3D HIGH RESOLUTION SEISMIC IMAGING OF MIDDLE – LATE QUATERNARY DEPOSITIONAL SYSTEMS, SOUTHEAST GREEN CANYON, SIGSBEE ESCARPMENT, GULF OF MEXICO

A Thesis

Presented to

the Faculty of the Department of Geosciences

University of Houston

In Partial Fulfillment

of the Requirements for the Degree

Master of Science

By

Oluwayomi Oyedele

August 2005

3D HIGH RESOLUTION SEISMIC IMAGING OF MIDDLE – LATE QUATERNARY DEPOSITIONAL SYSTEMS, SOUTHEAST GREEN CANYON, SIGSBEE ESCARPMENT, GULF OF MEXICO

Oluwayomi Oyedele

Approved:

Dr. William Dupre', Chairman

Dr. Kurt Marfurt, Co-Chairman

Mr John Sharp

Dean, College of Natural Sciences and Mathematics

ACKNOWLEDGEMENTS

My special thanks go to the Author and Finisher of my faith, GOD ALMIGHTY for His grace and mercy throughout the duration of my study. I thank my advisor Dr Dupre' and committee members Dr Kurt Marfurt (Uof H), and Mr. John Sharp (BP) for their guidance and encouragement. I thank BP Inc. and partners for giving me the privilege to work on this data. I am also grateful to Bob Bruce, Chuck Bluementritt, Dr Don Van Nieuwenhuise, John Brand, Kolla Venkatarathnam, and Vitor Abreu for their useful discussions. Finally, I thank my family, friends, and members of the Living Word Chapel (RCCG) for all their support.

3D HIGH RESOLUTION SEISMIC IMAGING OF MIDDLE – LATE QUATERNARY DEPOSITIONAL SYSTEMS, SOUTHEAST GREEN CANYON, SIGSBEE ESCARPMENT, GULF OF MEXICO

An Abstract of a Thesis

Presented to

the Faculty of the Department of Geosciences

University of Houston

In Partial Fulfillment

of the Requirements for the Degree

Master of Science

By

Oluwayomi Oyedele

August 2005

ABSTRACT

My study describes the architecture and facies distribution of Middle-Late Quaternary depositional systems along the Sigsbee escarpment, Southeast Green Canyon, Gulf of Mexico. The Sigsbee escarpment defines the seafloor expression of the down-slope limit of the mobile allochthonous shallow salt. My study area is located within the lower continental slope in water depths of approximately 4500' (1370m), and is focused largely on the upper 500ms (approximately 400m) of sediment.

Previous work in the area delineated several fan systems landward of the escarpment. My objective was to perform a more detailed analysis of the depositional systems, including their age, lithofacies, seismic reflections, and architectural elements. Most of my work was based on interpreting 3D HR seismic data covering an area of 48 sq km. The seismic data were supplemented with four electric well logs, each with both gamma ray (GR) and resistivity logs, and one well boring from which five biostratigraphic age dates had been obtained.

The depositional systems I studied include a channel-lobe complex, channel-like features, and mass transport complexes (MTCs). The oldest of these systems was a channel-lobe complex that accumulated within a minibasin; it is composed of at least four distinct channel-lobe systems. It formed between 500 and 550 Ka, perhaps during an early rise in sea level. Numerous curvi-linear channels (best imaged using seismic attributes) are probably glide tracks, however a turbiditic origin for some is possible.

The MTCs studied are characterized on seismic by chaotic reflections, failure scars, scoured bases (basal shear surfaces), and mounded and lobate external geometry.

MTC A and MTC B were likely formed during major drops in sea level (~ 470Ka and ~ 370Ka respectively). MTC C and MTC D were probably triggered by salt-driven uplift; however two younger, widespread MTCs (not studied in detail) appear to coincide with sea-level drops at ~290 Ka and ~75 Ka.

The slope depositional systems were mainly controlled by the interplay of sea-level changes and salt tectonics. The changes in sea level dictated the volume of sediment supplied and also accommodation space for deposition. Salt movement affected the slope's depositional gradient and slope stability, as well as created localized accommodation space in the form of intraslope basins.

CONTENTS

Chapter 1

INTRODUCTION

1.1 PURPOSE

The purpose of my research is to better understand the depositional systems and geologic history of the lower continental slope region of the northern Gulf of Mexico basin. Previous workers have delineated the geometry of fan systems ponded behind the escarpment rim, as well as some mass transport complexes on the Escarpment; however, a detailed analysis of deposystems within the lower continental slope has not been done. By integrating seismic facies analysis with well data, I intend to do the following:

- Perform a detailed seismic facies analysis of deposystems within the study area.
- Infer the factors controlling the transport and deposition of those deposystems.
- Describe the depositional history of the stratigraphic section of interest.

1.2 STUDY AREA

My study area is located in the southeast Green Canyon blocks where the base of the northern Gulf of Mexico continental slope meets the continental rise at the Sigsbee escarpment (Figure 1). The basin has been strongly influenced by salt movement that in turn controls the facies characteristics and geometry of the systems. Nibbelink & Martinez (1998) used seismic attributes to describe and delineate the turbidite systems in the area. Nibbelink (1999) proposed the turbidite systems as analogues for deeper targets.

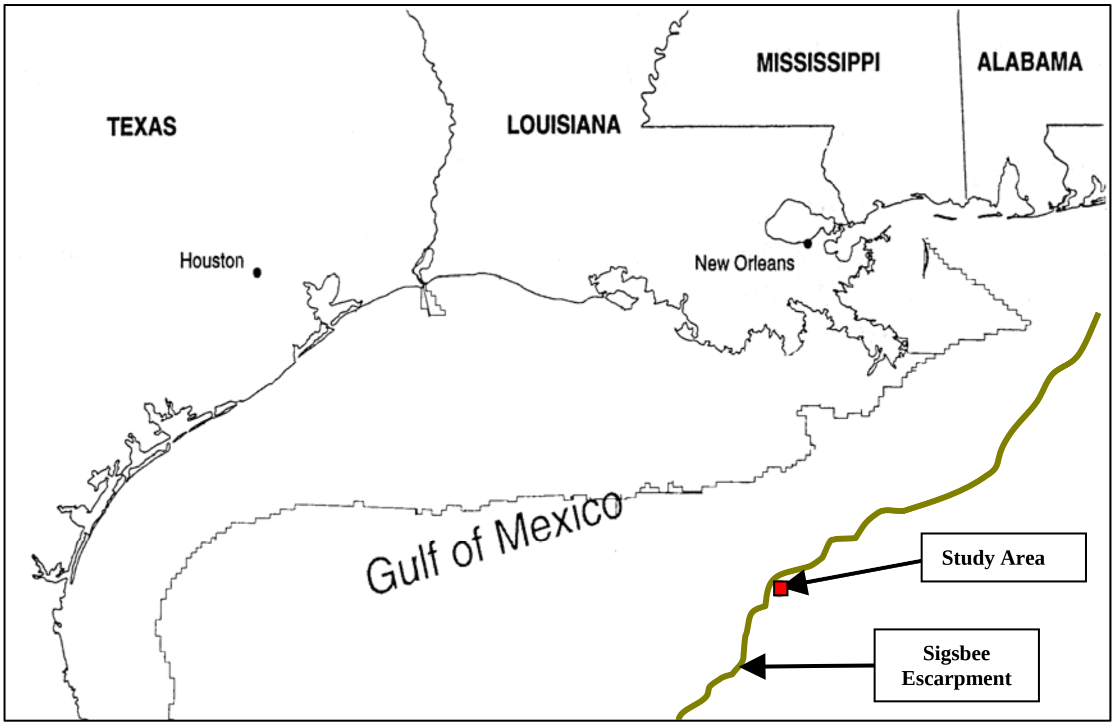

Figure 1: Map showing the location of the study area along the Sigsbee Escarpment, Gulf of Mexico.

The area was subdivided into three provinces (Figure 2): the lower continental slope, the face of the escarpment, and the upper continental rise (Orange *et al*., 2003). My study area covers approximately 48 km^2 within the lower continental slope, and is limited to the upper 500 ms (~400m) of sediment.

The *lower continental slope* at the top of the escarpment occurs in an average water depth of approximately 4500ft (~ 1370m). It is characterized by extensional faults, including a northwest trending graben associated with a local salt diapir. Some buckle folds also exist above the seaward-mobile salt, which suggest some component of regional compression (Orange *et al*., 2004).

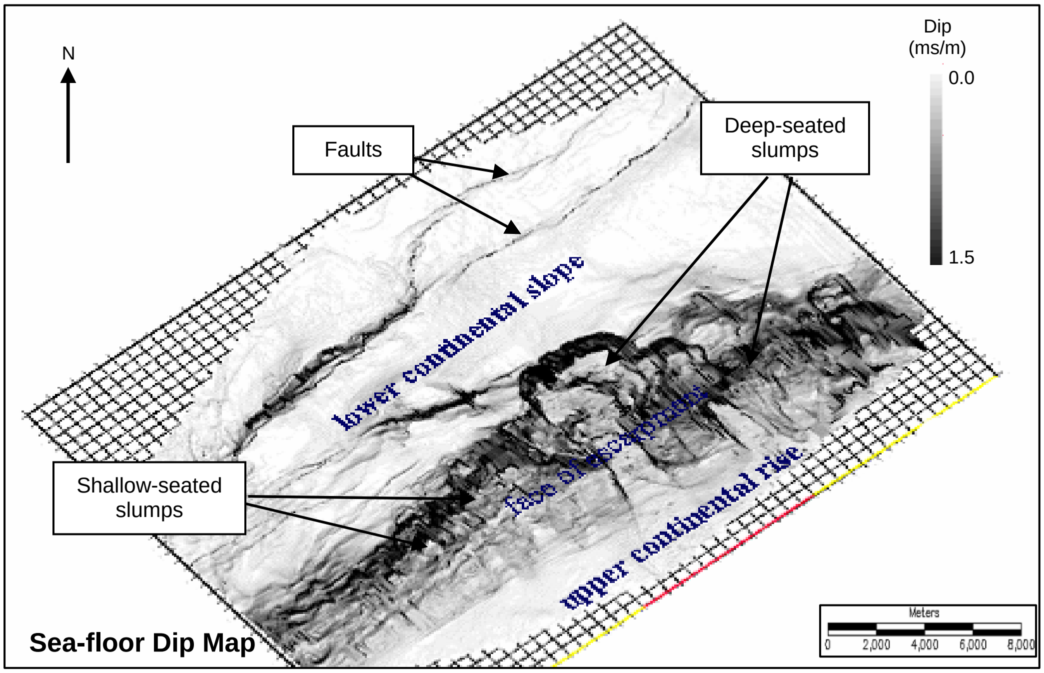

Figure 2a: Seafloor dip map showing the 3 distinct provinces: lower continental slope, face of the escarpment, and upper continental rise (after Orange *et al.*, 2003).

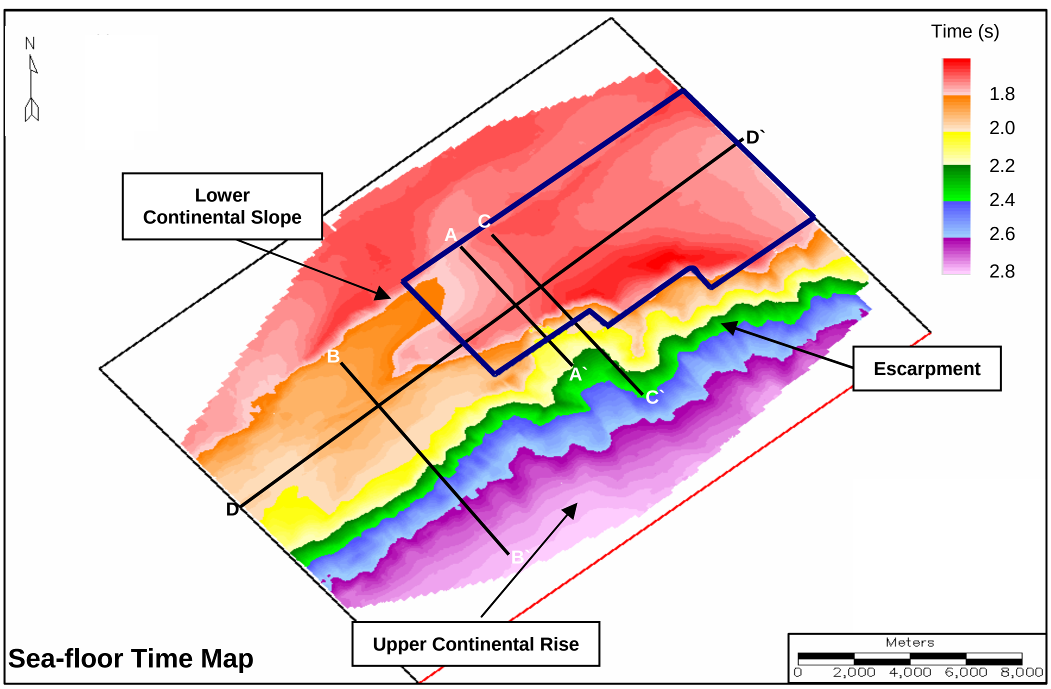

Figure 2b: Seafloor time map. The blue polygon represents my study area.

Nibbelink and Martinez (1998) delineated ponded fan systems within the lower continental slope approximately 500 ms (~400m) below the seafloor (Figure 3). Orange *et al*. (2003) noted that one of the fan systems (Hrz 25) identified by Nibbelink and Martinez (1998) occurs approximately at the same elevation as the base of a main headscarp. They noted that the unit is laterally restricted to the northeast portion of the study area, and concluded it was acting as a barrier to confine underlying overpressure (Figure 4). Calculated sediment accumulation rate in some areas within the province was less than 12cm/Ka during the last 8.50 Ka, which implies that the area has been relatively stable with respect to mass movement during the Holocene (Slowey *et al*., 2003).

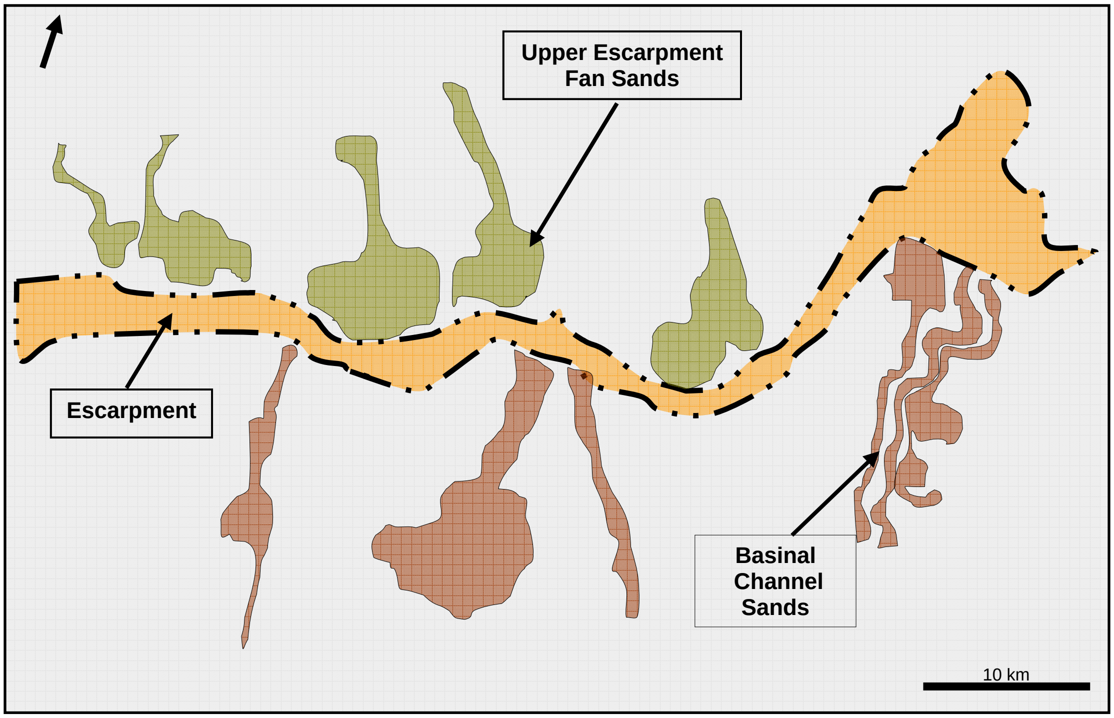

Figure 3: Line drawing along the escarpment based on coherence and amplitude map showing fan sands ponded behind the escarpment and channel systems in front of the escarpment (modified after Nibbelink & Martinez, 1998).

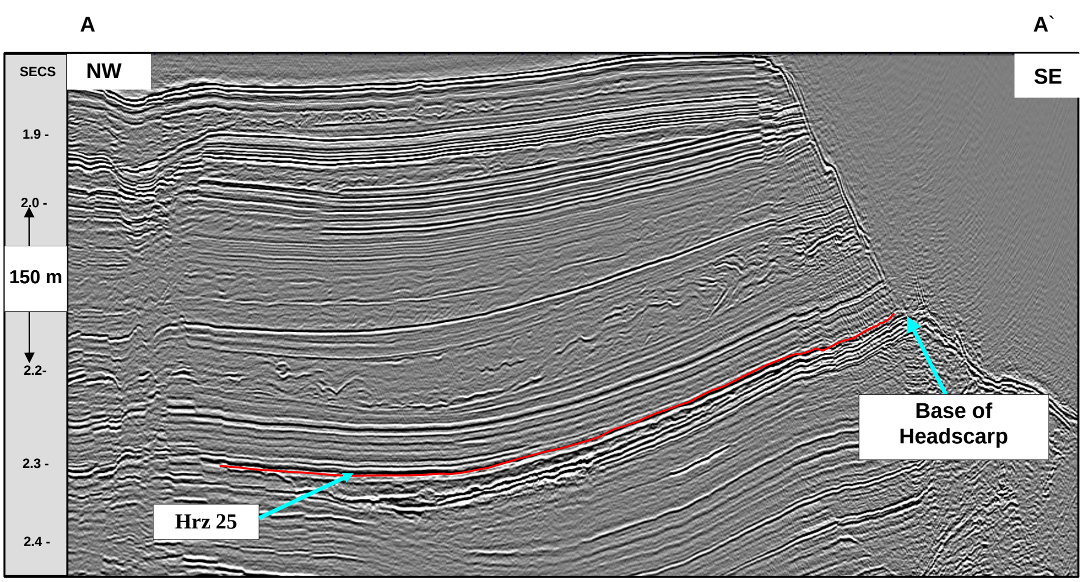

Figure 4: NW-SE seismic profile showing the sheet sand (Hrz 25) at the base of the headscarp. See Figure 2b for location.

The *face of the escarpment* occurs at an average water depth of approximately 5600ft (~1700m). Two distinct types of slumps characterize the area. Deep-seated slumps with amphitheatre-shaped head-scarps occur along the central/northeastern portion of the escarpment, whereas shallow-seated slumps with small-scale head-scarps occur along southwest side of the escarpment. The shallow-seated slumps were triggered by salt-induced oversteepening, whereas the deep-seated slumps were internally triggered by pore pressure fluctuations, which may not be directly linked to salt activity (Orange *et al.*, 2003). The differences observed in the slumps' triggering mechanisms reflect the strong influence of salt movement on the supra-salt section. Figure 5 shows how the shallow placement of the salt in the southwest area promoted oversteepening conditions as expressed by seaward dipping of beds and faults. In contrast, the strata in the northeast area are truncated at the seafloor because of slumping caused by movement of the laterally extensive underlying salt. The slumps were suggested to be presently dormant based on the recovery of Holocene sedimentary layers draping the escarpment (Young *et al.*, 2003).

The *upper continental rise* occurs in an average water depth of 6800ft (~ 2070m). The region is characterized by contractional toe-thrust faults and folds. Depositional features in the area include debris flow and turbidite deposits, probably derived from the slumped escarpment (Nibbelink, 1999).

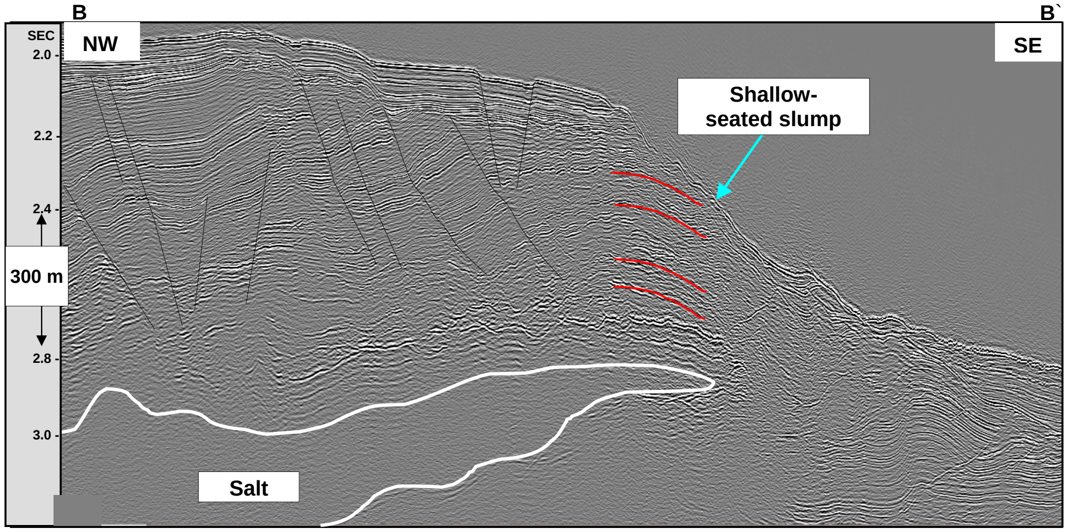

Figure 5a: NW -SE showing how shallow placed salt in the southwest promoted sea-ward dipping of beds and faults. See Figure 2b for location.

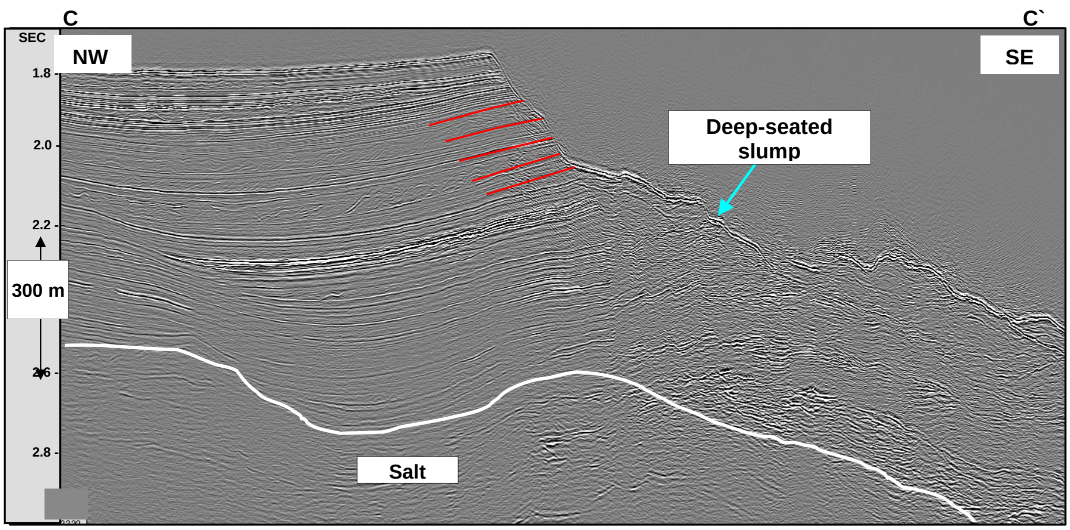

Figure 5b: NW -SE showing how deeply placed salt in the northeast area resulted into the occurrence of the strata at high angles with the seafloor. See Figure 2b for location.

1.3 BACKGROUND

The deep water Gulf of Mexico has received tremendous attention from both the oil companies and academic community in recent years due to increasing hydrocarbon discoveries in the region. In order to maximize production from these reservoirs, research has increasingly focused on better understanding the internal architecture and facies distribution of the turbidite systems. The architecture and facies associations of turbidite systems are determined by a variety of factors that influence the transportation and deposition of the sediments (e.g. Reading and Richards, 1994; Prather *et al*., 1998; Weimer and Slatt, 1999; Armentrout *et al*., 2000; Sikkema and Wojcik, 2000; Bouma, 2001; Samuel *et al*., 2003). A good understanding of these factors is therefore imperative.

Detailed studies of these turbidite systems have been achieved by integrating seismic data (and in some cases side – scan sonar data) with data obtained from wells (wire line logs, core, biostratigraphic, and engineering data) and outcrop studies. Conventional seismic data are normally used to interpret deeper targets. Where high-resolution (HR) shallow seismic data exist, the HR can be used as analogues for the deeper lower-resolution targets. The advantage of the HR is that it allows for a more detailed interpretation. Outcrop studies also provide useful analogues for subsurface interpretation. The outcrops provide bed-scale architectural analysis which otherwise are not obvious on seismic data. Ground Penetrating Radar (GPR) has also been used in recent years in imaging these bed-scale features (Young *et al*., 2003). Outcrop studies have proven to be very useful; however, their utility is somewhat restricted due to their limited lateral continuity.

The integration of the aforementioned data sets allowed the definition of seismic facies, which in turn aided in inferring depositional processes and thereby provided a more detailed understanding of deepwater systems in the basin. Prather *et al*., (1998) developed a seismic facies scheme tailored specifically for the intraslope basins in deep-water Gulf of Mexico. Seismic facies schemes comparable to those defined by Prather *et al*., (1998) was proposed by Beaubouef *et al*., (2000).

1.4 TURBIDITE SYSTEMS

A turbidite system refers to the sediments or sedimentary rocks and associated sedimentary structures (in the subsurface or outcrop) that were deposited by sedimentary gravity flows (Bouma, 2000 pg. 9). Sediment gravity flows are usually triggered by factors such as storm waves, slope oversteepening, fault offset, pore pressure fluctuations, earthquake ground motion, and sea-level changes.

Pioneering studies on turbidite systems were marked by the introduction of the Bouma sequence into the academic community. Based on outcrop studies, Bouma (1962) described an idealized sequence of sedimentary structures in rocks deposited by turbidity currents (as cited by Weimer and Slatt, 2004). The complete sequence was characterized by a fining upward pattern (normally graded bedding) with their associated sedimentary structures. Subsequent studies later identified incomplete Bouma sequences in the rock record that were either deposited as incomplete sequences or altered by other flows. The 2-dimensional limits encountered in most outcrop studies were in part overcome in later years by the acquisition of subsurface seismic data. The integration of seismic data with well data, and outcrop studies provided a 3–dimensional view into the architectural elements of turbidite systems, which aided in reservoir characterization by providing insight into the systems’ depositional processes. Principal architectural elements defined by Chapin *et al*., (1994) from such integrated studies in deepwater depositional settings include levees, channel complexes, and sheet sands (as cited by Weimer and Slatt, 2004) (Figure 6).

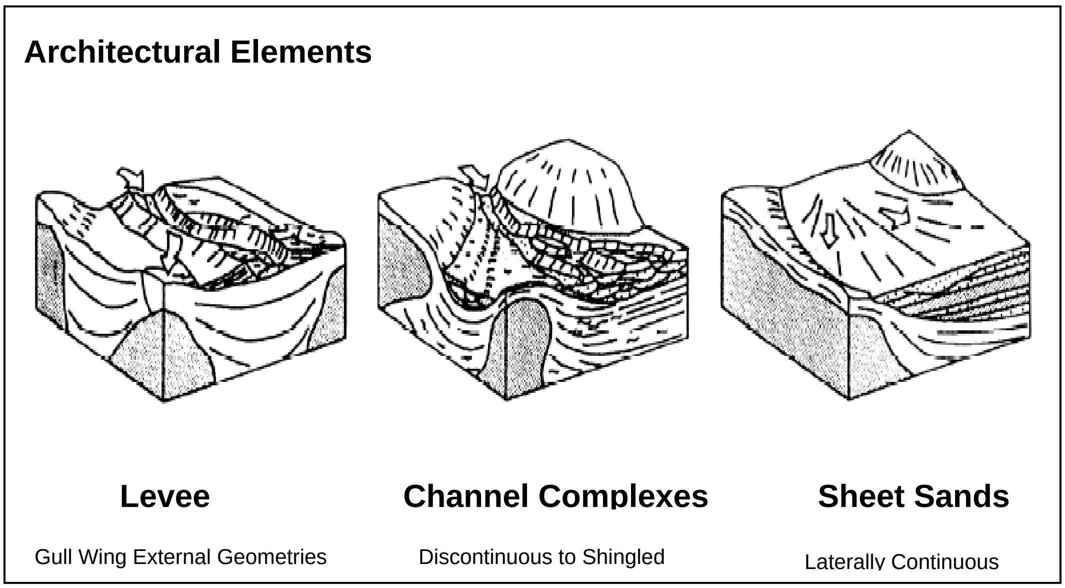

Figure 6: Principal architectural elements of deepwater clastic systems (Chapin *et al*., 1994).

1.4.1 Controlling Factors

Turbidite systems are controlled by three major factors: tectonics, climate, and sea level fluctuations (Figure 7). Tectonism influences the nature of the basin's drainage (i.e. its geometry, gradients, and provenance) as well as the bathymetry and geometry of the receiving basin (Reading *et al*., 1994; Bouma *et al*., 2000; Weimer and Slatt, 2004). Climate influences the rate and type of weathering, precipitation, and runoff, thereby determining the sediment type (i.e. grain size, shape, and mineral composition) as well as amount of sediment entering the basin. Major climatic changes (e.g. glacial and interglacial ages) result in sea-level fluctuations that affect the rate of sediment supply and type of sediment dispersal pattern The interplay of these various factors determines accommodation space and sediment supply in the deepwater which influences the systems' facies association and depositional elements.

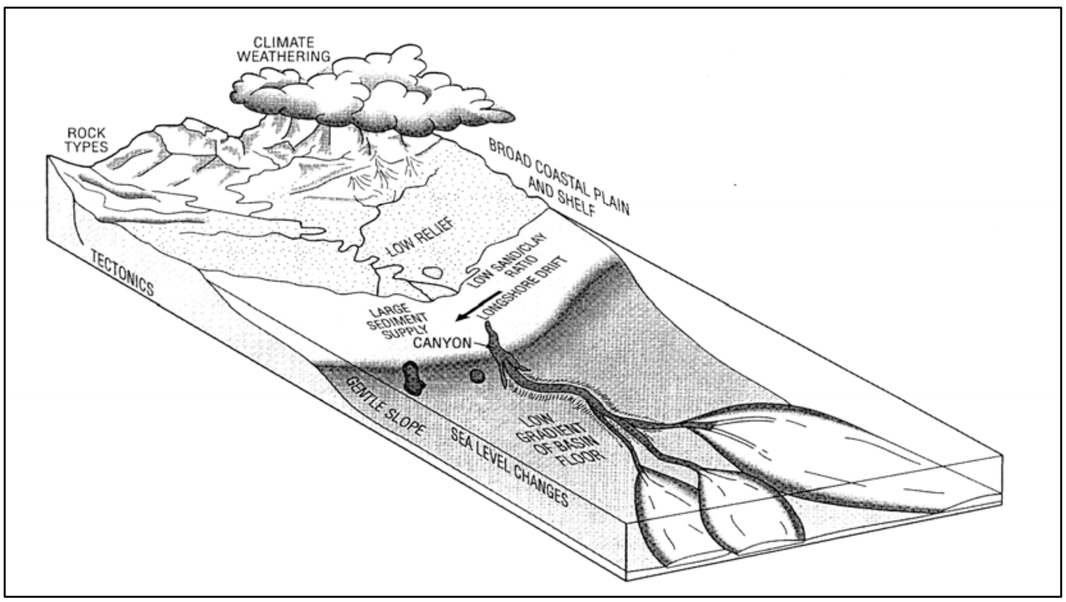

Figure 7: Diagram showing the principal factors influencing the process of erosion, transport, and deposition of depositional systems (Bouma, 2001).

Regional basin accommodation can be created by tectonic subsidence e.g. the opening of the Gulf of Mexico as a result of the breakup of the super-continent Pangea during the Mesozoic. Accommodation space within the basin can also change due to sea-level fluctuations. A relative rise in sea level creates increased accommodation space within the shelf region, whereas a relative drop in sea level decreases accommodation space within the basin. Locally confined accommodation space can also be generated by syn-depositional tectonic activity. Differential loading of sediments on salt or shale triggers their movement, which leads to the creation of intraslope basins. These localized "depressions" on the continental slope control the length of turbidite flows as they trap sediments along their paths. When the intraslope basins are filled, sediments spill over to the next basin down-slope via a bypass channel. The complex stratigraphic and structural framework of basins such as in the Gulf of Mexico, lower Congo basin (offshore Angola), and Niger delta is attributed to such salt/shale movement.

Several studies have looked at the evolution of intraslope basins in Gulf of Mexico (e.g. Prather *et al*., 1998; Beaubouef & Friedman, 2000; Sikkema and Wojcik, 2000; Prather *et al*., 2003). An idealized sequence for the basins was proposed by Beaubouef & Friedman (2000) based on the integration of seismic facies analysis with well data (Figure 8). The basin fill exhibits an overall fining upward pattern; the base is characterized by chaotic facies (Mass Transport Complexes), while the top of the sequence is characterized by draping facies (hemipelagic deposits). Other depositional elements within the sequence include, distributary channel complexes, channel-levee systems, and sheet sands. The draping facies are associated with major transgressions and channel avulsions as the basin fill reaches its spill point (Prather *et al*., 1998; Badalini *et* *al*., 2000; Beaubouef & Friedman, 2000). Incomplete sequences exist, however, because factors influencing depositional processes vary from basin to basin.

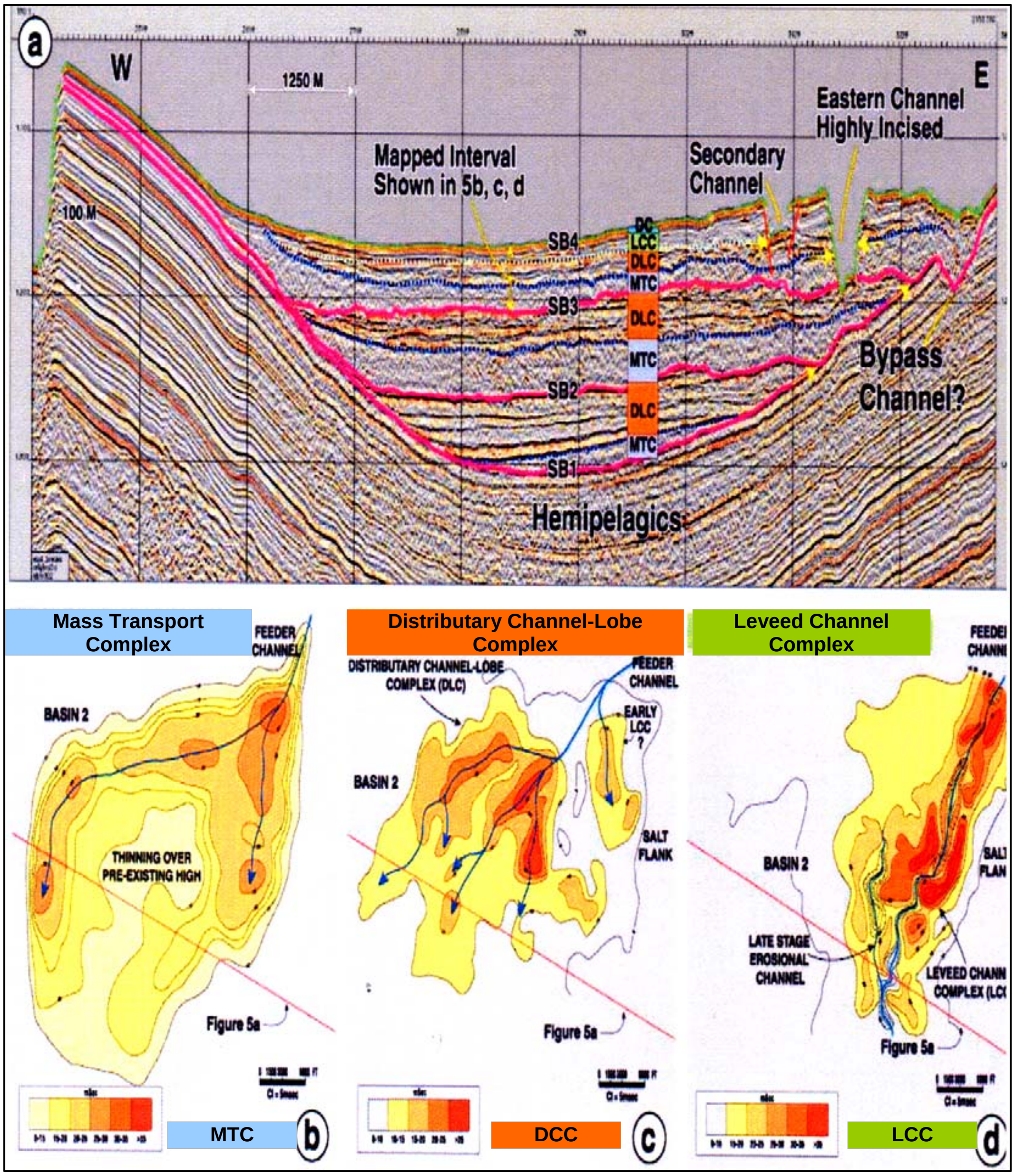

Figure 8: Idealized intra-slope basin sequence proposed by Beaubouef *et al*., (2000).

Other key factors influencing the architecture and facies of turbidite deposits include volume and type of sediment. The volume of sediment is strongly affected by changes in sea level. Lowstands of sea level are associated with high rates of sediment supply rate, whereas highstands of sea level are characterized by low sedimentation rates in the basin. Short pulses of sea-level rise and fall also affect sedimentation, though more typically within the shelf and slope regions.

Sediment type, (especially grain size) affects the flow velocity and distance of sediment transport. For example, mud-dominated systems transport sediments over long distances, whereas mud-deficient systems transport sediments over shorter distances (Reading and Richard, 1994). This is because the mud-rich systems exhibit a lower rate of momentum loss compared with the coarse-rich systems. In addition, the lengthy travel of the fine-grained sediments in some cases may also have been propelled by their large source. For example, the Mississippi fan was fed by a major delta (Reading and Richard, 1994). Mutti and Ricci (1981) described the mud-dominated systems as formed by high efficient flows and the sand-rich systems are formed by low efficient flows (as cited by Reading and Richard, 1994).

Distance of transport and flow velocity rates can also be affected by changes in slope gradients. Steep slopes allow for high flow velocities, which allows transportation further basinward, whereas, lower slope gradients result in decreased flow velocities which initiate sediment deposition, channel avulsions, and/or changes in the flow's architecture (Bouma, 1995; Galloway, 1998; Armentrout *et al*., 2000).

1.4.2 Turbidite System Models

The idea of developing a unifying turbidite system model has been discouraged by several authors (e.g. Bouma, 2000), because the factors influencing deposition are variable and their impact on individual fan often differ. Thus, numerous models exist in the literature based on a variety of controlling factors the authors deemed to be the most influential in the system's depositional process. As such, the application of these models should be done carefully.

Reading and Richard (1994) proposed 12 turbidite system models based on two factors; the type of feeder system (point-, multiple-, and linear sourced systems) and the grain size (mud-rich, mud/sand rich, sand-rich and gravel-rich systems) of the deposit. The authors felt that these two factors were dominant in controlling the travel distance, which ultimately determines the facies produced and their architecture. In contrast, based on the review of several other models, Bouma (2000) proposed and described two siliciclastic fan models based only on grain size. They are a coarse-grained, sand–rich submarine fan system and a fine–grained, mud-rich submarine fan system.

Bouma (2000) also discussed the relationship between slope gradient and architectural elements (Figure 9). Using his fine-grained turbidite system model, he demonstrated how changes in slope gradient influenced the external geometry of turbidite flows from the base of the slope to the abyssal plain. He proposed that the deposition of wide channel complexes at the base of the slope (upper fan) was initiated as a result of changes in slope gradient. While further reduction in slope gradient resulted in the deposition of levees and overbank systems in the middle fan and finally unconfined depositional lobes in the lower fan. Armentrout *et al*. (2000) discussed a similar progression of seismic facies; from upper slope confined flows (characterized by channel-levee/overbank elements) to down-slope less confined flows (characterized by sheet sand elements) (Figure 10).

In conclusion, considering the subjectivity of these models, a basic understanding of factors controlling deep-water systems is needed before choosing analogues from pre-existing models. Analogues appropriately applied help in inferring prevailing depositional processes and their associated facies product, which in turn facilitate proper reservoir characterization.

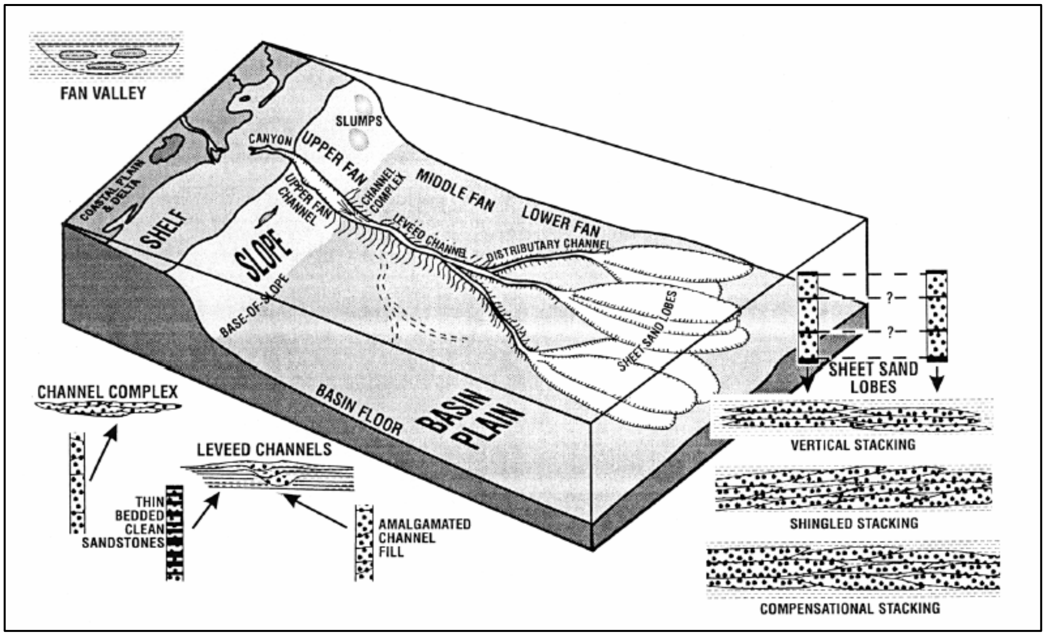

Figure 9: Block diagram showing fine-grained turbidite system model. The model demonstrates how changes in gradient affect the different depositional elements (Bouma *et al*., 2000).

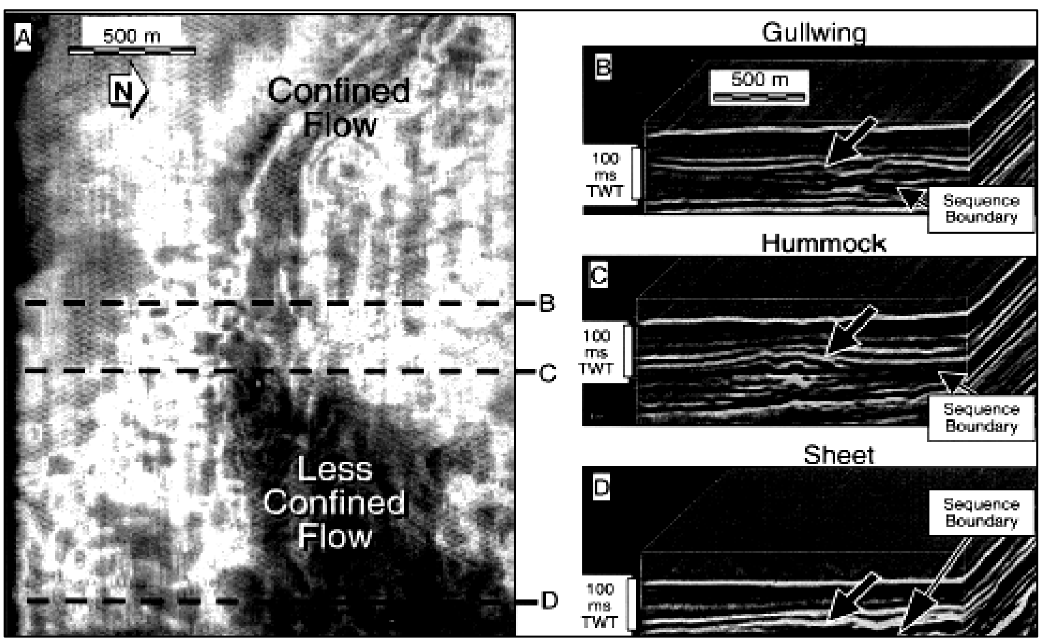

Figure 10: RMS amplitude extraction of an early channel to sheet system. Change in depositional element reflects the influence of gradient changes on deposition (Armentrout *et al*., 2000).

Chapter 2

REGIONAL GEOLOGY

The breakup of the super-continent Pangea was accompanied by Triassic rifting along extensive fracture zones leading to the separation of North America from South America and Africa and subsequently the development of the Gulf of Mexico and the central Atlantic. By the Callovian (middle Jurassic), the basin experienced a major influx of seawater from the Pacific. Salvador (1987) suggested that the influx probably occurred occasionally during periods of hurricanes or exceptionally high tides. Restricted seawater circulation under arid climate conditions resulted in the precipitation of evaporites over an extensive area in the basin (Salvador, 1987; Worrall *et al*. 1989; Marton *et al*., 1993). The salt initially accumulated in a widespread, shallow basin, which later became separated as a result of Middle to early Late Jurassic sea-floor spreading. Presently, these salt deposits are found in major allochthonous evaporitic belts in the northern and southern part of the basin (Figure 11).

The Northern region is characterized by the Louann salt, underlying the coastal plains and offshore regions of Northeastern Mexico, Texas, Louisiana, southern Arkansas, Mississippi, Alabama, part of the Florida panhandle and adjacent areas of the continental shelf and slope of the Gulf of Mexico. The Southern region occupies a portion of the southern deep Gulf of Mexico (Challenger salt), north of the Campeche Escarpment, the Bay of Campeche, adjacent onshore Mexico to the south (Isthmian salt) and the southern eastward concave belt along the west and northwest flank of the Yucatan Peninsula (Salvador, 1987; Worrall *et al*., 1989).

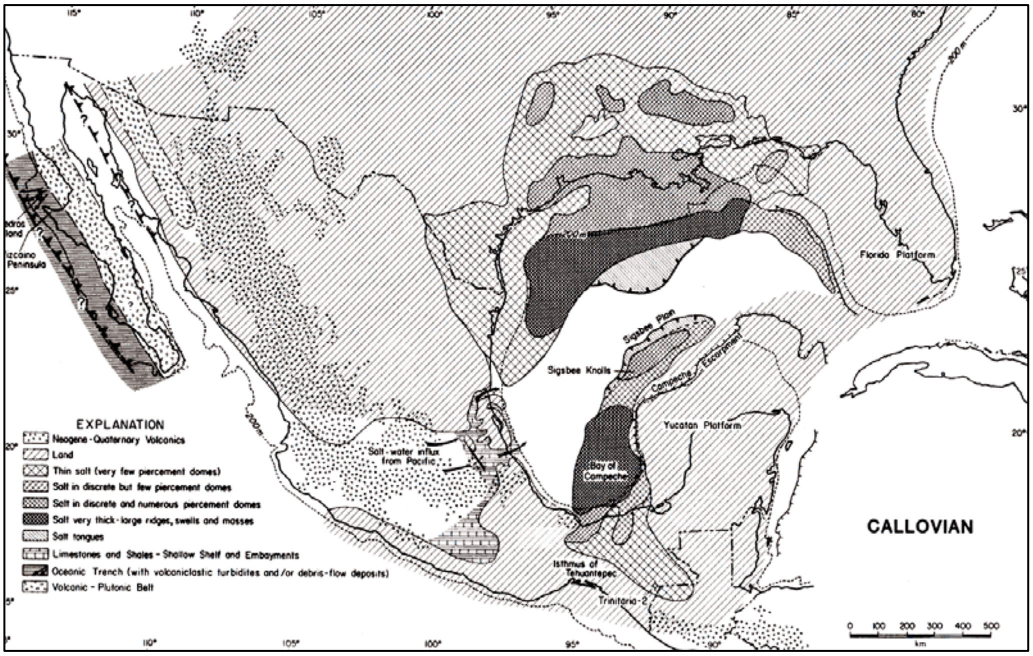

Figure 11: The two major evaporitic salt regions in the North and South of the Gulf of Mexico basin caused by seafloor spreading during the Callovian (Salvador, 1987).

The change from evaporitic conditions to normal marine conditions occurred during the late Jurassic Oxfordian Stage. During this period, the Gulf region experienced the first major widespread and prolonged marine transgression with unrestricted seawater circulation. The creation of new oceanic crust resulted in the Southern rotation of the Yucatan block to its present position, which probably created open marine conditions within the proto-Caribbean and the newly developing Atlantic Ocean (Salvador, 1987; Worrall *et al*., 1989). The Oxfordian stage also recorded the deposition of heterogeneous carbonates. These units are characterized by evaporitic and shallow lagoon facies reflecting deposition in shallow- to deep-water marine environments.

Deposition of carbonates and evaporites during late Jurassic- earliest Cretaceous was followed by a major siliciclastic influx into the gulf region during the Tithonian (uppermost Jurassic) to Berriasian (earliest Cretaceous). The Cenomanian (mid-Cretaceous) recorded the drowning of early Cretaceous shelf margin reef cycles, which was followed by the deposition of chalks, marls, and shales during the late Cretaceous.

Differential sediment loading of the Oxfordian transgressive sequences on the Louann strata triggered salt movement, which deformed into extensive massifs, pillows, ridges, and swells of salt. Salt tectonics became intensified during the Cenozoic as a result of rapid sedimentation caused by the uplift of the Cordillera and sea-level fluctuations. (Worrall, 1989; Feng *et al*., 1996; Galloway *et al*., 2000). This resulted in complex faulting, folding, and a progressive southward squeezing of the salts into a bulge of salt at Sigsbee Escarpment area (Figure 12). The escarpment therefore defines the seafloor expression of the down-slope limit of mobile allochthonous shallow salt in the Northern region of the Gulf of Mexico (Humphris, 1979; Walper *et al*., 1979; Salvador, 1987; Worrall *et al*., 1989). In 1998, Nibbelink and Martinez proposed a model describing how the escarpment was formed. They suggested that the escarpment developed from the influence of deep currents eroding the supra-salt sediments, which caused salt dissolution at the seafloor and subsequent sediment slumping towards the abyssal plain (Figure 13).

The Gulf of Mexico’s complex stratigraphic and structural framework is the result of the interplay of high sedimentation rates and salt tectonics. These factors remain the primary factors controlling depositional processes within the basin.

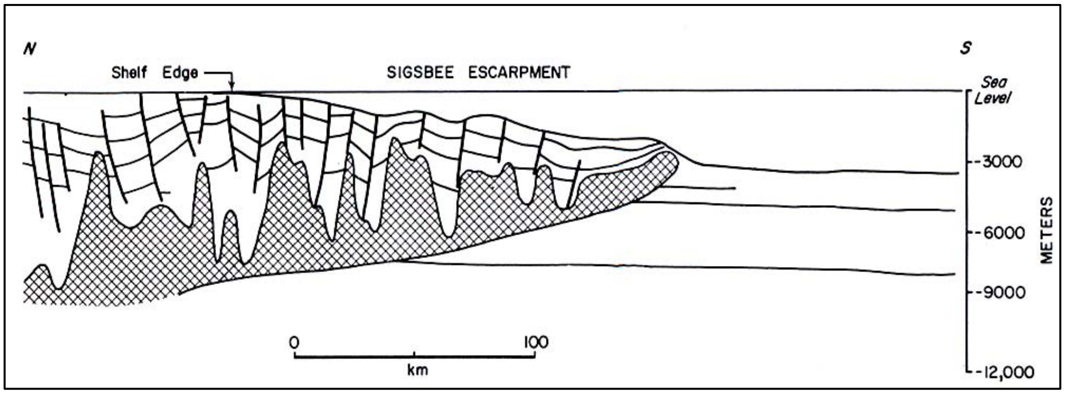

Figure 12: Southward squeezing of salt resulted into a bulge at the Sigsbee Escarpment (Salvador, 1987).

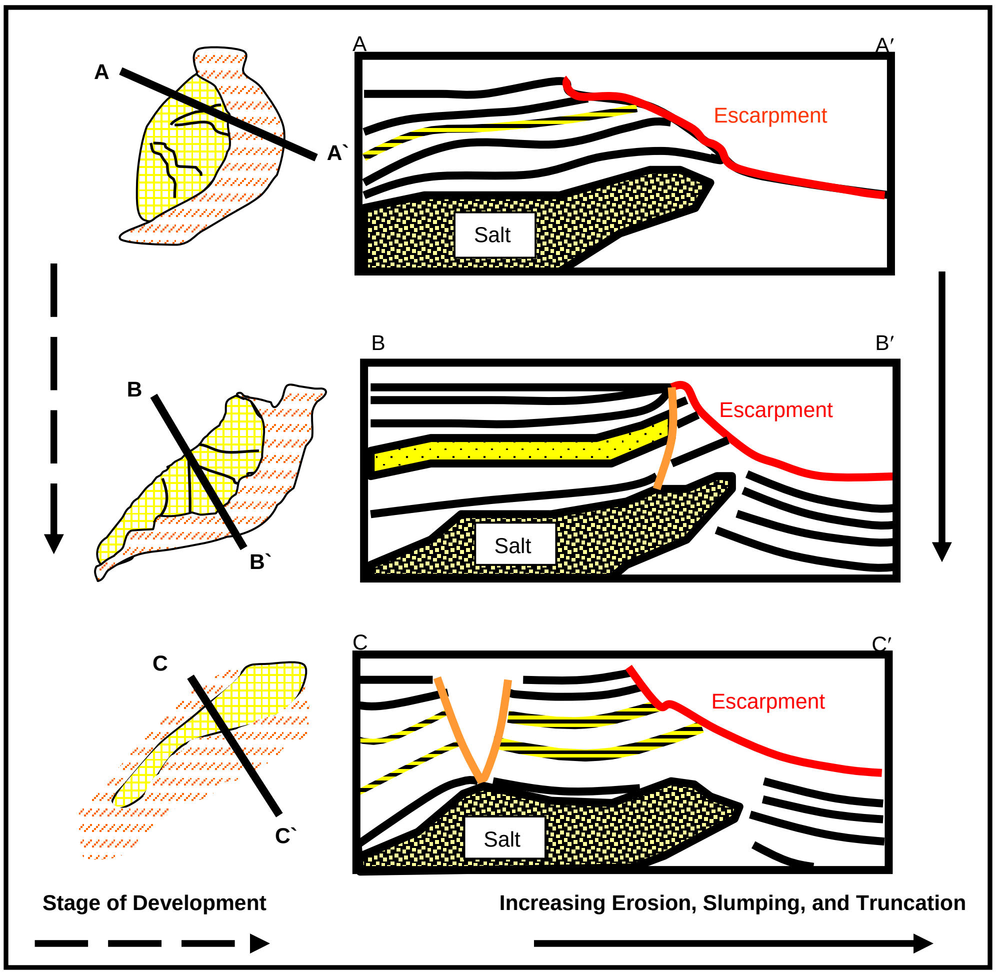

Figure 13: Escarpment model: (a) rounded front-smooth, gentle slope; (b) scalloped front-fault slump escarpment; (c) truncated, flat front-fault slump escarpment with graben (modified after, Nibbelink & Martinez, 1998).

Chapter 3

METHODOLOGY

3.1 DATA DESCRIPTION

The increasing discovery of turbidite systems as prolific reservoirs has inspired the detailed understanding of these systems. Maximal development and exploitation of producing fields have been achieved by integrating seismic data with all available geologic and engineering data and even outcrop studies. Such an integrated approach has been useful in understanding the transport and depositional processes of the systems and ultimately defining their facies association and depositional element.

Due to the limited data (gamma ray and resistivity logs, checkshot data, and shallow borings analysis reports) acquired within my area of interest, my interpretation was primarily dependent on seismic facies analysis of a three-dimensional high-resolution (3D-HR) seismic data. The HR seismic provided an edge in my interpretation over conventional 3D seismic because of its improved vertical and lateral resolution that aid in defining and differentiating the reservoir’s external geometries and facies to a degree that can only be hoped for at the exploration objective. Such high-resolution images can help us construct detailed analogues that may allow us to better understand reservoir heterogeneities.

3.1.1 Seismic Data

The entire 3D-HR seismic data covers an area of 205 sq km. The seismic data has a peak frequency of 170 Hz and were processed at 0.5-millisecond sample rate. The survey consists of 2500 NW-SE inlines spaced at 7.5m and 2250 SW-NE crosslines spaced at 6.25 m. My study is limited to approximately 48 sq km within the lower continental slope.

3-D-HR seismic data provide better images than conventional 3D data because of the broader frequency bandwidth and higher frequency that improves both vertical and lateral resolution. In general, HR surveys are acquired with a short cable, providing only limited multiples suppression. Due to the depth of the water (~1.3 km) these multiples arrive well after the “shallow” objectives imaged by the Green Canyon survey. As a result, HR surveys are primarily used for shallow geohazards assessments.

Geohazards assessment refers to the identification of geologic features that may pose a threat to successful drilling and processing activities at well sites. Such features include pockmarks (fluid exclusion craters), near-surface faults, shallow water sands, gas chimneys, and shallow gas pockets. The accurate assessment of these hazards is very important in making drilling and production decisions such as well placement and facilities positioning, especially while drilling exploratory wells (Rader and Medvin, 2002; Heggland, 2004).

Reservoirs imaged by HR seismic data at relatively shallow depths offer a better understanding of the reservoir’s internal architecture and true thickness. This enhances a more precise estimation of the field’s volume, which otherwise may be hampered by tuning effects (Beydoun *et al*., 2002). In addition, acquisition foot-print that can obscure accurate interpretation are minimized at this depth.

3.1.2 Well Data

Four electric well logs (BH1, BH2, BH3, and BH4), each with both gamma ray (GR) and resistivity curves are available within the study area (Figure 14). The electric logs extend to a maximum depth of 10700’ (~3300m) below sea-bottom. The gamma ray log is primarily sensitive to shaliness in formations and therefore indicates different types of lithology (especially sand verses shale content). Resistivity logs are responsive to fluid content (either water or hydrocarbon). Other available data include bostratigraphic dates from deep sample boring BH5. The boring has a maximum depth of 1400’ (~ 430m).

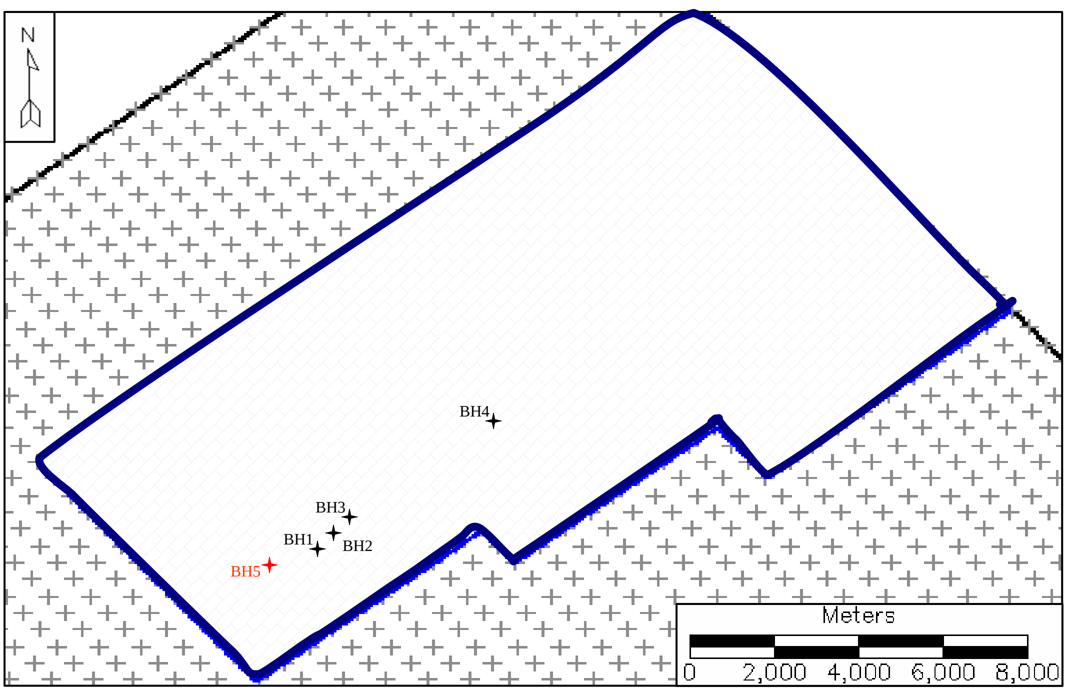

Figure 14: Basemap showing the location of well logs BH1-4 and deep sample boring (BH5). The blue polygon represents the study area.

3.2 MAPPING TECHNIQUES

The advent of long 2-D seismic lines provided a major breakthrough in understanding modern deepwater systems. One of the advantages of these data was the ability to image systems at scales well beyond the limits of outcrop studies. Structural interpretation was enhanced and the link between seismic reflection and lithology allowed for detailed facies analysis. Over the years, 3D seismic data led to better imaging of deepwater systems, allowing for more robust and accurate stratigraphic analysis compared to the earlier "layer–cake stratigraphy" theory.

Mapping 3D seismic for exploratory purposes normally requires a good understanding of the basin's structural framework and seismic facies analysis. In contrast, mapping in developed fields is usually initiated by tying production results to the regions of interest. Such mapping entails the interpretation and correlation of existing wells in the vicinity and tying the zones of interest from the logs to the seismic data. Gamma ray and SP logs are very useful in inferring deposystems, whereas an integration of these logs with resistivity, and neutron /density curves aid in identifying potential reservoirs. Tying the logs to seismic data is achieved by generating a synthetic seismogram from density and sonic logs. The product of density and velocity (from the logs) equals acoustic impedance, which is a function of lithology changes. This approach therefore helps in establishing the link between lithology and fluid content (from logs) with corresponding seismic response. However, in the absence of a synthetic seismogram, well-log information can be correlated to seismic using checkshot data. Checkshots do not offer as detailed a match but since it is measured at seismic versus sonic log frequencies, misties due to velocity discrepancies are avoided.

I used the second approach in my study because of the lack of sonic and density logs in the supra-salt section. An integration of this tie and seismic facies analysis was used in the detailed interpretation of the packages of interest. These packages included a channel-lobe complex, channel-like features and mass transport complexes (MTCs) (Figure 15). A detailed interpretation of these systems is presented in Chapter 4.

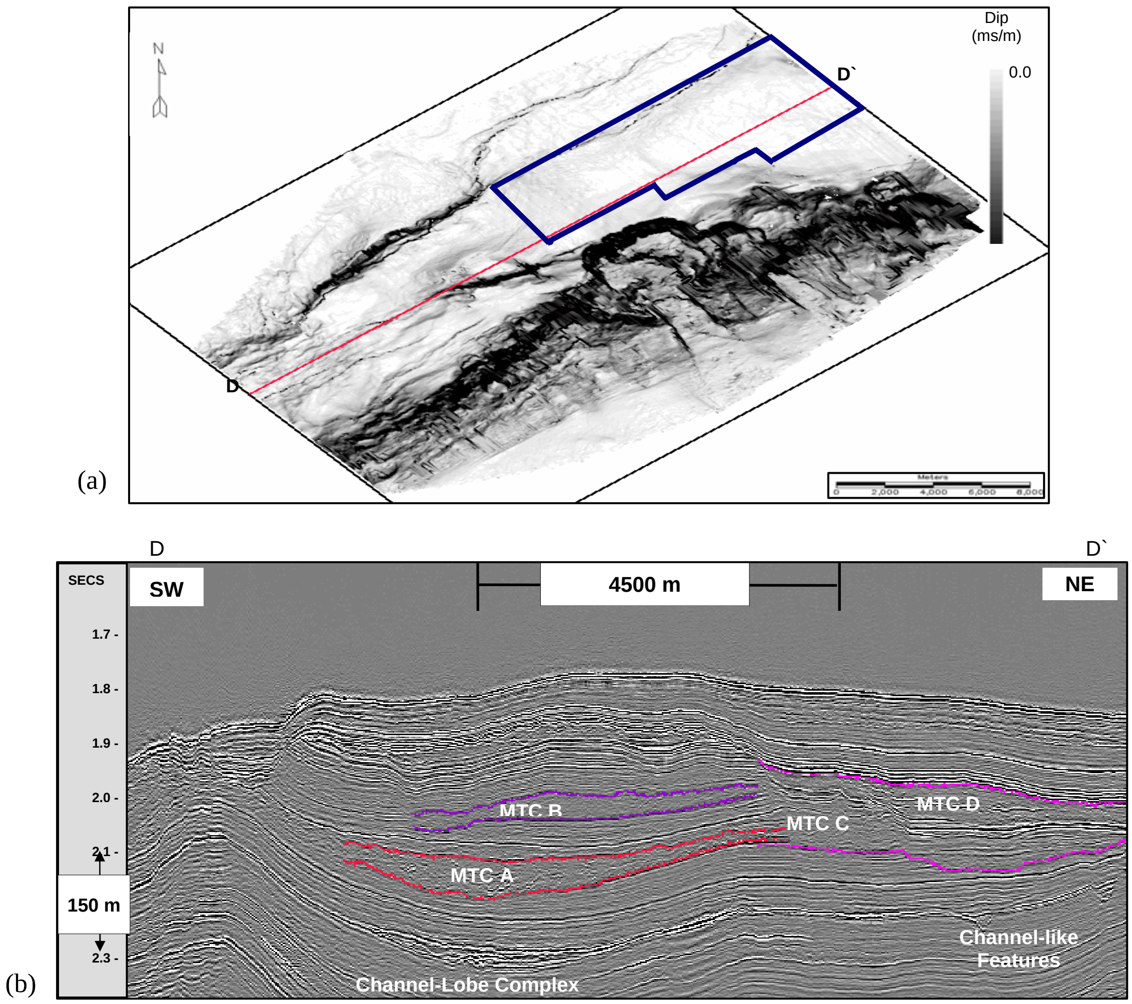

Figure 15a: Seafloor dip map, the blue polygon represents my area of study within the Lower Continental Slope (b) Seismic line DD' showing the mapped seismic facies.

I mapped key horizons across the study area using a 20 x 20 grid of inlines and crosslines. Areas that required more detailed mapping were mapped using smaller grids. Loop-tying the horizons in the inline and crossline directions helped in reducing mis-ties that could under/over-estimate the unit’s areal extent. After the manual horizon picking was concluded, the horizons were auto-picked. The auto-pick operation allowed the software to track events along bedding planes across the entire seismic volume, using the hand picked horizons as a constraint.

After auto-picking, I generated horizon slices through the seismic and attribute volumes. I also generated window-based attributes (attributes extracted within a window around the picked event) about the horizons. Horizon slices can be generated along either the top or base of the package. Rijks and Jauffred (1991) demonstrated that attributes generated along the top of the package offer more comprehensive geological information in contrast to horizon slices along the base of the package (Figure 16) . Horizon slices along the base usually represents the incision stage of the system, which is not only stratigraphically less interesting but also seismically more complicated, since the incision may cut lithologies having laterally varying impedances. Window-based attribute however integrates information above and below the reference horizon and therefore better represent the “sedimentary” package in contrast to point-based attributes. Window-based attributes are particularly useful in areas where there is difficulty carrying the top or base horizons accurately across the area either as a result of amplitude loss event discontinuity, and lateral changes in lithology.

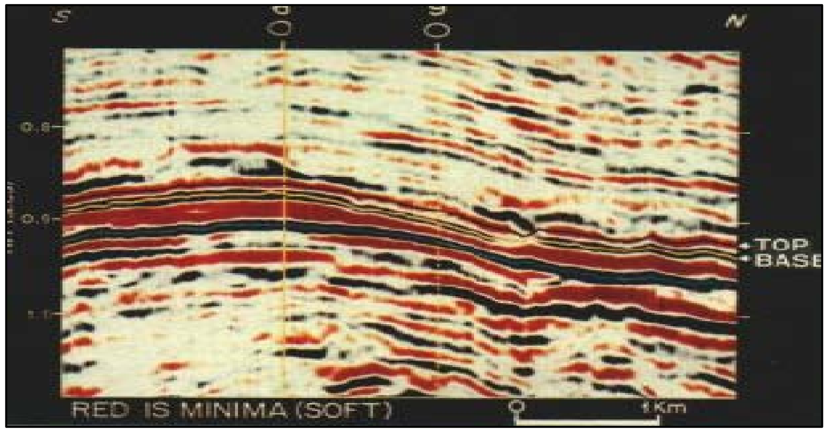

(a)

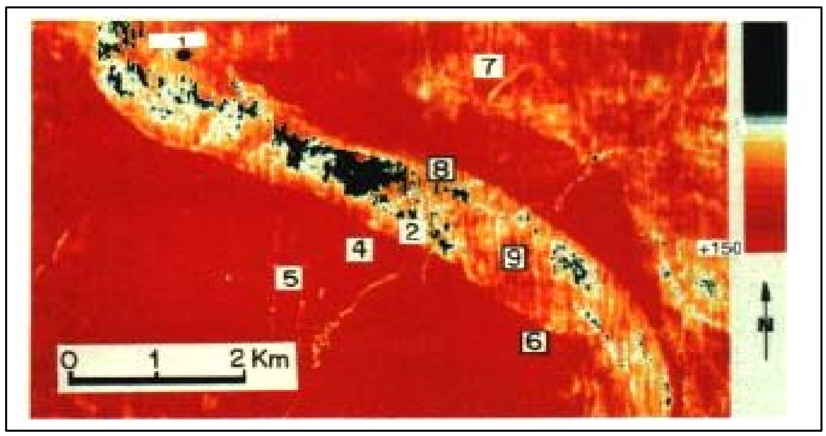

(b)

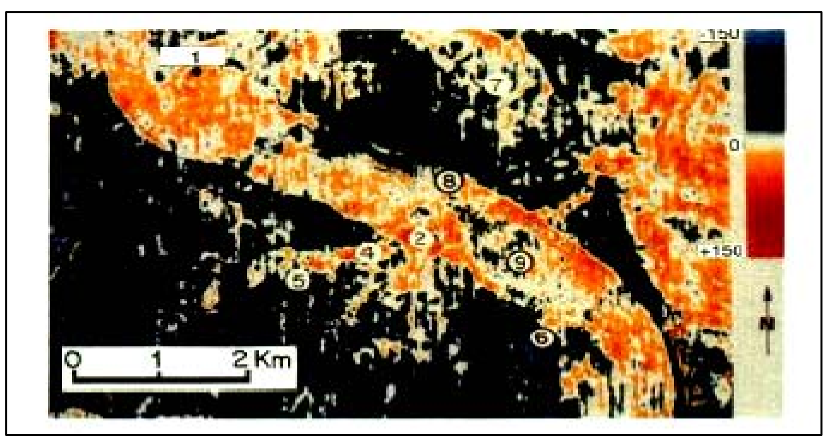

(c)

Figure 16: (a) Seismic line of channel, Balingian Province, Malaysia; (b) Amplitude map extracted from base sand; (c) Amplitude extracted from top sand (Rijks and Jauffred, 1991).

Intermediate slices were generated by flattening attribute volumes, thereby creating a suite of phantom horizons. The phantom horizons remove structural deformation that allows imaging of packages under conditions similar to the time of deposition. The evolution of a depositional system can be imaged by using flattened volumes which provide images at different seismic times, which correspond to different stages in the system's development. Flattening; however, fails when applied to areas with very strong structural control such as minibasins. Images extracted from such environments do not express the true extent and framework of the packages, as some of the strata appear as inclined beds. A summary of the methodology is presented below.

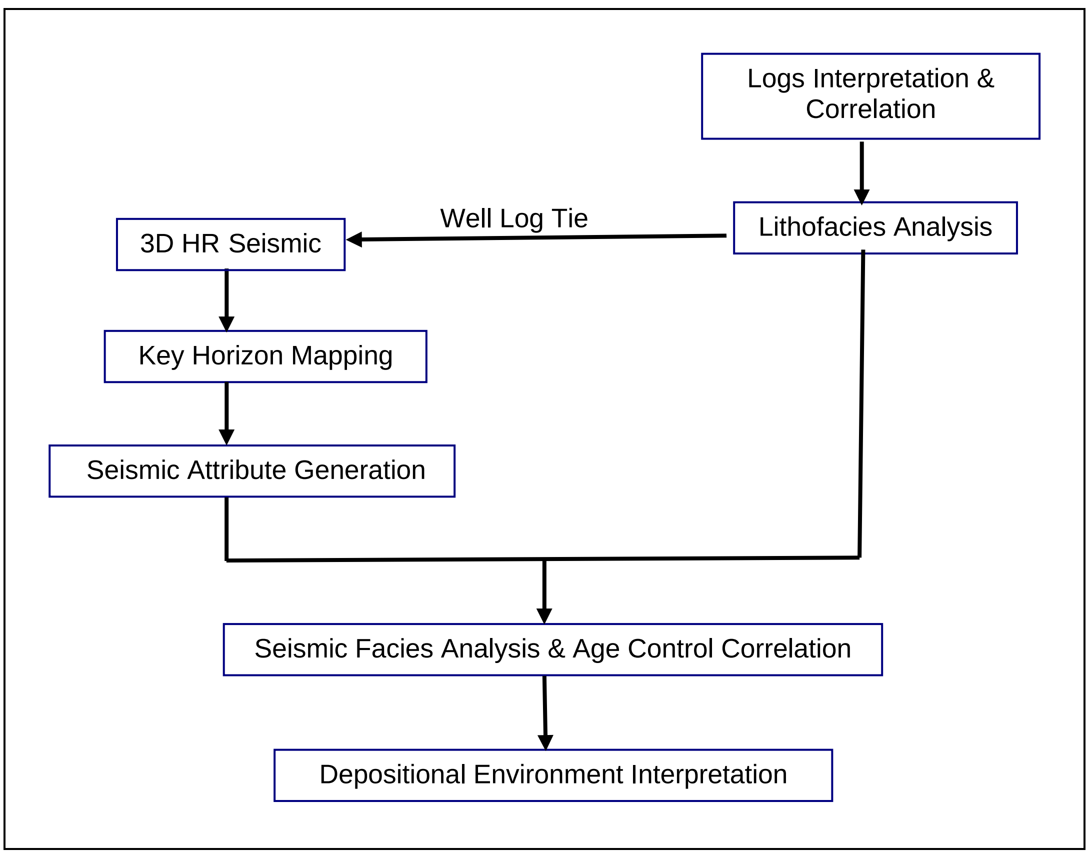

Figure 17: Flowchart of methodology

3.3 SEISMIC ATTRIBUTE ANALYSIS

Brown (1996) defined a seismic attribute as a “derivative of a basic seismic measurement”. Seismic attributes are used in imaging stratigraphic and structural details, which are otherwise less obvious on migrated time slices. In addition, the integration of these attributes with well data can provide information on reservoir properties such as porosity and fluid fill (Chopra, 2001). Seismic attributes include amplitude-derived attributes (e.g. Root Mean Square and average peak amplitude), time–based attributes (e.g. time, dip, azimuth) and waveform similarity attributes (e.g. coherence).

3.3.1 Time-based Attributes

Time-based attributes include time structure, isochron, dip, azimuth, and curvature. Isochron maps show thickness in time (ms), allowing an interpreter to infer relative changes in accommodation and sedimentation rates thereby providing an idea of the stratigraphic evolution of the basin. Dip and azimuth maps highlight the direction of dip and strike of a bed and subtle faults on mapped horizons. Areas of similar dip and/or azimuth may be structurally related. Curvature attributes measures the maximum and minimum bending of a surface at each imaged point. Consequently, “anticlinal” surfaces such as overbank deposits (levees and splays) display a positive curvature whereas “synclinal” features such as the channel axis have a negative curvature (Figure 18).

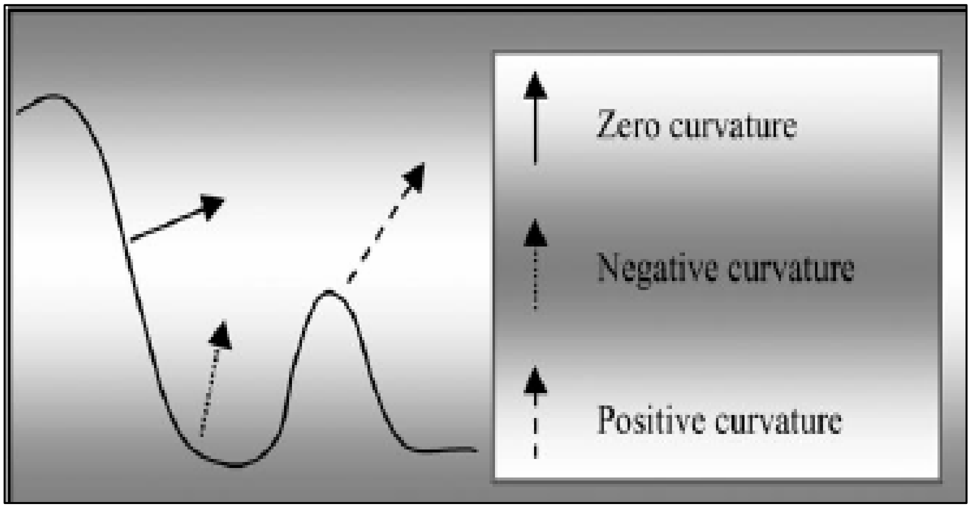

Figure 18: Positive curvature represents anticlinal features such as overbank deposits, whereas negative curvature represents synclinal features such as the channel axis (Sigismondi and Soldo, 2003)

3.3.2 Amplitude-based Attributes

Amplitude varies with lithology. High amplitude is typical of sand-rich deposits whereas low amplitude may denote a mud-rich system. Anomalous seismic amplitude (e.g. bright spots) is primarily used as hydrocarbon indicators, although they can also be associated with lithology changes (Rijks and Jauffred, 1991; Chen and Sidney, 1997). As a hydrocarbon indicator, bright spots reflect the changes in acoustic impedance such as when shale overlies gas sand. Anomalous amplitude may also be represented as dim spots, in which case the seismic event shows as weak amplitude rather than a strong one. Similarly, dim spots may be indicative of hydrocarbon or lithology changes. In both cases, the hydrocarbon or stratigraphic change reduces the acoustic impedance. Also, some other attributes such as spectral decomposition are sensitive to both amplitude and layer thickness. Window-based seismic amplitude attributes include Average Peak

Amplitude (those based on peak) and Root Mean Square (represents the root mean square averages between interpolated horizons or windows around mapped seismic events).

Inline and crossline energy gradients measure changes in reflectivity amplitude as energy crosses a discontinuity in the inline and crossline direction. This is useful in detecting features such as the boundaries between fault blocks and stratigraphic units and between hydrocarbon accumulation and diagenetic changes (Al-Dossary, 2004).

3.3.3 Waveform Similarity Attributes

Coherence measures waveform similarity or continuity (Gersztenkorn *et al*., 1999; Wood *et al*., 2000; Chopra, 2001; Rader & Medvin, 2002). Coherence volumes are used as a reconnaissance tool before commencing on a mapping project. Typically, a high coherence (similarity) is shown as lighter shades of gray whereas low coherence (similarity/continuity) is expressed as darker shades of gray. Faults, fractures, unconformities, channel edges, reefs and salt edges generally show a low coherence whereas high coherence may reflect hiatus events and periods of slow deposition (Rader and Medvin, 2002) (Figure 19). High coherence may be associated with gas accumulations though this interpretation should be validated from the seismic amplitude response.

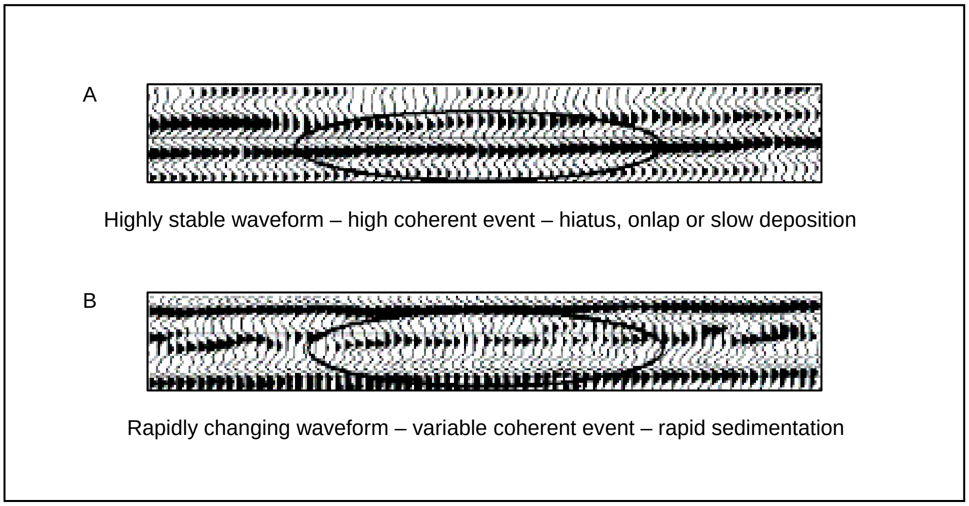

Figure 19: (A) shows a highly stable waveform corresponding to high coherence values; (B) shows a rapidly changing waveform that corresponds to varying coherence values (Rader and Medvin, 2002).

Coherence and curvature attributes are edge-detecting attributes as they aid in delineating channel margins and overbank deposits, from which stratigraphic details such as channel meander length and sinuosity can be inferred (Wescott and Boucher, 2000). However, the precise location of the channel axis and the areal extent of overbank deposits are better imaged by coherence.

3.4 SEISMIC FACIES ANALYSIS

Sangree *et al*. (1978 p. 89) defined seismic facies as the "seismic expression of a unit of sediments formed by a particular set of events and bounded by depositional surfaces". Numerous authors have developed different seismic facies classifications based on the integration of seismic data with geologic data from core, well logs, and biostratigraphy. (e.g. Sangree *et al*., 1978; McHargue & Webb, 1986; Bouma *et al*., 1987; Mitchum *et al*., 1991; Pacht *et al*., 1991; Vail & Wornardt, 1991; Liu & Watkins, 1992; Prather *et al*., 1998; Beaubouef *et al*., 2000).

For example, Prather *et al*. (1998) calibrated well data with seismic facies with which they were able to establish a link between lithology, seismic response, and depositional environment. They defined three primary seismic facies: convergent, draping, and chaotic (Figure 20). These were further subdivided into nine primary facies based on internal reflection configuration and reflectivity. Beaubouef *et al*. (2000) used high-resolution 2D seismic data, side-scan sonar images, and shallow penetration cores to identify four main seismic facies. These are: mass transport complexes (MTC), distributary channel-lobe complexes (DLC), leveed-channel complexes (LCC), and hemipelagic drape complexes (DC) (Figure 8). The authors also discussed the correlation between their seismic facies and classifications proposed by other authors such as Prather et al. (1998).

Although different seismic facies classifications have been proposed, the basis for their description has remained the same, thus their character remains very similar though appended with different names. These classifications are generally based on geometry and reflection character. Geometry describes the overall external geometry of the package, event geometry internal to bounding surfaces and bounding surface type, while reflection character describes seismic reflectivity and event continuity.

Commonly identified external geometries include gull-wing cross sectional profile characteristic of levee deposits, symmetrical or skewed "depressions" distinctive of channel-belts, and mounded chaotic forms characteristic of mass transport complex (slides, slumps, and debris flows). All these geometries are imaged on vertical seismic sections. Other geometries such as lobate forms associated with sheet sands, deltas (distributary mouth bars), and crevasse splays are best imaged on seismic attributes.

Seismic reflectivity and event continuity are important factors for inferring lithofacies assemblages and their associated depositional environments (Mutti and Normark, 1991; Prather *et al*., 1998; Broucke *et al*., 2004; Deptuck *et al*., 2003; Jennette *et al*., 2003; Posamentier, 2003; Abreu, 2003). High Amplitude Reflections (HAR) corresponds to coarse-grained lithology (sand-prone, sheet-like or pod-like deposits) whereas moderate to Low Amplitude Reflector (LAR) are primarily interpreted as fine-grained or mud-prone deposits. High Amplitude Reflections are formed in response to large impedance contrasts between lithology interfaces. Reflections may be parallel to sub parallel, continuous, or discontinuous to shingled, and they may exhibit terminations such as truncations, onlaps and downlaps against the bounding surface. Continuous, parallel to sub-parallel HAR corresponds to sheet sand, whereas discontinuous HAR showing onlapping and downlapping terminations may be interpreted as channel-fills or distributary mouth bars (Beaubouef *et al*., 2000; Deptuck *et al*., 2003). Low Amplitude Reflections result from the lack of strong internal impedance contrast between rock layers. Reflectors can be continuous, evenly spaced, or parallel to gently divergent. Such deposits are characteristic of periods of abandonment and sediment starvation or slow sedimentation. Depositional systems characteristic of LAR include hemipelagic deposits and levee deposits with downlapping reflections. Chaotic patterns exhibiting wavy, discontinuous, and nonparallel reflections are characteristic of mass transport complex systems (MTC). These include slumps, debris flows, and slides. The system sometimes demonstrates a variable internal reflection indicative of heterogeneous lithologies that may record a transition between a laminar and turbulent flow (Posamentier, 2003).

In conclusion, a proper integration of these parameters is needed in performing an accurate seismic facies analysis. This tool can be used in understanding prevalent controlling factors in a basin and in making inferences on the rate of sediment supply and accommodation.

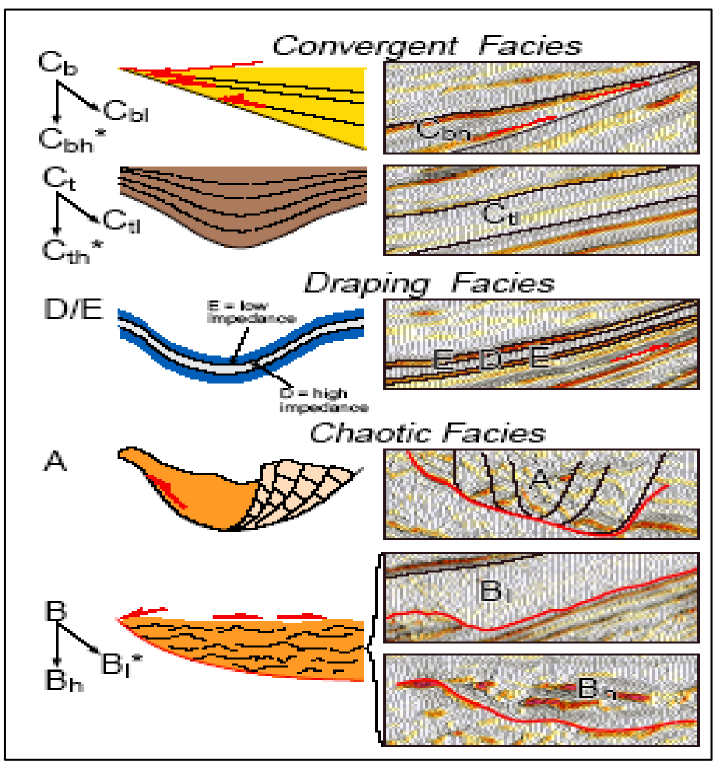

Figure 20: Idealized external and internal geometries that characterize the seismic facies (Prather *et al.*, 1998)

Chapter 4

INTERPRETATION

4.1 SEISMIC INTERPRETATION

The area of investigation is within the eastern region of the lower continental slope (Figure 21a) at a maximum depth of 2.4 seconds (~550 m) below the water bottom. Deposition of sediments within this area is strongly controlled by salt tectonics, as revealed by the ponding of turbidite systems and mass transport complexes within minibasins (Figures 21b and 21c).

I used seismic facies to define the different depositional systems based on reflection continuity, amplitude, and external geometry as imaged by seismic attributes. The seismic attributes were also useful in understanding the evolution of the systems and defining their transport direction. Depositional systems identified include a channel-lobe complex, channel-like features, and mass transport complexes (MTCs). The channel-lobe complex and channel-like features were identified at 2.2 to 2.3 seconds below the water bottom (~500m – 520 m) within the supra-salt section. The overlying sediments consisted mainly of mass transport complexes (MTCs) interbedded with parallel to sub–parallel seismic facies (Figure 21b). This pattern of deposition suggests periodic changes in sediment supply and accommodation within the basin. The MTCs correspond to periods of high sediment supply related either to early low-stands of sea level (Beaubouef *et al*., 2000) or to pore pressure fluctuations within the supra-salt section (Orange *et al*. 2003). Whereas, the parallel to sub–parallel seismic facies correspond to periods of low sediment supply in the basin associated with high-stands of sea level.

(a)

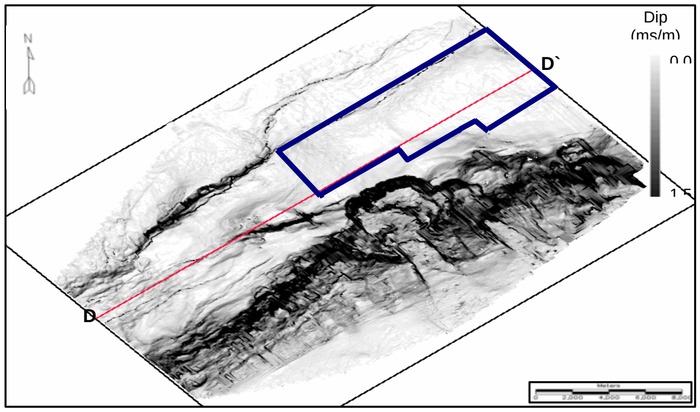

(b)

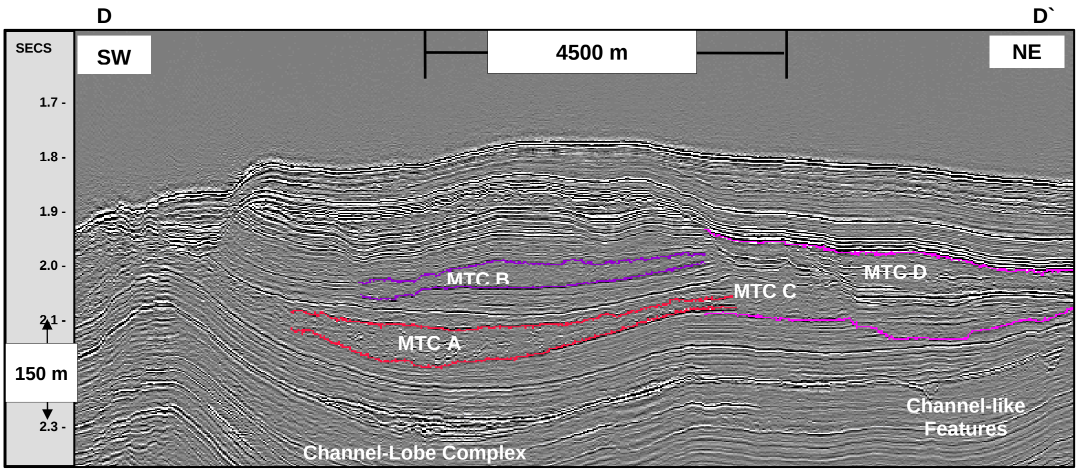

(c)

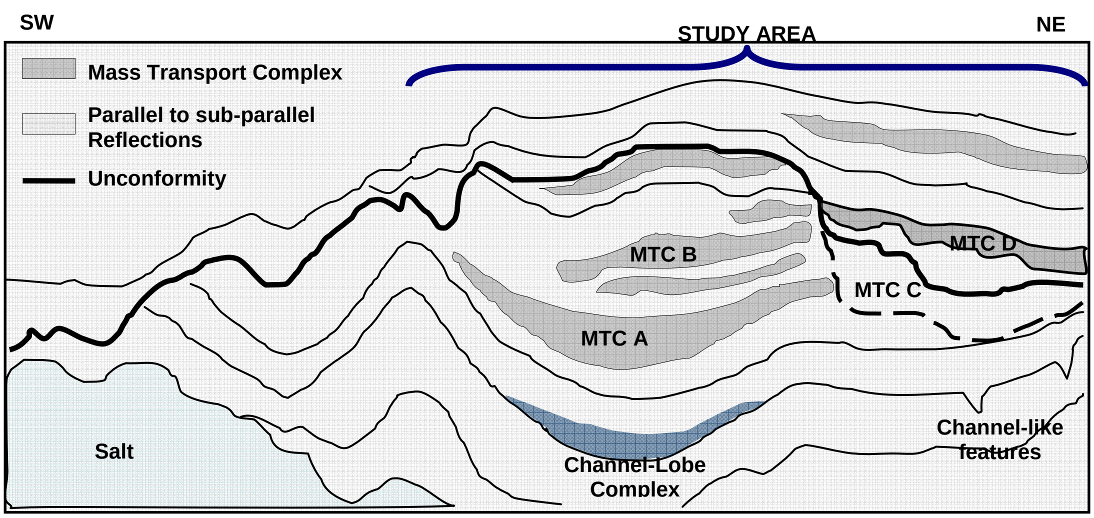

Figure 21: (a) Seafloor dip map showing the study area (blue polygon) (b) Seismic line showing mapped seismic facies. Description is based on seismic reflectivity, event continuity, and external geometry (c) Geologic interpretation of seismic line DD`. Observe the Influence of salt withdrawal on deposition and the prevalence of MTC packages above the channel-lobe complex.

Evidence of deformational activities (slumping and salt movement) within the overall area includes faults, failure scarps, linear features, blocky structures and hummocky features. The low coherent, hummocky features imaged by coherence map correspond to rapidly deposited mass transport complexes (debris flow and slumps). Whereas, I interpreted the blocky features on the upper continental rise as either undeformed blocks of sediments or outrunner blocks. The linear features are drainage features for brine water seeping through the sea floor as a result of the active slumping activity. These drainage features later become more modified and may act as conduits for turbidite flows (personal communication, Brand, J., 2005) (Figure 22).

(a)

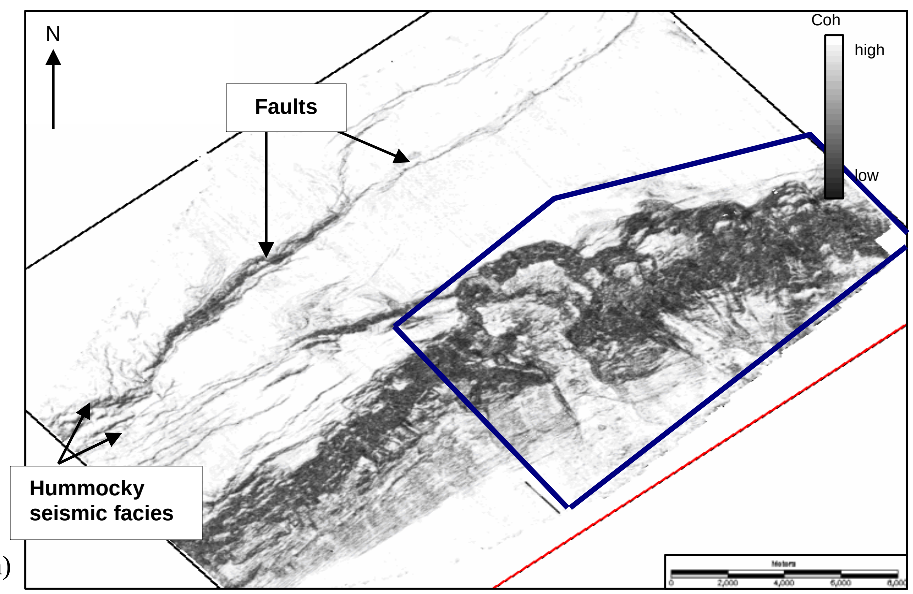

Figure 22a: Coherence extracted along the seafloor.

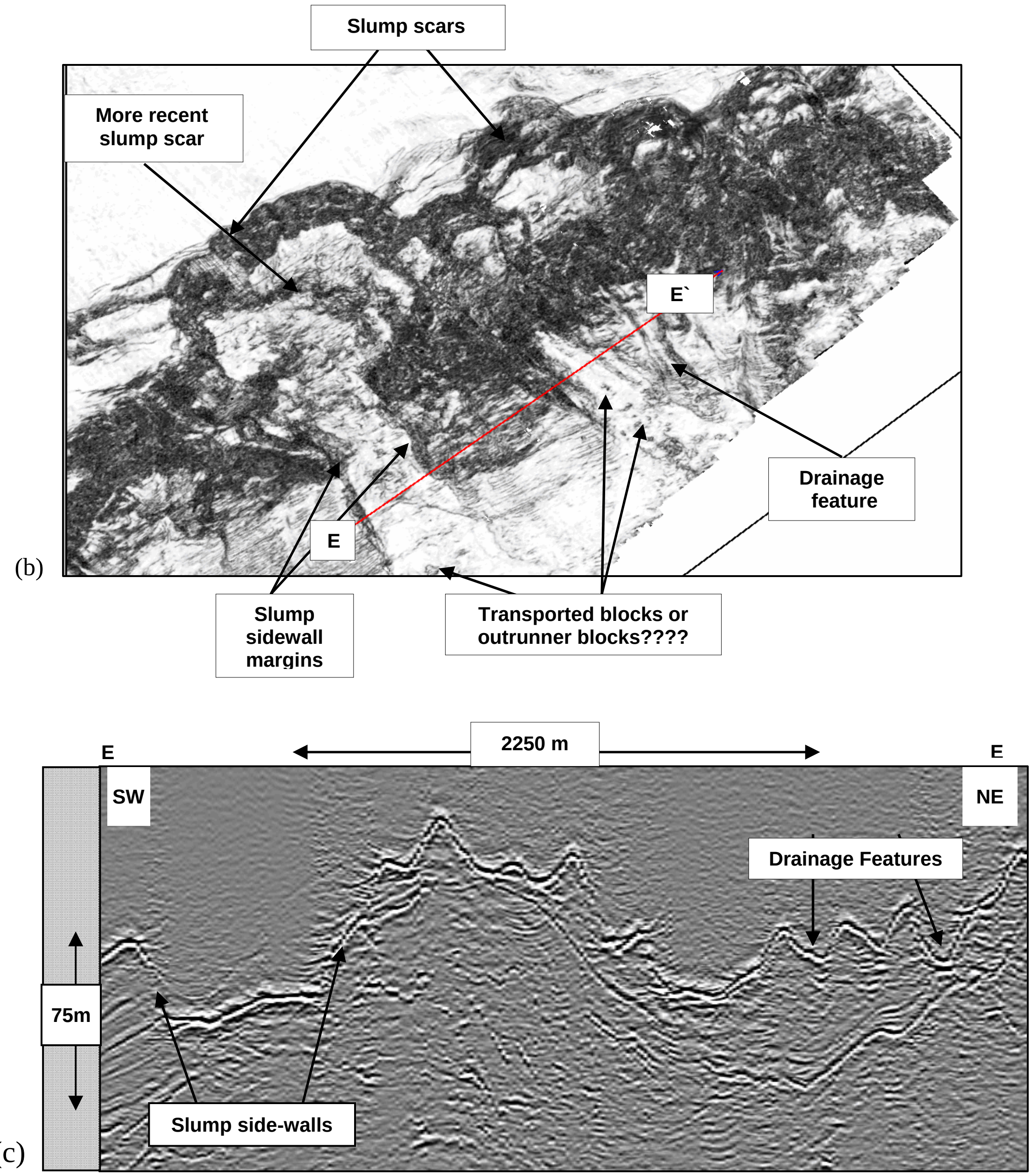

Figure 22: (b) Close-up on slumps (blue polygon) (c) Seismic profile showing the grooves on the lower continental rise.

4.2 TURBIDITE SYSTEMS

The major turbidite system identified in the study is a ponded channel-lobe complex in the middle portion of the upper continental slope (Figure 23). The channel-lobe complex was formed during different periods of deposition and subsequent erosion, as shown by reflection terminations (such as truncations and downlaps) within the complex. Some faulting is observed within the channel-lobe complex; however, there is no indication from flattened volumes that the faults influenced sedimentation. Therefore, I interpret the faults to be related to the slumping of overlying younger sediments, as the faults die out in the lobe complex.

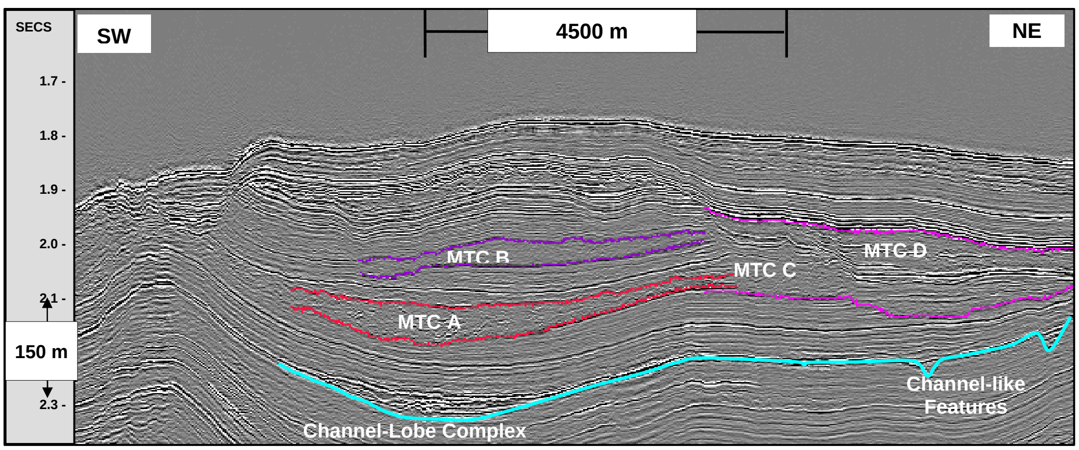

Figure 23: Seismic line showing mapped seismic facies. The channel-lobe complex represents the oldest of the depositional systems.

4.2.1 Channel-Lobe Complex

The channel-lobe complex is ponded within a mini-basin and is composed of at least four channel-lobe systems (Figure 24c). It has an approximate area extent of 3.2 km by 2.7 km, and a thickness of approximately 40m. The system is characterized by variable amplitude, shingled seismic reflections and a mounded external geometry. Its basal surface is defined by reflection terminations associated with incision into underlying strata. On map view, the system exhibits a lobate geometry indicating the influence of topography on deposition (Figure 24a).

The channel-lobe complex is composed of at least 4 channel-lobe systems with a younger channel-like feature capping the package (Figure 24b). Detailed analysis of these sub-units reveals different transport directions probably due to the interaction of sediment supply and lateral changes in gradient. The channel-lobe complex is subsequently overlain by low amplitude reflections interpreted as pelagic deposits. The pelagic drape suggests a period of slow sedimentation, which probably corresponds to a period of sediment influx decrease in the basin.

(a)

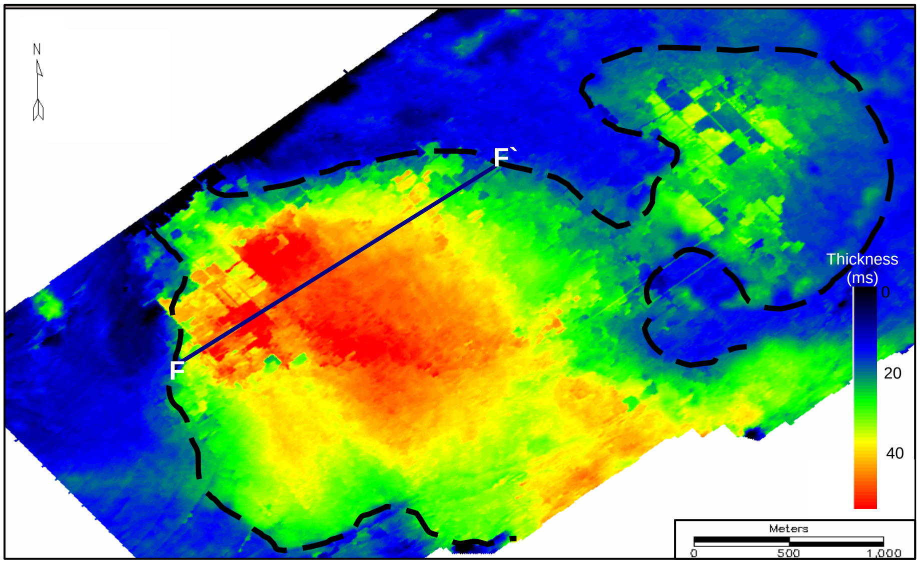

Figure 24a: Time thickness map of the channel-lobe complex.
The lobate geometry reflects the influence of topography on deposition.

(b)

(c)

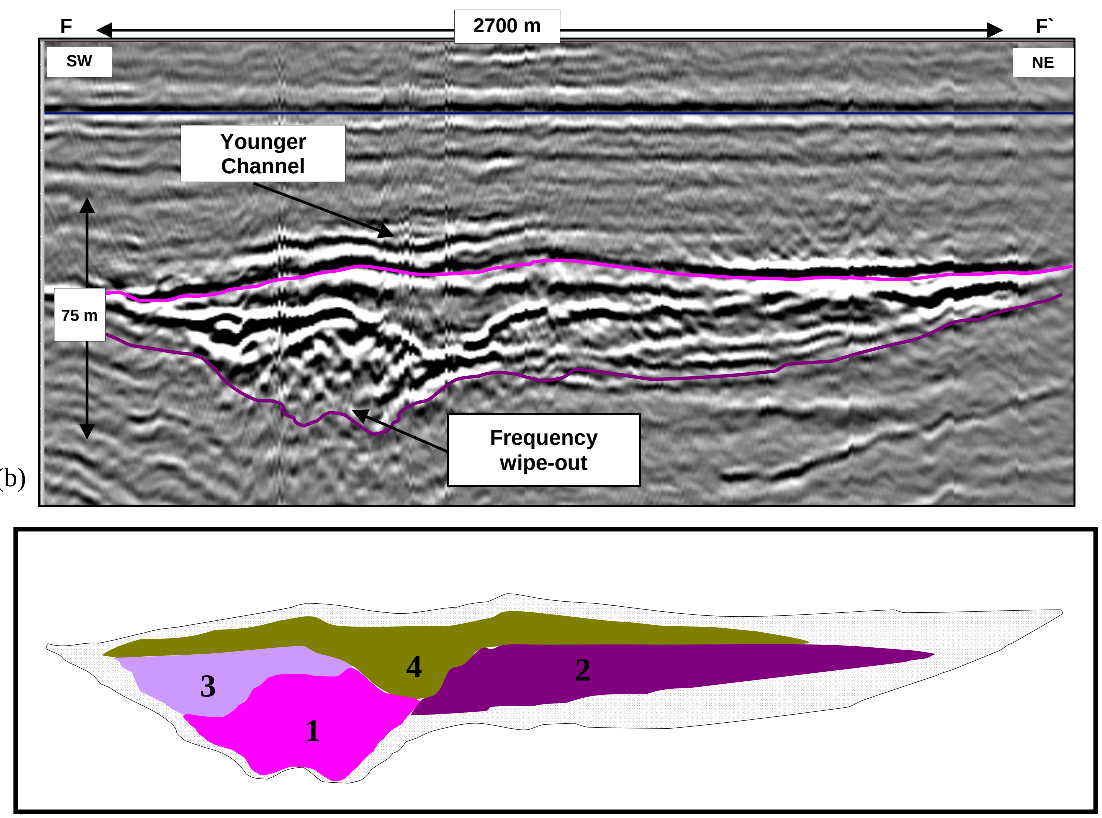

Figure 24: (b) Seismic line FF` showing channel-lobe complex characterized by variable amplitude. The channel-lobe complex is capped by a younger channel (c) Cross-sectional profile of the channel-lobe complex reveal that the system is composed of at least 4 channel-lobe systems.

4.2.2 Channel-Lobe Complex Evolution

In discussing the developmental history of the channel-lobe complex, I divided the system into a basal portion, comprised of channel-lobes 1- 3, and an upper portion comprised of channel-lobe 4 (Figure 24c). The RMS amplitude image of the basal deposits (1-3) shows a “confined” channelized flow grading down-slope into an “unconfined” ponded lobe (Figure 25). The change from a confined to an unconfined geometry correlates with seismic facies changes from shingled reflections (seismic facies 1- characteristic of a confined geometry), to parallel reflections (seismic facies 2- characteristic of an unconfined geometry) (Figure 26). The down-slope progression of seismic facies from confined to unconfined probably indicates the influence of changes in depositional gradient on deposition. Frequency wipe-outs beneath the basal deposits (Figure 24b) and anomalous amplitude on the RMS map suggest that the sediments may be gas-charged.

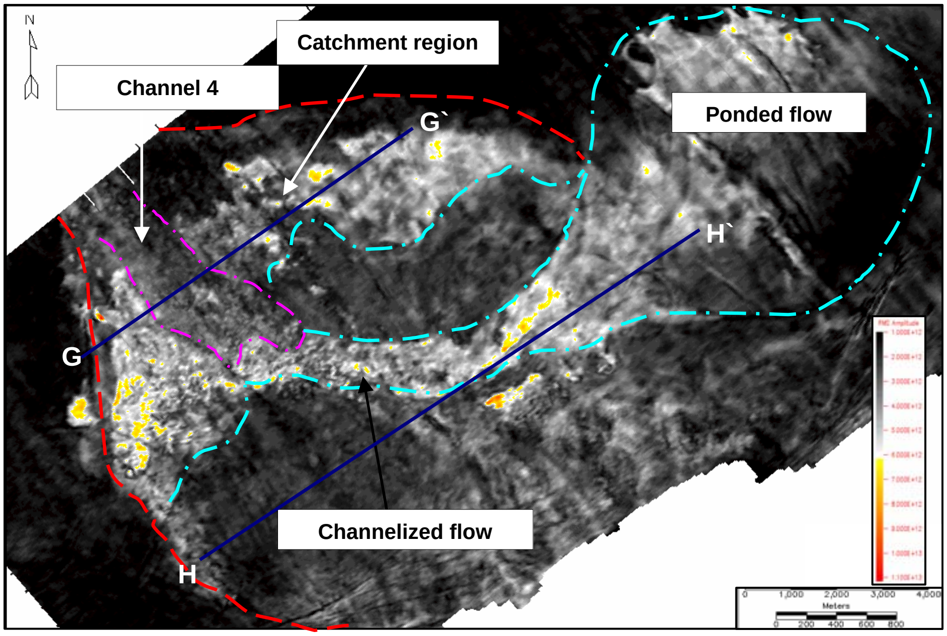

Figure 25: RMS amplitude extracted between the top and base of channel-lobe complex (1-4) shows a confined flow translating into a ponded flow.

(a)

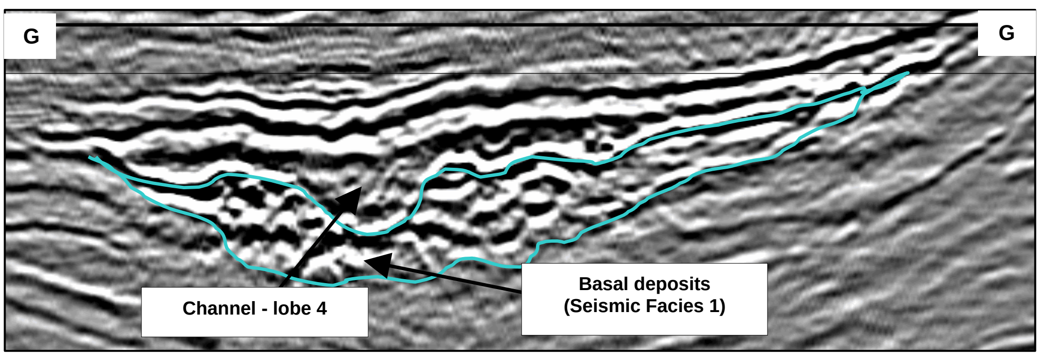

(b)

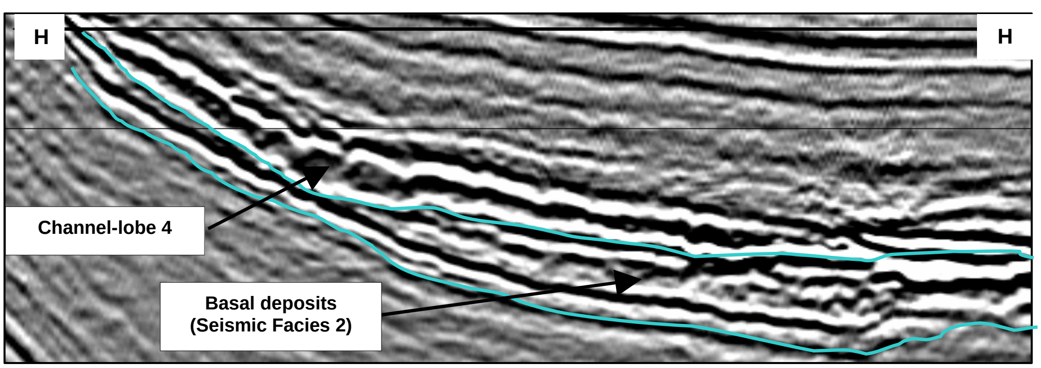

Figure 26: (a) Seismic line GG` in the up dip region of the basal deposits is dominated by shingled reflections (seismic facies 1) (b) Seismic line HH` in the down-dip region is characterized by parallel reflections (seismic facies 2) indicative of unconfined flow.

The most recent of the channel-lobe systems is channel-lobe 4. It has a maximum thickness of 22 m and maximum length of 2.5 km. An isochron map generated between the top and base of the unit shows that channel-lobe 4 is comprised of a main lobe unit with two other distributaries forming smaller lobes (Figure 27).

(a)

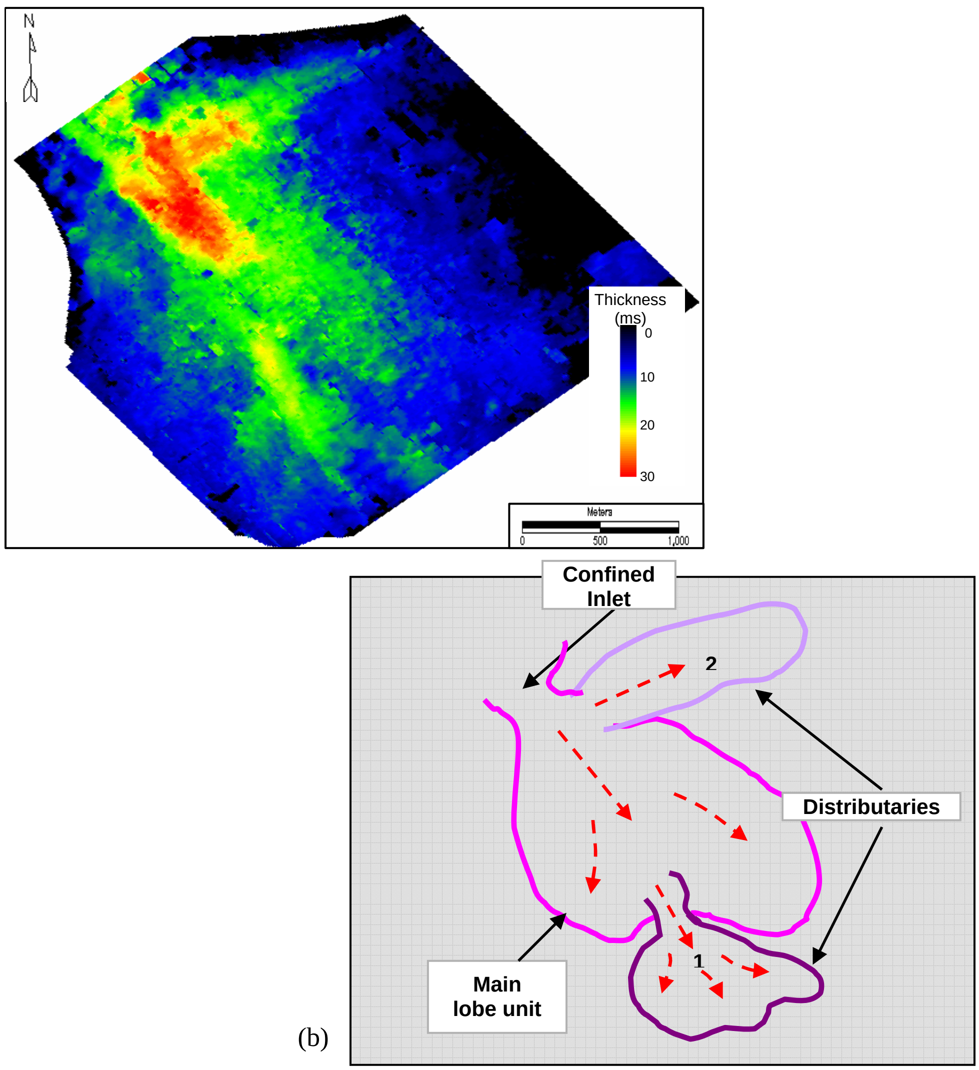

(b)

Figure 27: (a) Time thickness map of channel-lobe 4 (b) Diagram showing the main channel-lobe unit and its distributaries forming smaller lobes.

The up-dip portion of the flow inlet is characterized by a relatively confined scour that deepened in the middle portion. My interpretation is that scouring of the channel was caused by sand-rich facies; the spilling of the sediments in the middle region, as they are transported downslope is imaged on seismic by the levee deposits (Figure 28c). Alternatively, the deepened scour may have resulted from repeated erosional events rather than a single flow event. Further down-dip, erosion decreases as the flow became more unconfined, as characterized by sheet-like reflection on seismic (Figure 28d).

(a)

(b)

(c)

(d)

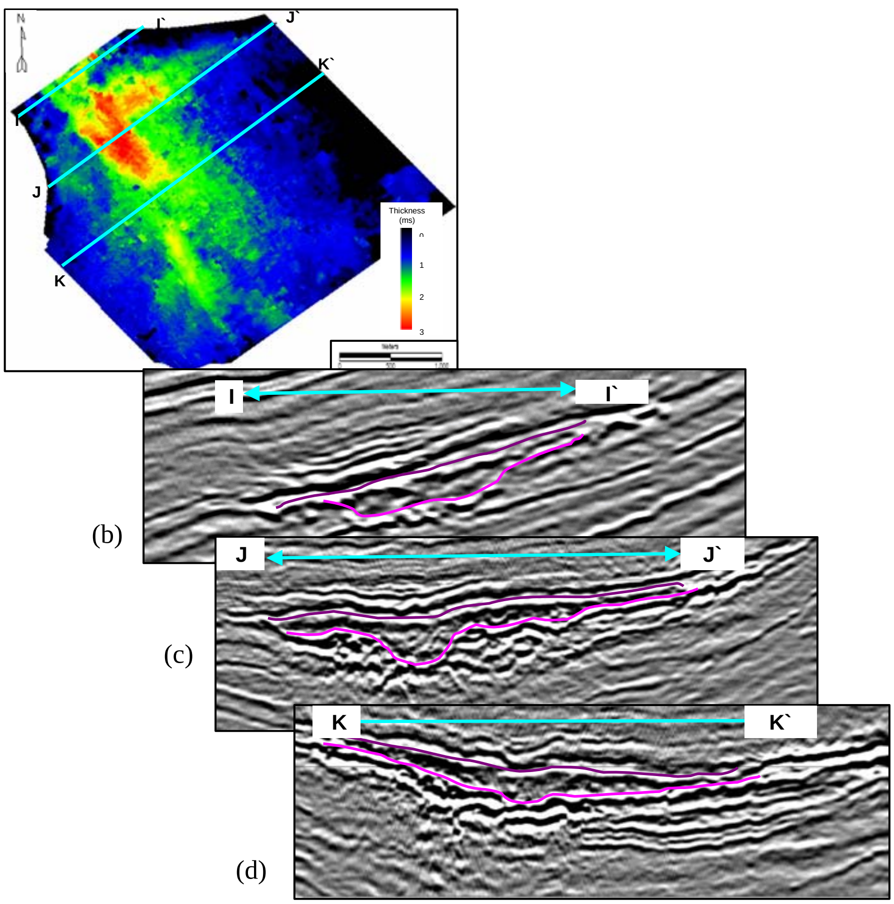

Figure 28: Cross-sectional seismic profiles of the channel-lobe 4 from the up-dip to down-dip regions (a) Time thickness map (b) The up dip portion is characterized by a confined channel (c) The mid-portion is characterized by a deepened scour and overbank deposition "channel-levee" system (d) The down-dip is characterized by an unconfined flow geometry which forms the main lobe.

In summary, I propose that as the flow traveled down-slope, it deposited coarse-grained sediments along its path in the up dip region as probably evidenced by increased scouring and relatively confined channel. Meanwhile, the fine-grained sediments travel further basinward in a plume and later spread out downslope, forming the unconfined geometry characteristic of lobe deposits. The progression from (coarse-grained) confined to (fine-grained) unconfined geometry is attributed to depositional gradient changes.

The system's evolution is further analyzed on amplitude horizon slice below the blue horizon (Figure 29). The channel is shown to terminate abruptly and then reinitiated into another lobe unit down-dip at 76 ms below the blue horizon. My interpretation is that the main channel-lobe unit got obstructed along its path by erosional remnants of basal deposits (1-3). Channel-lobe 4 probably was not able to erode the underlying sediments due to its waning erosive power. However, a distributary (bypass channel) from the main flow continued deposition further downdip. Though on a smaller scale, the bypass lobe also exhibited characteristics similar to the main lobe unit; scouring increased with increase in erosion in the middle portion, while the erosion became less intense down-dip (Figure 28a).

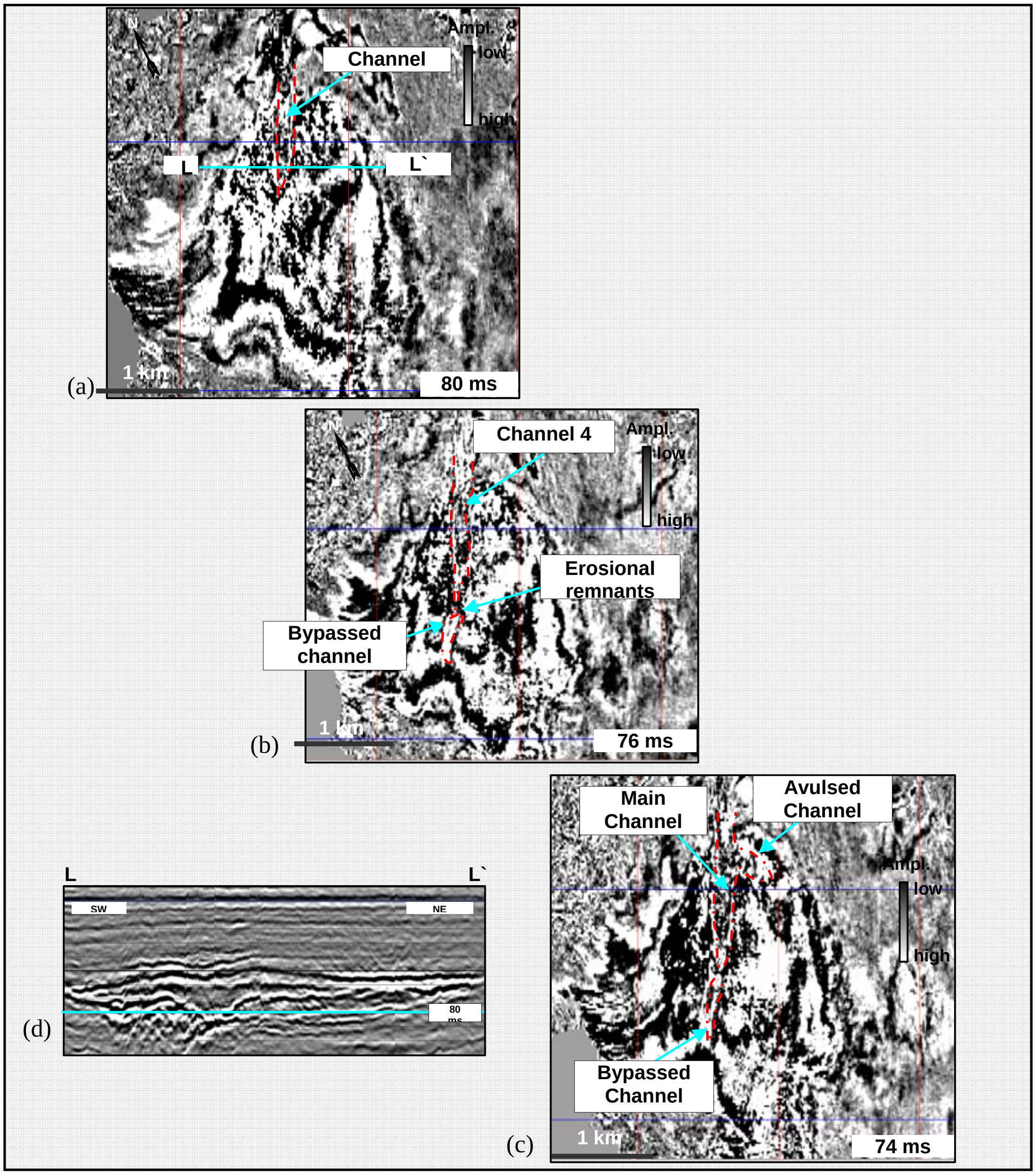

Figure 29: (a-c) Horizon amplitude slices below the blue horizon. On horizon slice 76ms 29(b) observe the abrupt termination of the main channel and the initiation of the bypassed channel down-dip (d) Seismic line showing channel-lobe 4.

Hoyal *et al*. (2003) and Wagoner *et al*. (2003) described features using a Turbulent Jet or Jet Plume Pair Model that was similar to those features discussed above. The model describes the behavior of sediment flows as it expands and decelerates from a point source under constant conditions. Hoyal *et al*., (2003) suggested that the erosional scour observed at the inlet was caused by the strong turbulence of sediments flowing from the single orifice. As such, bedload sediments were deposited close to the orifice, whereas suspended load were transported downstream in a plume and deposited in the down dip region (Figure 30).

Van Wagoner *et al*., (2003) further explained that the jet flows normally branch out following through optimal pathways in an attempt to dissipate energy. Preferred pathways are usually areas of lower resistance adjacent to the main flow. Continuous jetting of sediments promotes more channel avulsions, which eventually evolve the system into a tree-like sedimentary body. They suggested that this mechanism played a major role in the development of deposits such as deepwater fans, delta mouths and river bars that demonstrate similar dendritic patterns. In addition, they observed that long flow durations might trigger the formation of smaller jets (flows) at the margins of the deposits (Figure 31).

Vitor *et al*. (2004) applied the results from this experiment in describing the upper fan deposit of an intra-slope basin in western Gulf of Mexico. Their interpretation was that the upper fan was fed by jet flows; the up-dip portion of the fan was characterized by a confined channelized scour which deepened its scouring in the middle portion and finally became weakly erosional down dip. However, the tree-like structure observed in the experiment was not seen in their study. They described the architecture of this upper fan as a Scour-base Lobe.

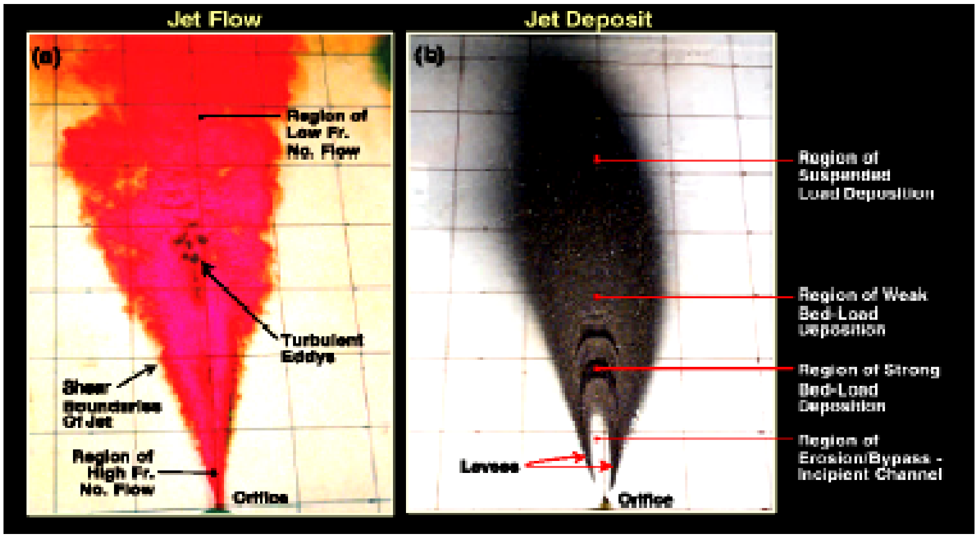

Figure 30: Jet Plume pair flow and deposit. The scoured channel inlet is attributed to the turbulence sediment inflow (Hoyal *et al*.,2003).

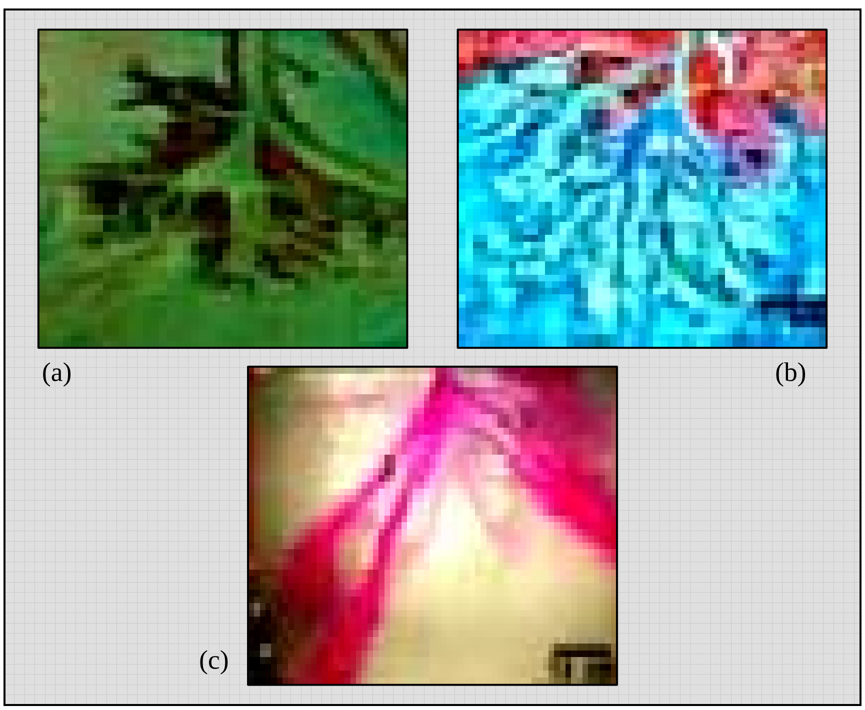

Figure 31: Shapes of sedimentary bodies formed in fluvial, and deltaic environments. (a) Mississippi Delta Complex (b) Wax Lake bay-head delta, LA. (c) ExxonMobil Upstream Research Company (URC) Jet model tank experiment. The sedimentary bodies display tree-like structures (*Van Wagoner et al*., 2003).

Similarities between results from the jet model and channel-lobe 4 suggest the experiment may provide an analogue in describing the behavior of the system under study (Figure 32). I propose that the development of the bypassed lobe beyond the terminus of the main flow reflects the system's attempt to dissipate energy, having been obstructed in its path by the basal deposits (lobes 1-3). Furthermore, the process of dispersing flow energy is expressed in the presence of smaller channels (jets) formed at the fringe of the bypassed lobe and a second distributary (avulsed lobe) formed adjacent to the main lobe.

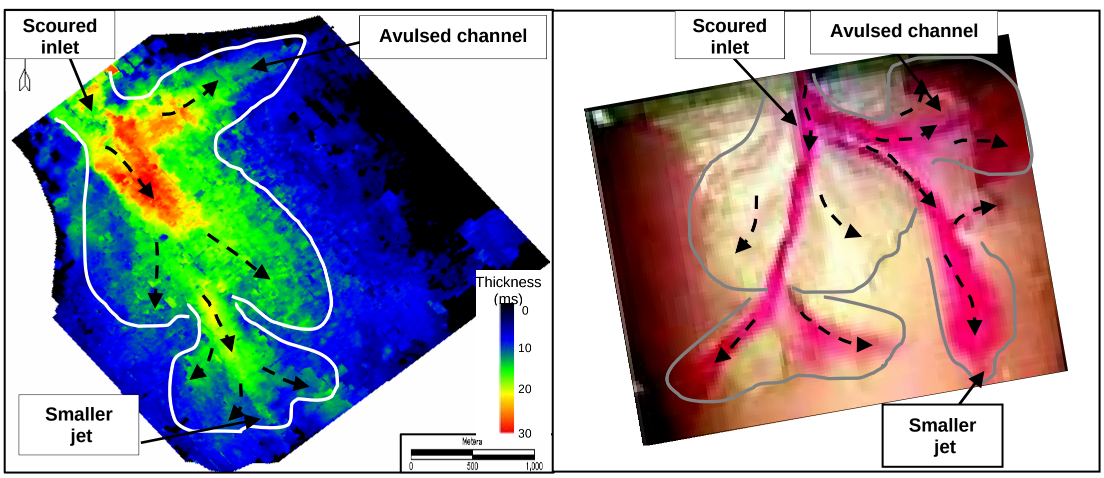

(a) (b)

Figure 32: Comparison between channel-lobe unit 4 and the Jet Plume pair flow (a) Time thickness for channel-lobe 4 (b) ExxonMobil Upstream Research Company (URC) Jet model tank experiment (Van Wagoner *et al*., 2003).

The inception of the avulsed lobe was identified on amplitude horizon slice 74 ms below the blue horizon (Figure 29c). The new transport direction created adjacent to the main flow unit represents the most optimal pathway available to dissipate flow energy (Figure 33). Similar to the other units, the isochron map shows, a flow inlet that deepens in the middle region and then becomes less erosive in the down-dip portion.

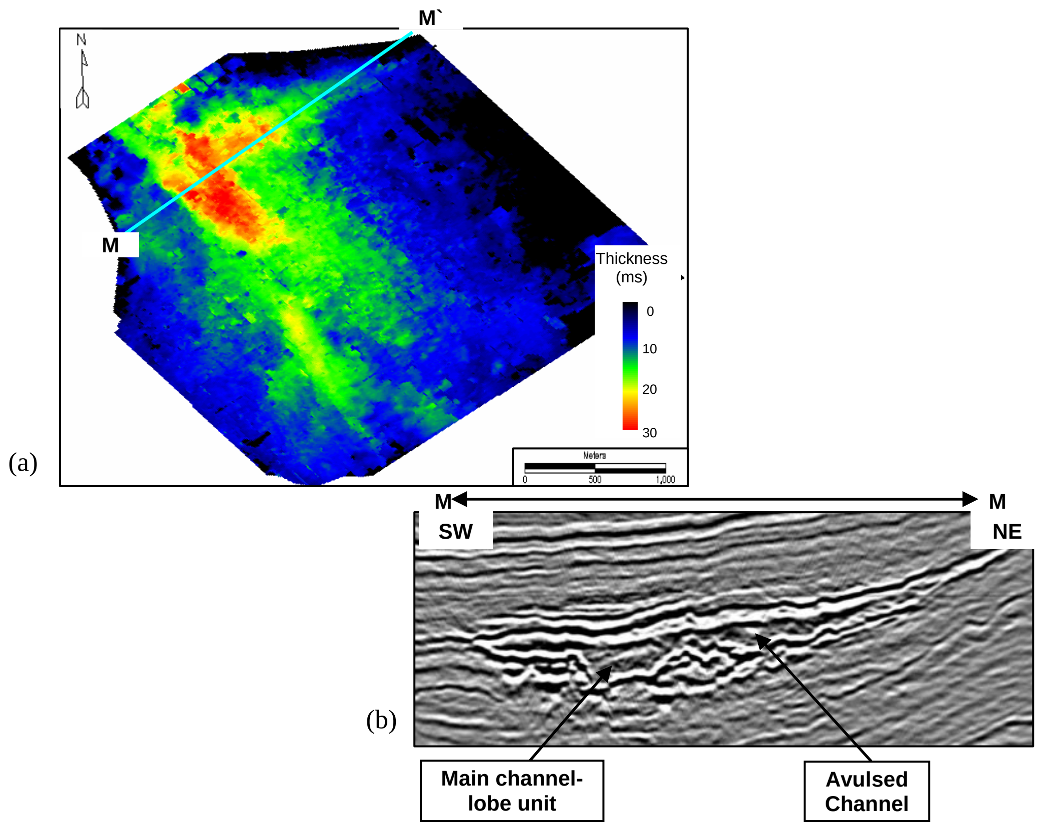

Figure 33: (a) Time thickness map of channel-lobe 4 (b) Seismic profile showing the main channel-lobe and its distributary.

In summary, the overall geometry of the most recent channel-lobe deposit (i.e. channel-lobe 4 and its distributaries) suggests prolonged flow duration, probably attributed to constant sediment supply into the mini basin. The unit is characterized by a main sediment flow inlet and "secondary" bypassed and avulsed sub-inlets. The up-dip regions of these systems are characterized by confined scouring that deepens in the mid-section with bedload deposition probably occurring around the inlet. While, the down-dip portions are characterized by less erosional bases, unconfined flows, and probably fine-grained sedimentation.

4.3 CHANNEL-LIKE FEATURES

Three distinct channel-like features were identified to the northeast of and at approximately the same seismic horizon as the previously described channel-lobe complex. On seismic, these features (channels A, B, and C) were defined by v-shaped, linear depressions, suggesting either turbidite or debris flow/glide block origin (Figure 34). The channels' linear to curvi-linear geometry as shown by edge-detecting attributes (coherence and curvature) (Figure 35) suggests a glide block or debris flow origin; however, the channels' fill (channel C) and associated overbank facies (channel B) are more typical of a turbidite origin. The linear geometry could be a reflection of the effect of prevailing depositional gradient on turbidity current. Alternatively, the channels may have been formed by glide block or debris flow action, later modified by turbidite flow.

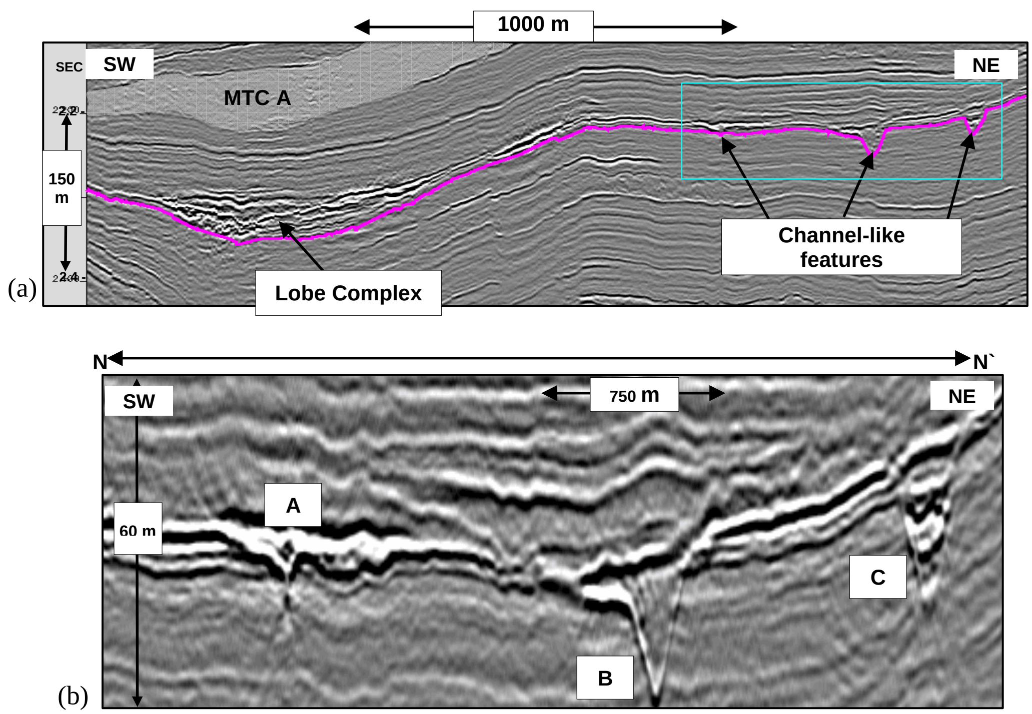

Figure 34: (a) Seismic profile showing the channel-lobe complex in relation to the channel-like features (b) A close-up on the channel-like features.

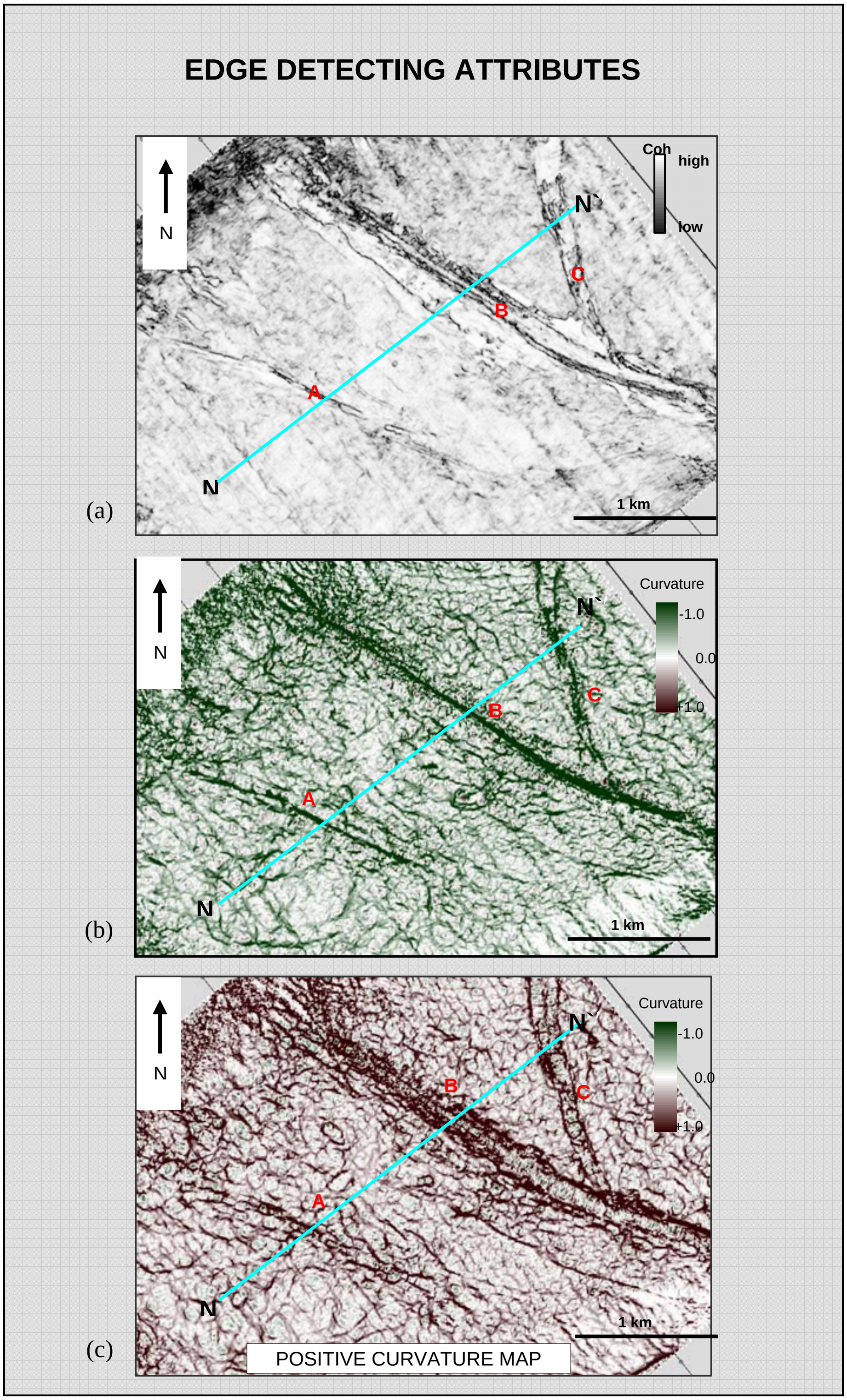

Figure 35: Edge detecting seismic attributes generated on the base of the linear features
(a) Coherence imaging changes in waveform (b) Negative Curvature delineating the channel axis
(c) Positive Curvature delineating the flank deposits. Observe the linear geometry of the channels.

4.3.1 Channel-like Feature A

Channel A is characterized by a small depression cutting into underlying strata. It has an area extent of approximately 3 km by 200m with 8m thickness. Channel A shows a curvilinear geometry in map view, and is flanked by high amplitude deposits interpreted as sand-prone sediments (levees?). Channel A can be interpreted as a channel-levee system based on the consistency of the sand-prone unit flanking the channel margin (Figure 36); however, the straightness of the channel on map-view suggests it might be a glide track, rather than a turbidite channel.

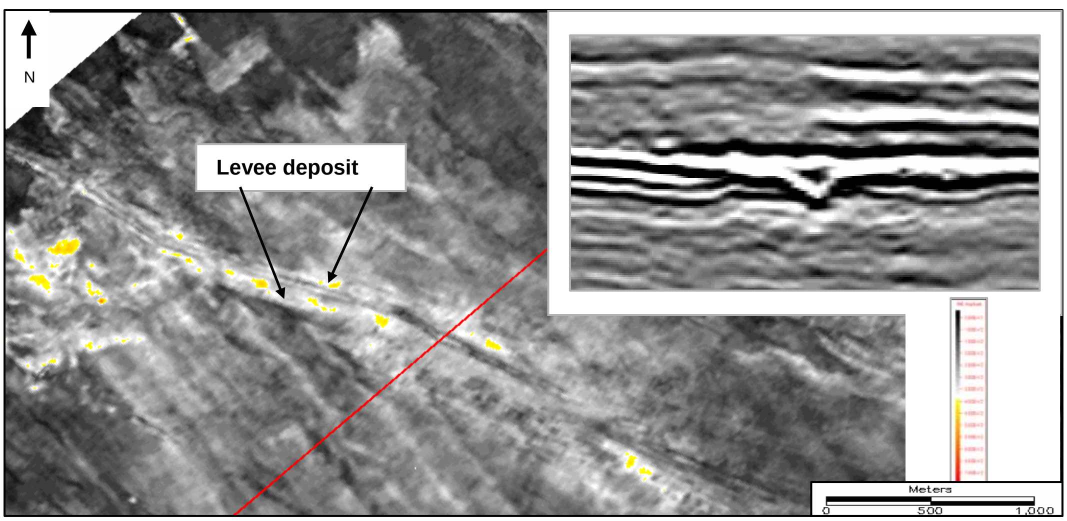

Figure 36: RMS amplitude showing flank deposits running parallel to the channel margins.

4.3.2 Channel-like Features B and C

On seismic sections, features B and C are characterized by unusual V-shaped depressions (Figure 34b). Channel B has an area extent of approximately 5 km by 450m with 25m thickness, whereas channel C has an area extent of approximately 2.3 km by 400m with 20m thickness. On map view they are characterized by straight to curvilinear geometry (Figure 35)

On seismic profile and map views, Channel B is characterized by a “localized” High Amplitude Reflection (HAR) on the left flank of the channel margin (Figure 37). The restriction of the HAR to the left side of the channel margin could be due to earlier structural deformational events that changed the depositional gradient prior to erosion of the marginal sediments. Channel B’s lack of sinuosity suggests it might have originally been a glide plane; however, I propose that it was subsequently modified by turbidite flow. My interpretation is based on the presence of the HAR at the left flank of the channel and also the presence of a younger channel within the channel axis (Figure 37c). The stacking nature of the 2 channels shows an aggradational pattern that indicates that the system was deposited under conditions of equal accommodation and sedimentation.

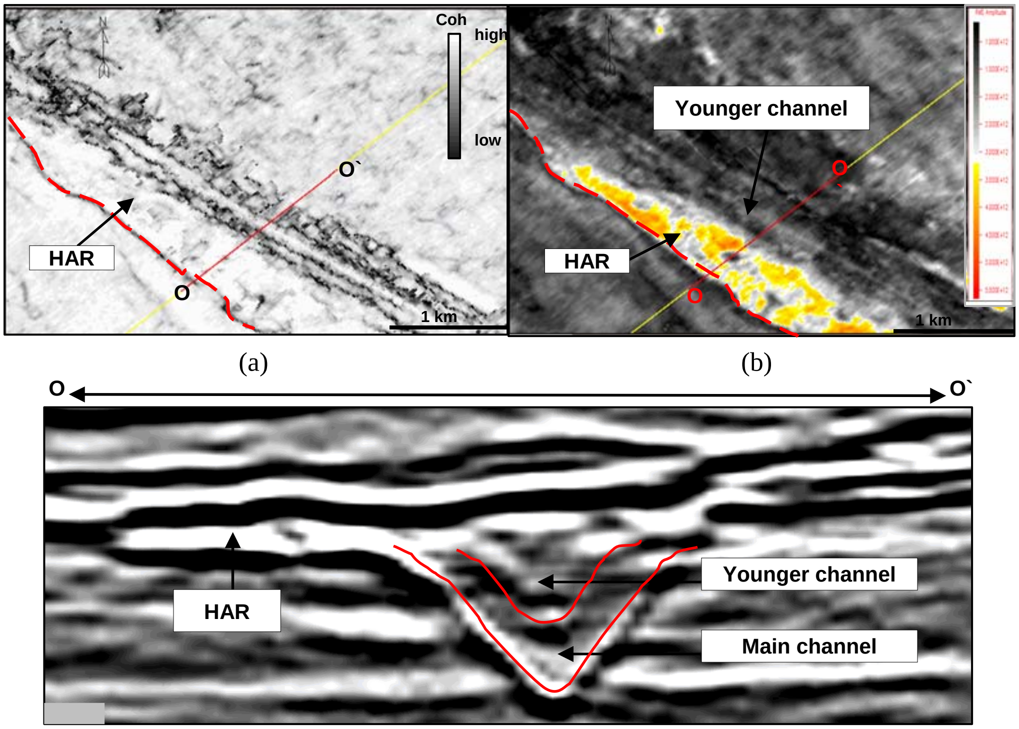

Figure 37: (a) Coherence map showing the HAR deposit on the left flank of the channel
(b)RMS amplitude extraction showing a younger channel within channel B
(c) Seismic profile showing an aggradational stacking pattern.

Channel C on seismic is characterized by a high amplitude channel fill (Figure 38b). A close observation of the negative curvature map shows that the channel is formed by 2 other channels that merged in their paths (Figure 38a). Although channel C seem to merge with channel B, it looks more obvious from the negative curvature map that channel B only truncated channel C along its path while it continued downdip (Figure 38a). This interpretation suggests that channel C must have stopped abruptly, a behavior more characteristic of a glide plane with an outrunner block at its terminus. Although this is a possible interpretation, it still stands questionable because of the character of its channel fill. A glide plane fill would probably be more chaotic than layered in nature as seen on the vertical seismic section (Figure 38b). On the other hand, it is possible that the glide plane channel subsequently funneled turbidity currents, leaving behind the layered HAR.

(a)

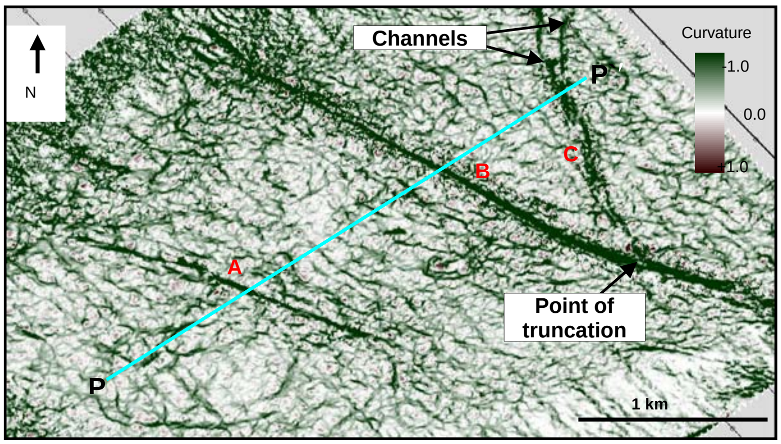

(b)

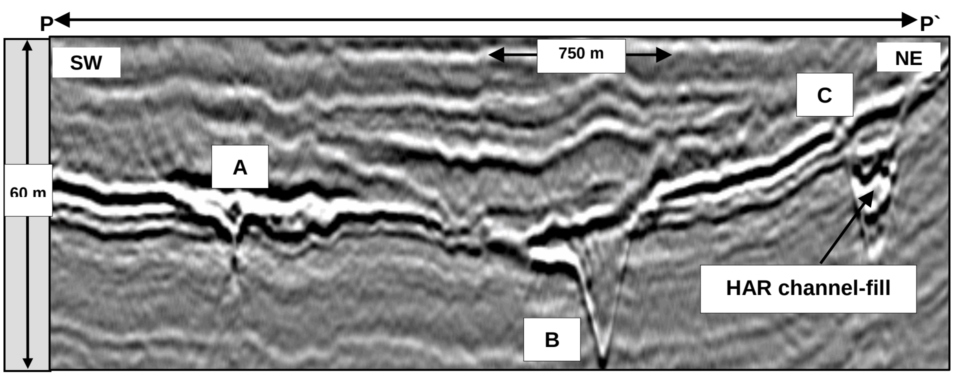

Figure 38: (a) Negative curvature reveals that channel C is made up of 2 channels that merged into a single flow. Channel C was subsequently truncated by channel B (b) Seismic section showing channel C filled with layered HAR seismic facies.

4.4 MASS TRANSPORT COMPLEXES (MTC)

Numerous mass transport complexes are present in the study area; however, I have only described four in detail: MTC A, MTC B, MTC C, and MTC D (refer to Figure 23). These deposits are characterized on seismic by chaotic reflections, failure scars, scoured bases (basal shear surfaces), mounded external geometry, and in some cases erosional remnants. I also identified associated depositional features such as glide tracks and out-runner blocks. The glide tracks record the path traveled by debris blocks that were detached from the main flow, whereas the out-runner blocks are detached blocks at the end of the glide tracks.

Detailed study of MTC A and B reveal that each of the units is made up of two distinct flow events based on subtle differences in their basal shear surfaces and internal fabric. On the other hand, MTC C and MTC D are products of very complex failure activities which may have been more episodic in nature. MTCs A, B, and D exhibit southeast transport directions, the absence of headscarps within the area I interpreted suggest their presence further updip.

4.4.1 MTC A

MTC A is the oldest of the mass transport packages that I studied. It is approximately 3km by 6km in area extent, with a maximum thickness of 56m. The deposit is characterized by variable amplitude chaotic reflections, a mounded external geometry, and scoured base. The high amplitude of the basal shear surface corresponds to changes in acoustic impedance, which most likely corresponds to changes in lithology.

A close examination of the unit suggests the deposit was formed by 2 different events. The first event is represented by less deformed, ductile (folded) reflections, whereas the second event is characterized by a more chaotic, low amplitude reflection (Figure 39).

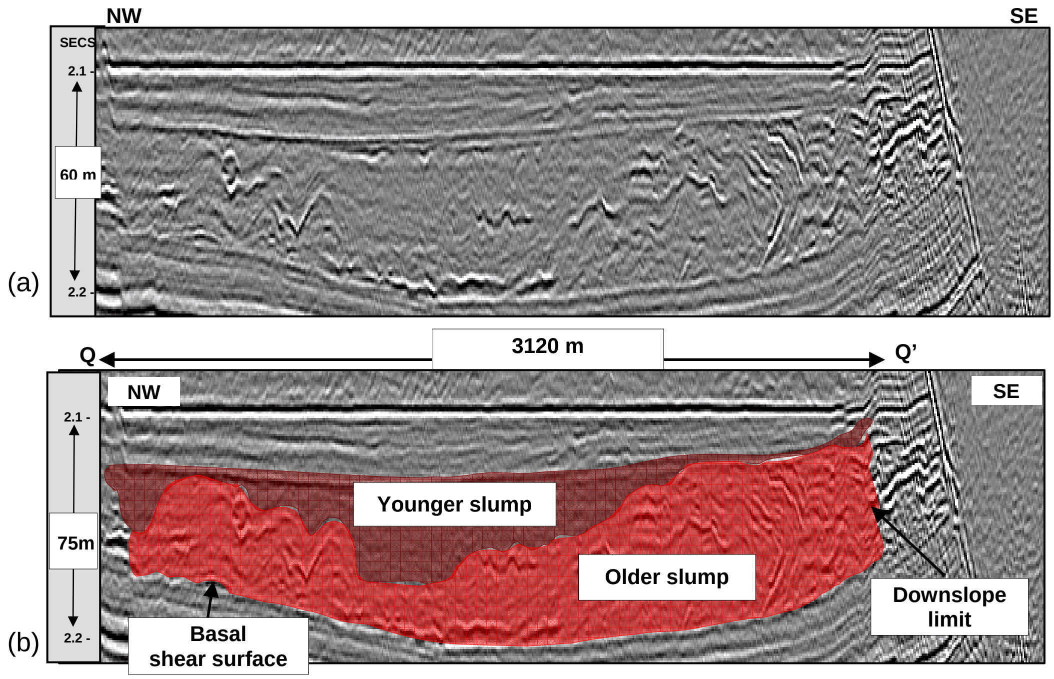

Figure 39: (a) Uninterpreted (b) Interpreted seismic data along QQ` showing MTC A. Observe the differences in internal fabric demarcated an erosional base.
See Figure 41a for location.

The apparent ductile nature of the first slump event suggests it resulted from a low-magnitude failure activity, which allowed only a short travel distance. Thus explaining its less chaotic internal fabric. In contrast the more chaotic nature of the second event is presumed to have resulted from a longer travel distance that promoted a more intense reworking of the sediments. The high amplitude reflections (HAR) within the older MTC appear as bright shades (high coherence) on coherence horizon slice at 70 ms below the green horizon. In contrast, the dark shades (low coherence) on the slice correspond to the chaotic reflections that are indicative of rapidly deposited sediments (Figure 40). Both isochron and coherence horizon slices show evidence of a southeast transport direction; however, the headscarp was not identified within the area interpreted suggesting its presence further updip. MTC A is characterized by a lobate geometry that indicates topographic influence on deposition (Figure 41a). The change from a confined inlet to an unconfined (ponded) flow may also indicate the influence of changes in depositional gradient on the flow.

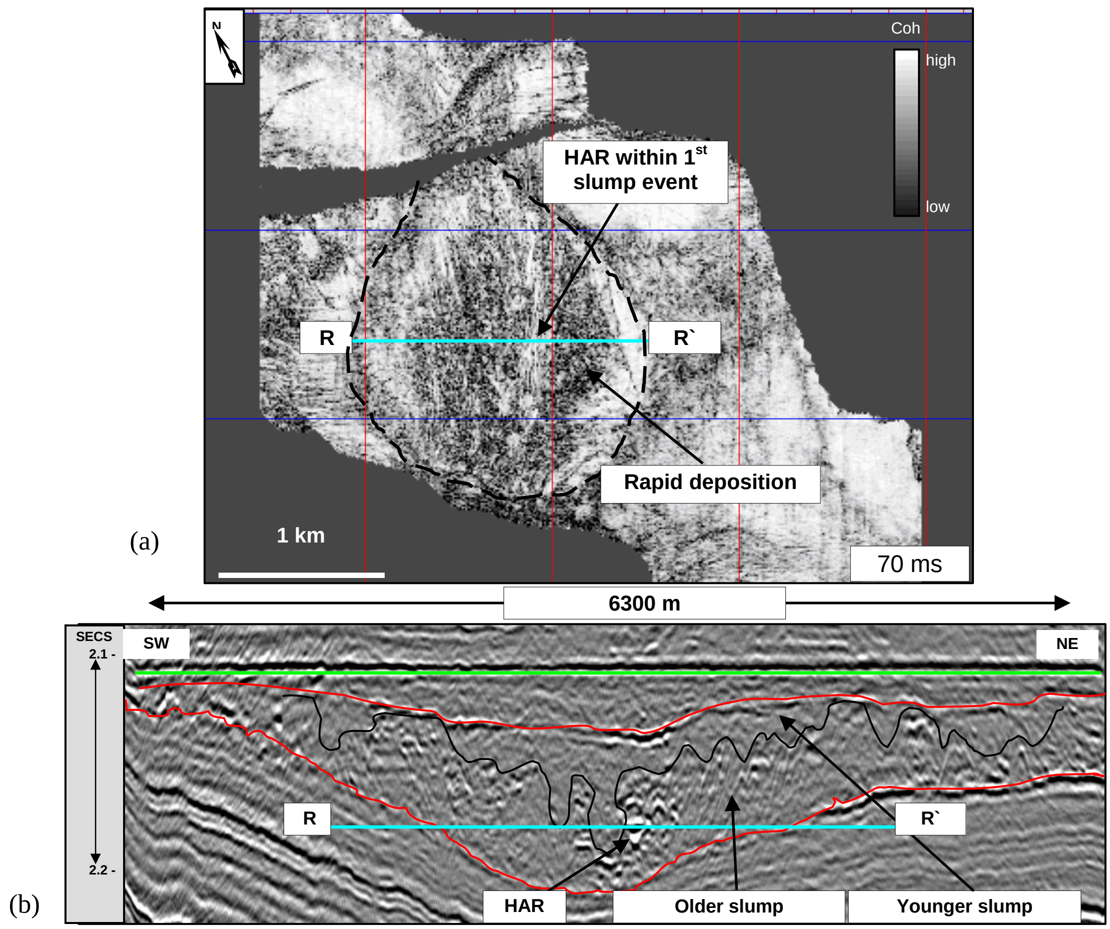

Figure 40: (a) Coherence horizon slice at 70ms below the green horizon imaged high coherent features (HAR) within the slump (b) Seismic line showing the HAR within the older slump.

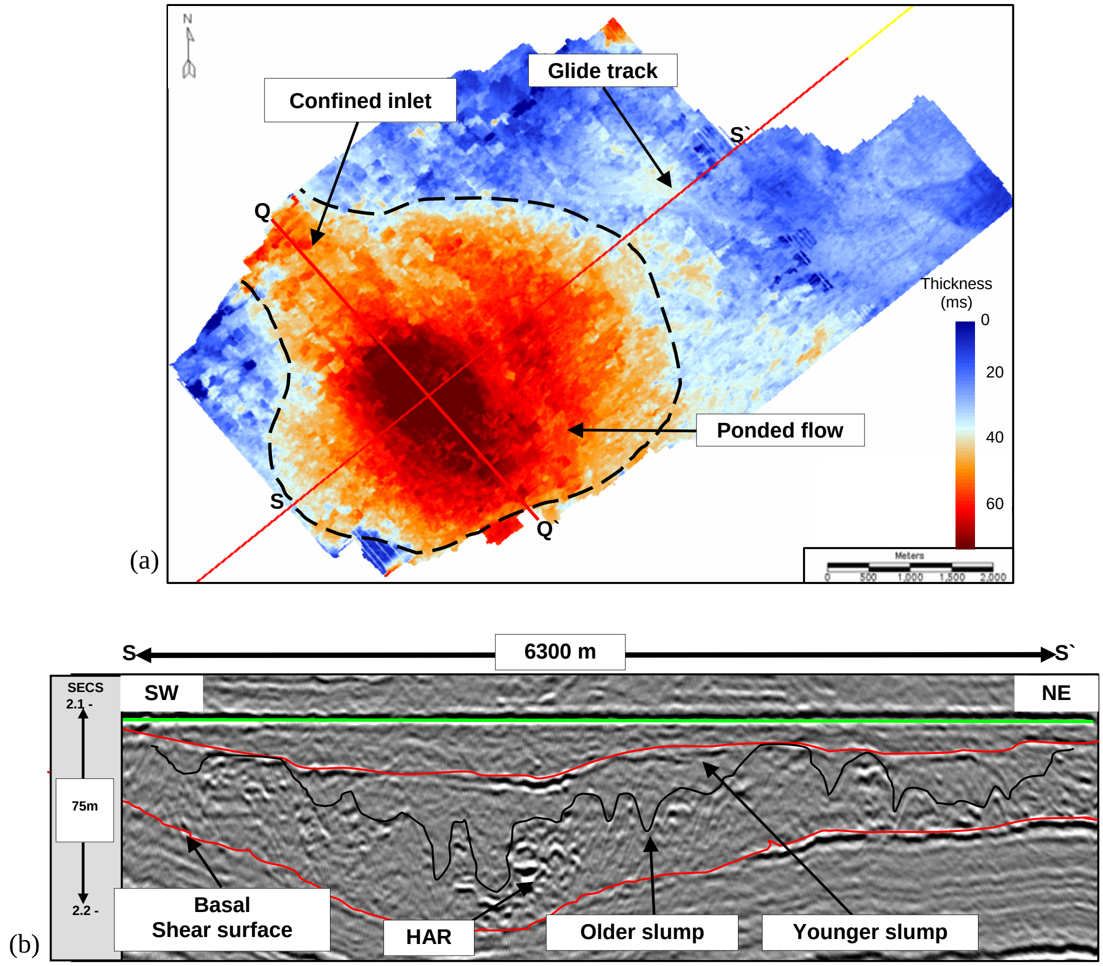

Figure 41: (a) Time thickness map shows an overall lobate geometry that reflects the influence of topography on deposition (b) Seismic line showing MTC A.

Figure 42 shows a prominent glide track with an out-runner block at its terminus on a coherence horizon slice 60ms below the green horizon. The glide track is approximately 1.8km long and 10 m wide while the outrunner block has a maximum thickness of 10m. Longer glide tracks (up to 12km long) with associated out-runner blocks up to 10 m thick have been identified on the Nigerian continental slope by Nissen *et al*., (1999).

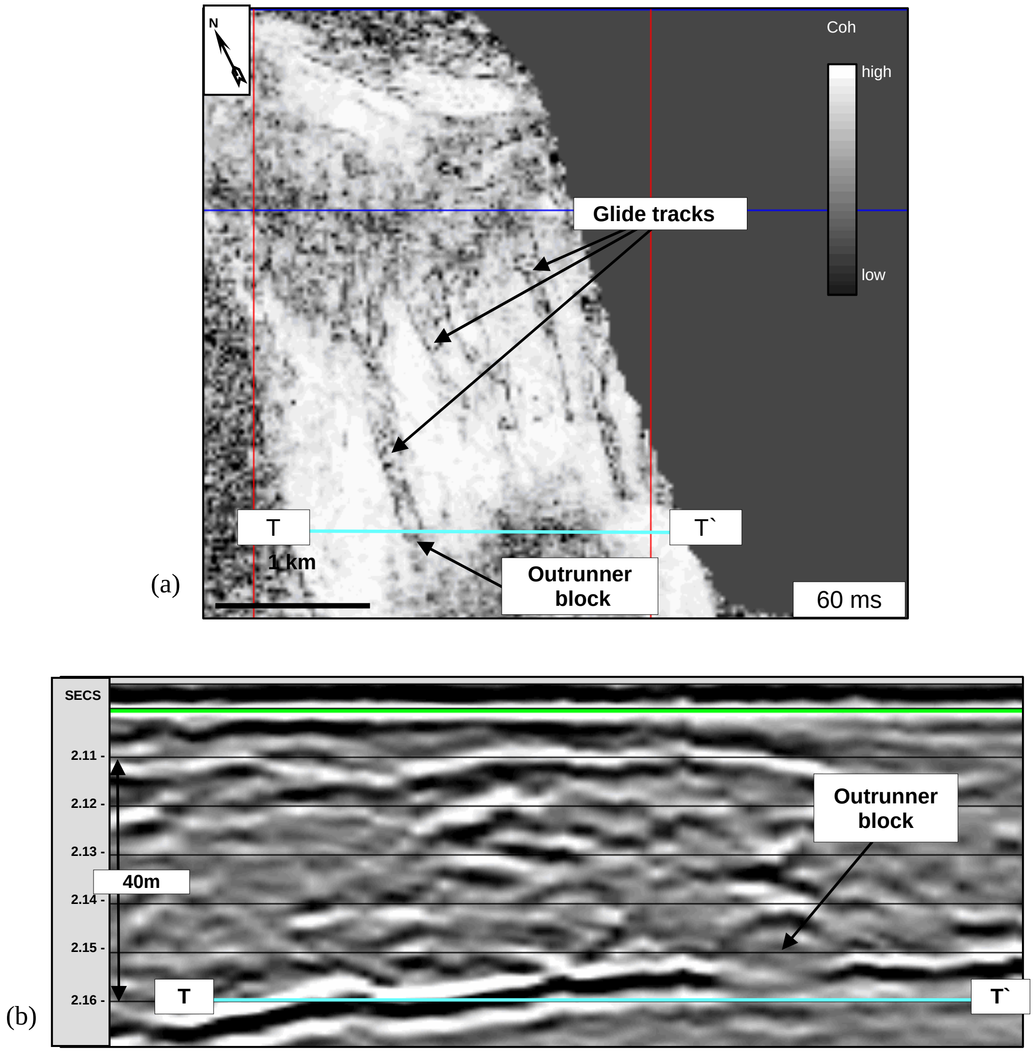

Figure 42: (a) Coherence horizon slice at 60ms below the green horizon imaged linear features interpreted as glide tracks with outrunner blocks at their terminus (b) Seismic traverse imaging the outrunner block.

4.4.2 MTC B

MTC B is approximately 3km by 4km in aerial extent, with a maximum thickness of 56 m. The unit is characterized by low amplitude chaotic reflections, and it comprises 2 different slump packages (Figure 43). However, unlike MTC A, both slumps exhibit similar internal fabric of low amplitude chaotic reflections, which correlates with dark shades on the coherence slice. Consequently, similar internal fabric implies that both packages were rapidly deposited. The main contrasting feature between the sub-units is their basal shear surface. The younger deposit is characterized by a more erosive basal surface in comparison to the older deposit (magenta colored). This difference may be related to their lithologic composition; I propose that the younger slump was coarser and had higher erosive power compared to the older slump, hence its more rugged basal surface.

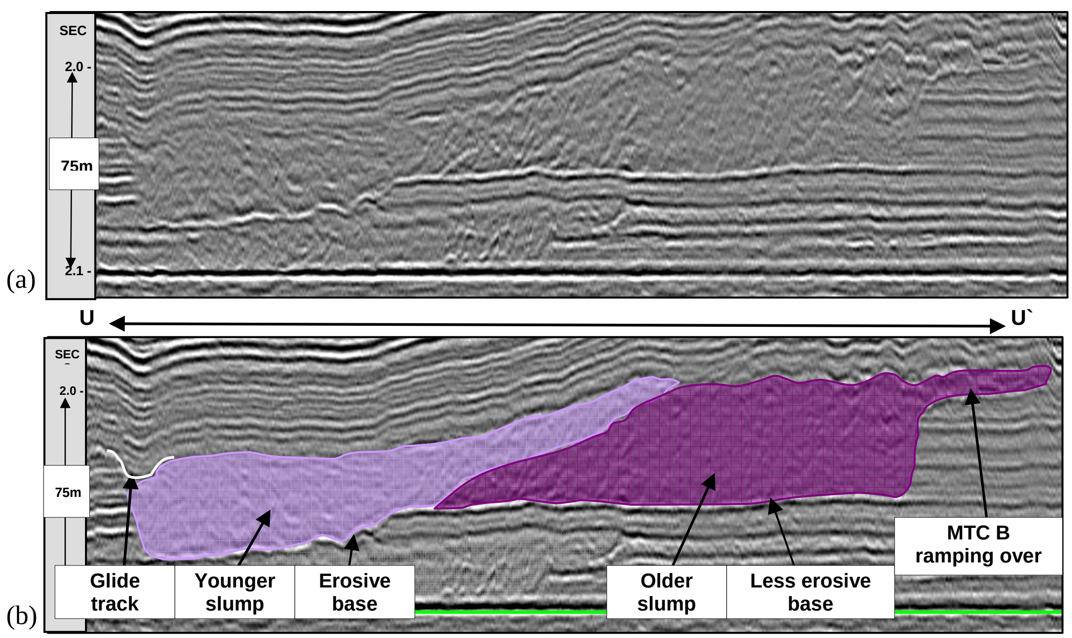

Figure 43: (a) Uninterpreted (b) Interpreted traverse line HH` showing MTC B's subunits. The more recent event (lilac-colored) is characterized by a more erosive basal surface in comparison to the earlier event (magenta-colored). See Figure 44b for location.

A southeast transport direction is deduced from map views (coherence horizon slices and isochron map) and the absence of a headscarp within the coverage area also suggests its presence further updip (Figure 44). In the map views, MTC B is shown to terminate abruptly against a pre-existing scarp in the toe region. This abrupt termination is imaged on seismic profile, but rather than having the MTC come to a definite stop, the slump ramped over the pre-existing scarp (Figure 43b). The behavior of the slump as it ramps over the scarp suggests prolonged flow duration. Similar "ramping over" of slumps was observed by Martinez *et al*., (2005) along the continental margin of Israel. In addition, the authors observed compressional features such as pressure ridges and thrust faults in the toe region of the slumps, features that were not identified in my study. MTC B was subsequently truncated in the eastward portion by a younger MTC package.

A major glide track corresponding to a small depression on seismic was identified on a coherence horizon slice at 70 ms above the green horizon (Figure 44a). The depression was approximately 8m deep, 2.8 km long, and 10 m wide. Though not directly associated with MTC B, the glide track indicates the occurrence of slumping events updip of the study area.

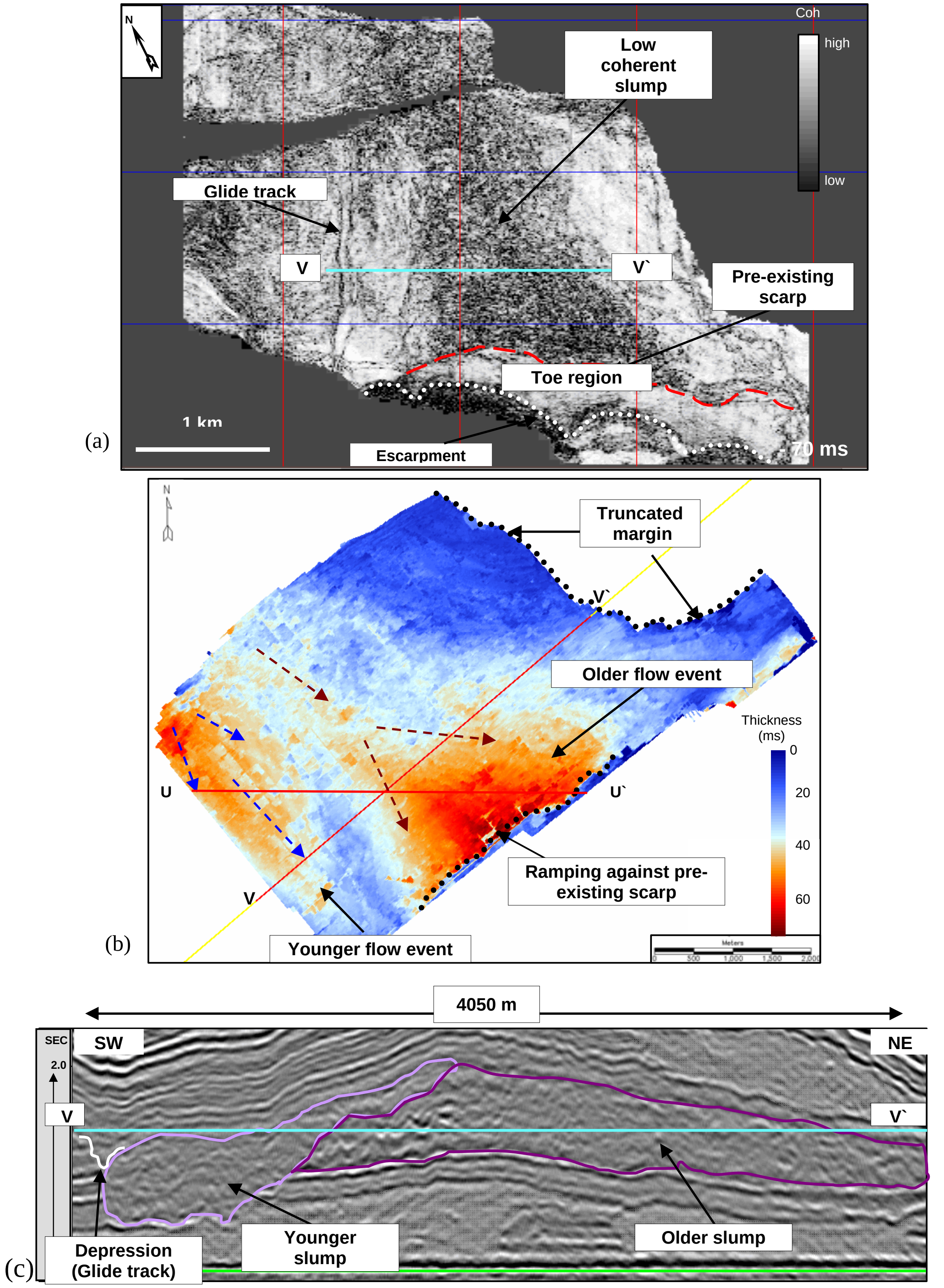

Figure 44: (a) Coherence horizon slice at 70ms above the green horizon imaged a prominent glide track running parallel to the direction of transport (b) Time thickness map of MTC B (c) Seismic line showing MTC B.

4.4.3 MTC C and MTC D

My interpretation shows that MTC C and D were triggered by differing mechanisms though on seismic they overlie each other and are only separated by a HAR unit that thickens updip (Figure 45). MTC C is shown to truncate MTC A and MTC B, while MTC D is underlain by a major angular unconformity. For discussion purposes MTC D is divided into MTC D Lower and MTC D upper (Figure 45b).

(a)

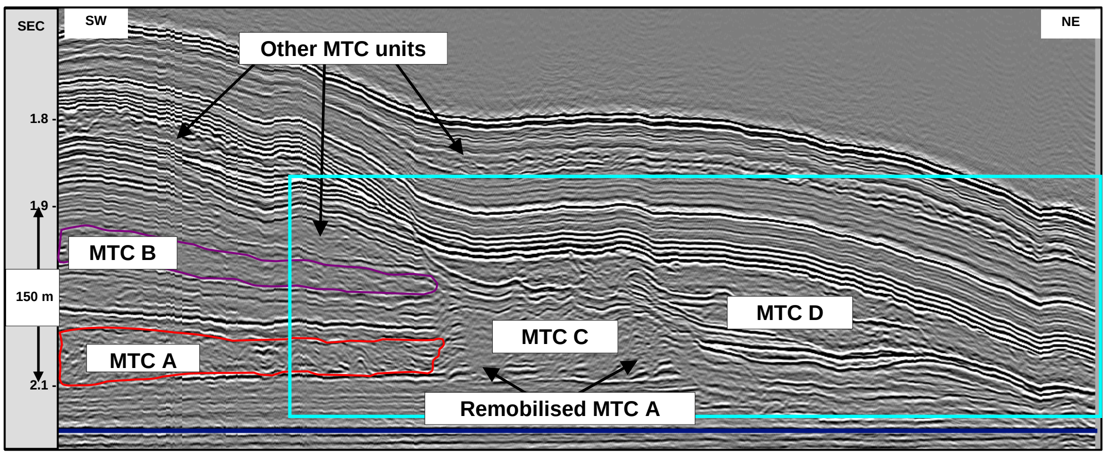

(b)

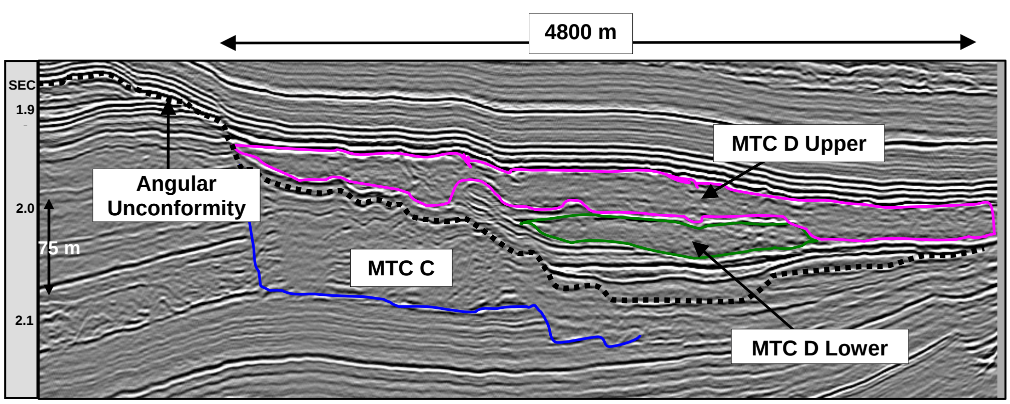

Figure 45: (a) Seismic line showing MTC C and MTC D separated by a HAR unit (b) Seismic line showing MTC C deposited eastward of MTCs A and B whereas MTC D is underlain by an angular unconformity.

4.4.3.1 MTC C

MTC C covers an area of approximately 2.6 km by 1.3 km, with a maximum thickness of 68m. It is characterized by a steep scarp sidewall, scoured base, and undeformed (coherent) blocks within the low amplitude chaotic mass. My understanding is that MTC C was triggered by some sort of structural activity that led to the failure of MTC A. The slumping that ensued from this failure is characterized by undeformed blocks within the chaotic mass. A correlation of these blocks with portions of MTC A further validates that MTC C failed from MTC A (Figure 46).

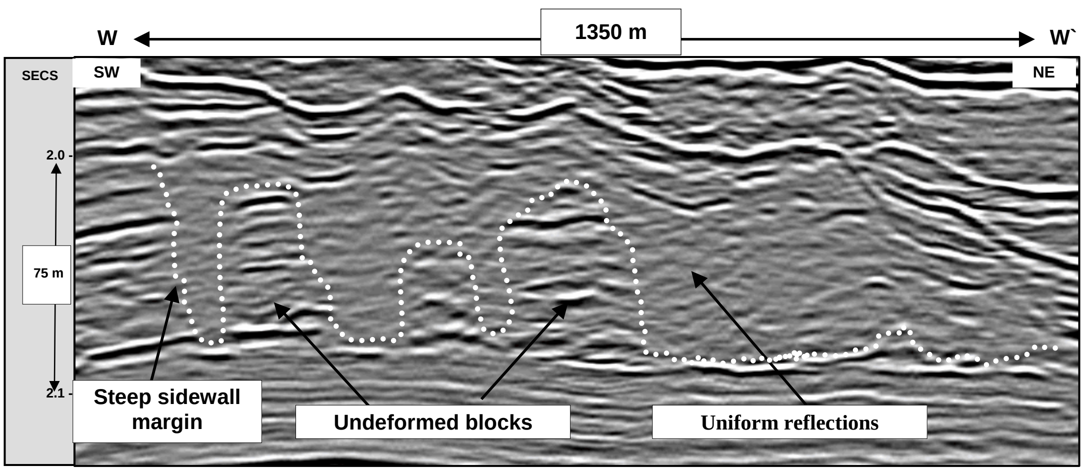

Figure 46: Seismic line showing MTC C characterized by undeformed blocks within the chaotic mass. An apparent correlation between the blocks and a portion of MTC A further validates the fact that MTC C ensued from the failure of MTC A.

The coherence map generated along the white horizon on Figure 46 reveals alternating high and low coherence features. The high coherence (light shades) correspond to the erosional remnants, whereas the low coherence features are associated with the chaotic slump mass (Figure 47a). Interpretation of the negative curvature attribute generated off the same surface also supports this conclusion. The negative values correspond to synclinal features, in this case the chaotic mass, whereas the positive values correlate with anticlinal features associated with the undeformed blocks (Figure 47b). The linear features imaged on the negative curvature map are interpreted as older glide tracks.

(a)

(b)

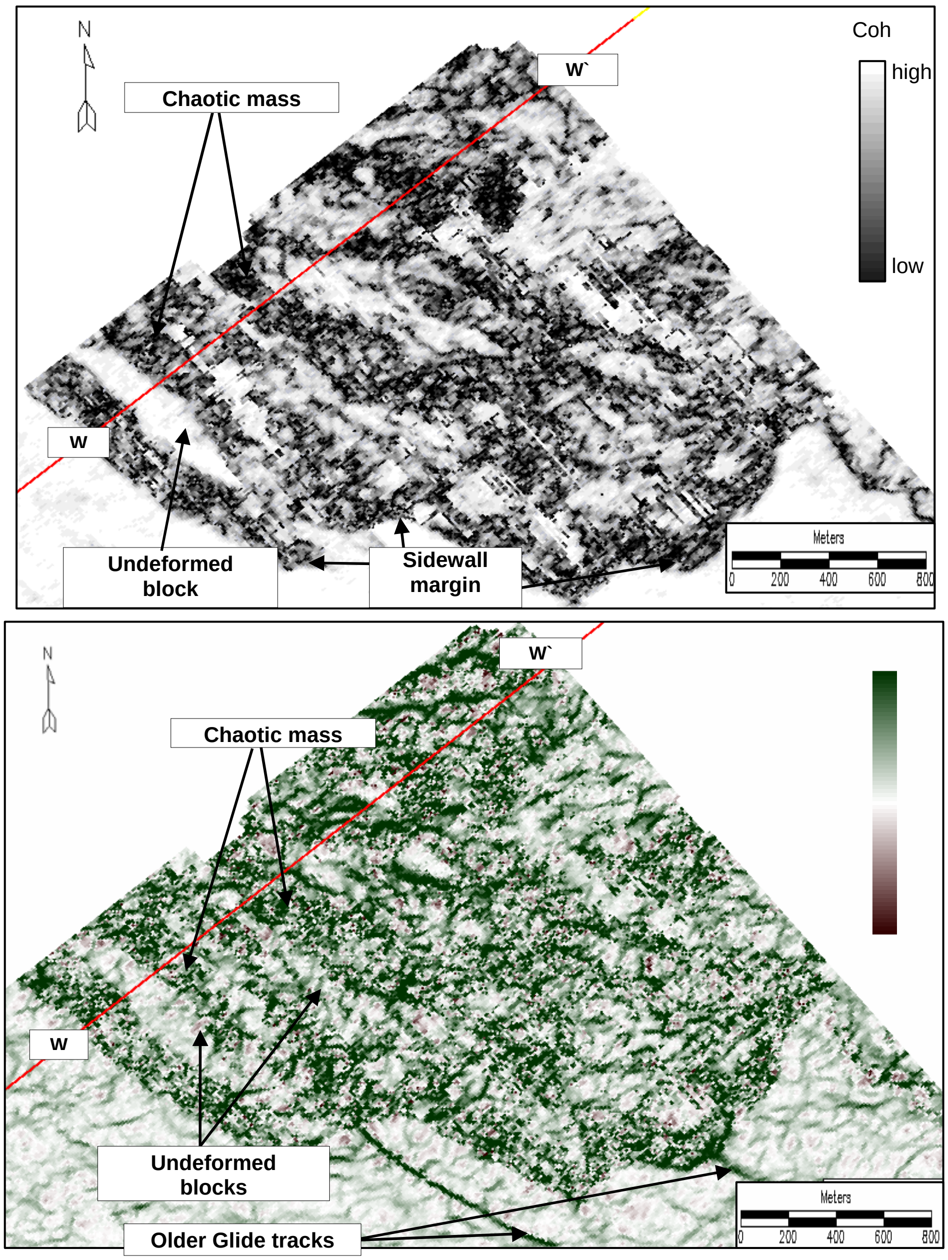

Figure 47: (a) Coherence map (b) Negative curvature. Map views imaged coherent blocks within the chaotic mass.

4.4.3.2 MTC D

Following the deposition of MTC C was a period of structural uplift probably related to salt movement and thereafter erosion marked by an angular unconformity (Figure 45b). The angular unconformity is overlain by a HAR unit and 2 other MTCs. The older MTC of the 2 units is clearly shown as eroding into the underlying HAR unit, while the younger MTC unit overlies it. Both MTC units are labeled MTC D with the younger being MTC D Upper and the older unit MTC D Lower (Figure 45b).

MTC D Lower has an area extent of approximately 4.4 km by 1.8 km, with a maximum thickness of 30m. The unit is characterized by a mounded external geometry filled with chaotic low amplitude reflections (Figure 48). The small area extent of MTC D Lower in comparison to the overlying MTC suggests that the slump may have resulted from a small scale failure event that eroded only a small volume of sediment.

(a)

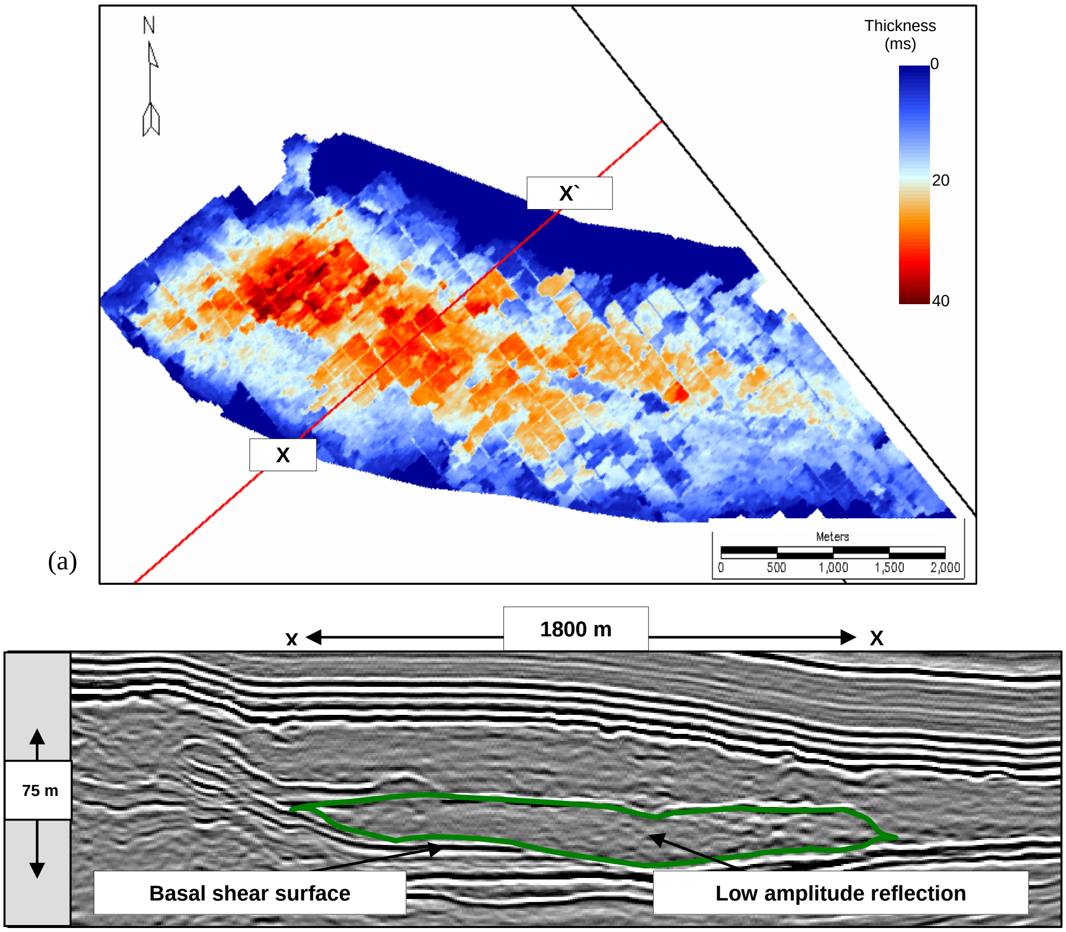

(b)

Figure 48: (a) Time thickness map (b) Seismic line XX` showing MTC D Lower.

MTC D Upper has an area extent of approximately 6 km by 4.8 km, with a maximum thickness of 30 m. The package is characterized by chaotic variable amplitude reflections, which suggest a mixed lithology composition (Figure 49). The lengthier extent of this unit in comparison to MTC D Lower suggests that it resulted from a failure-event that eroded a higher volume of sediments. MTC D Upper was subsequently draped by high amplitude continuous reflections.

(a)

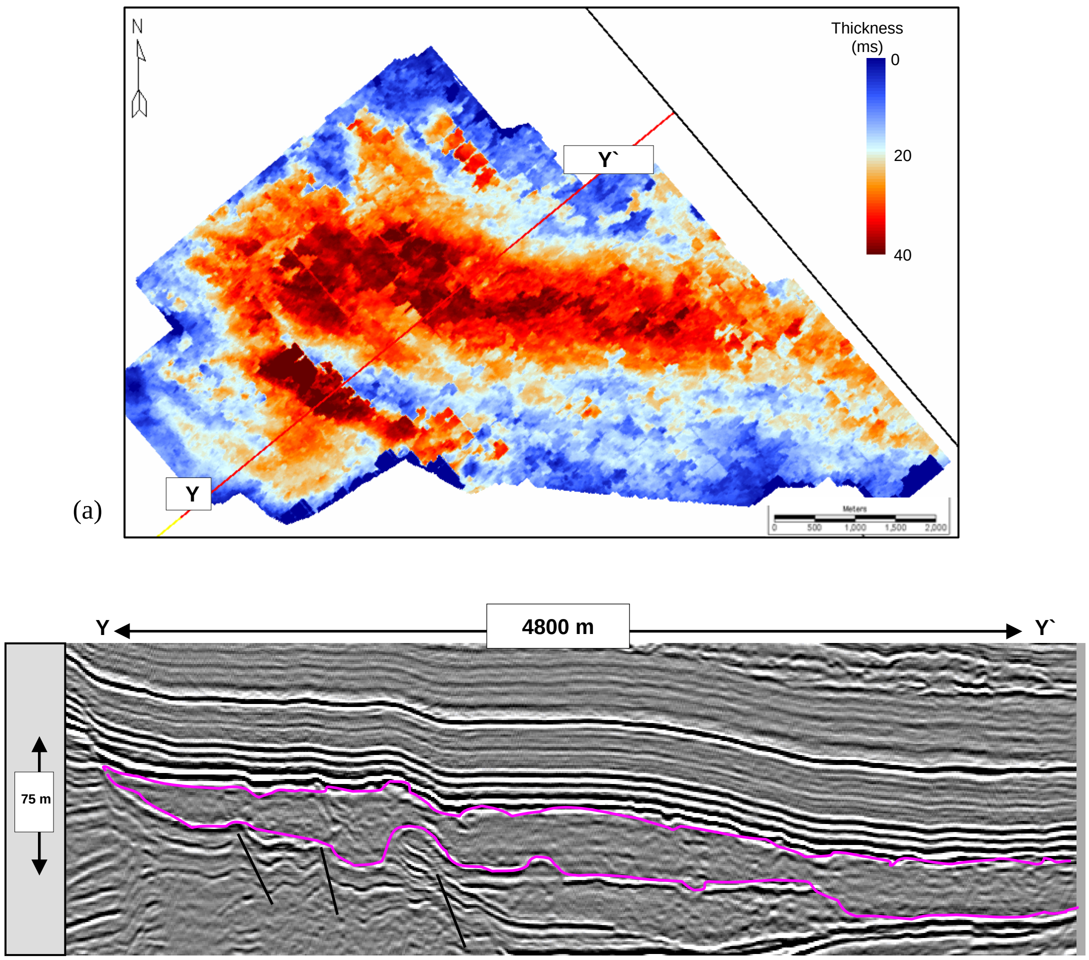

(b)

Figure 49: (a) Time thickness map (b) Seismic line YY` showing MTC D Upper.

4.5 WELL LOG INTERPRETATION

Logs from BH1-BH4 were tied to the seismic data using a checkshot data. Due to the close spacing of BH1, BH2, and BH3, the log curve with the best correlation to the seismic response was used as the type log (i.e. BH3) (Figure 50). The less sand-prone unit in the lower portion of the GR curve correlates with the channel-lobe complex, while another sand-prone unit in the upper section of the log correlates with a coherent block within the MTC A.

A relatively good correlation of the “ratty” channel-lobe complex was established across BH1 to BH3 (Figure 51). Posting these log curves on channel-lobe 4’s isochron map correlates with the “unconfined flow” region of the deposit (Figure 52). This correlation validates initial discussion on how the channel-lobe complex is characterized by bed-load sediments in the confined region and less coarse-rich sediments in the lobe area (unconfined region).

The sand-prone unit within MTC A could not be correlated to the other logs in the area (Figure 51). Since the unit was correlated to coherent seismic facie on the seismic section, its limited area extent therefore suggests that it might be a transported block within the chaotic slump mass (Figure 53).

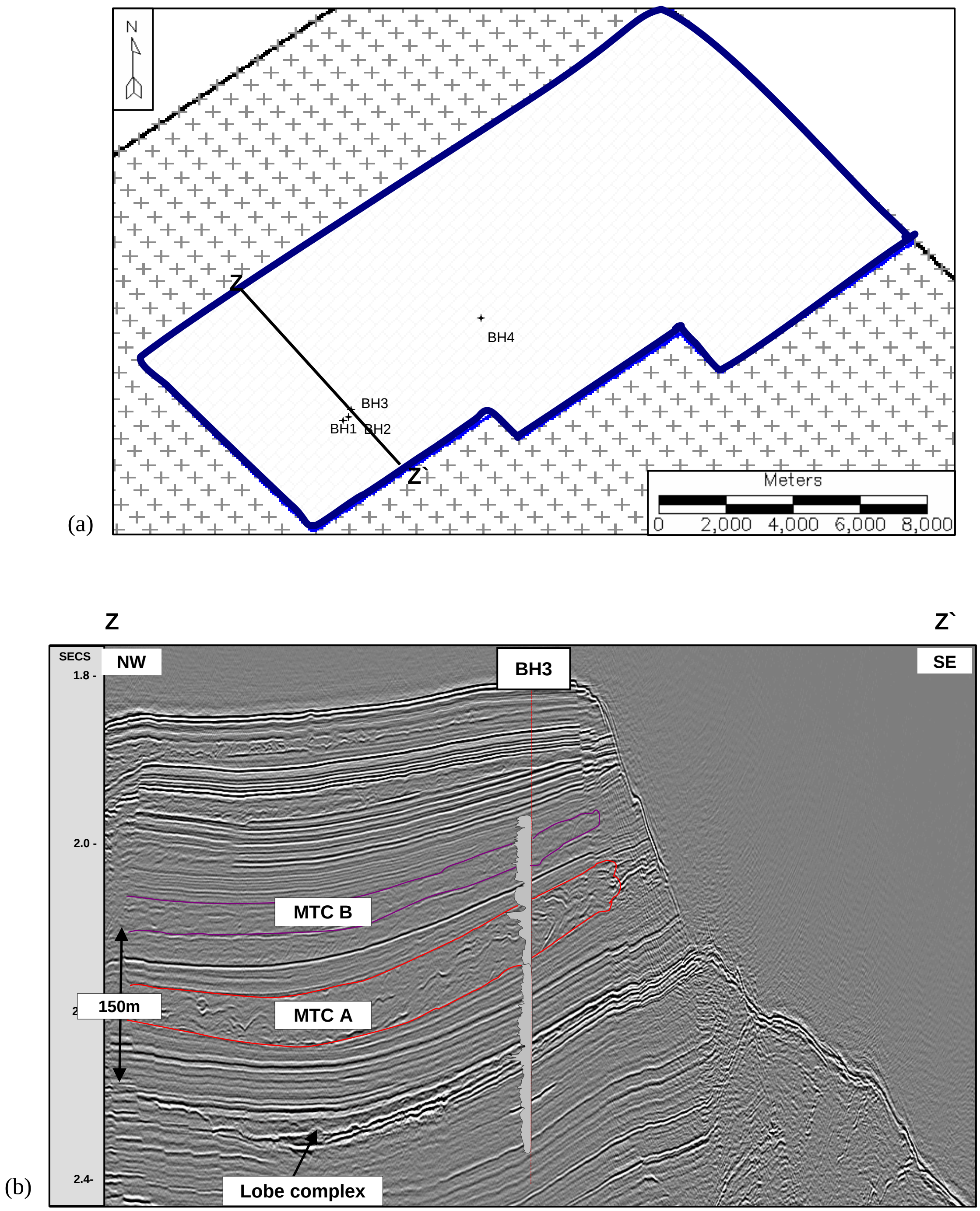

Figure 50: (a) Basemap showing the boreholes (b) NW-SE line showing the correlation between the type log (BH3) and seismic response.

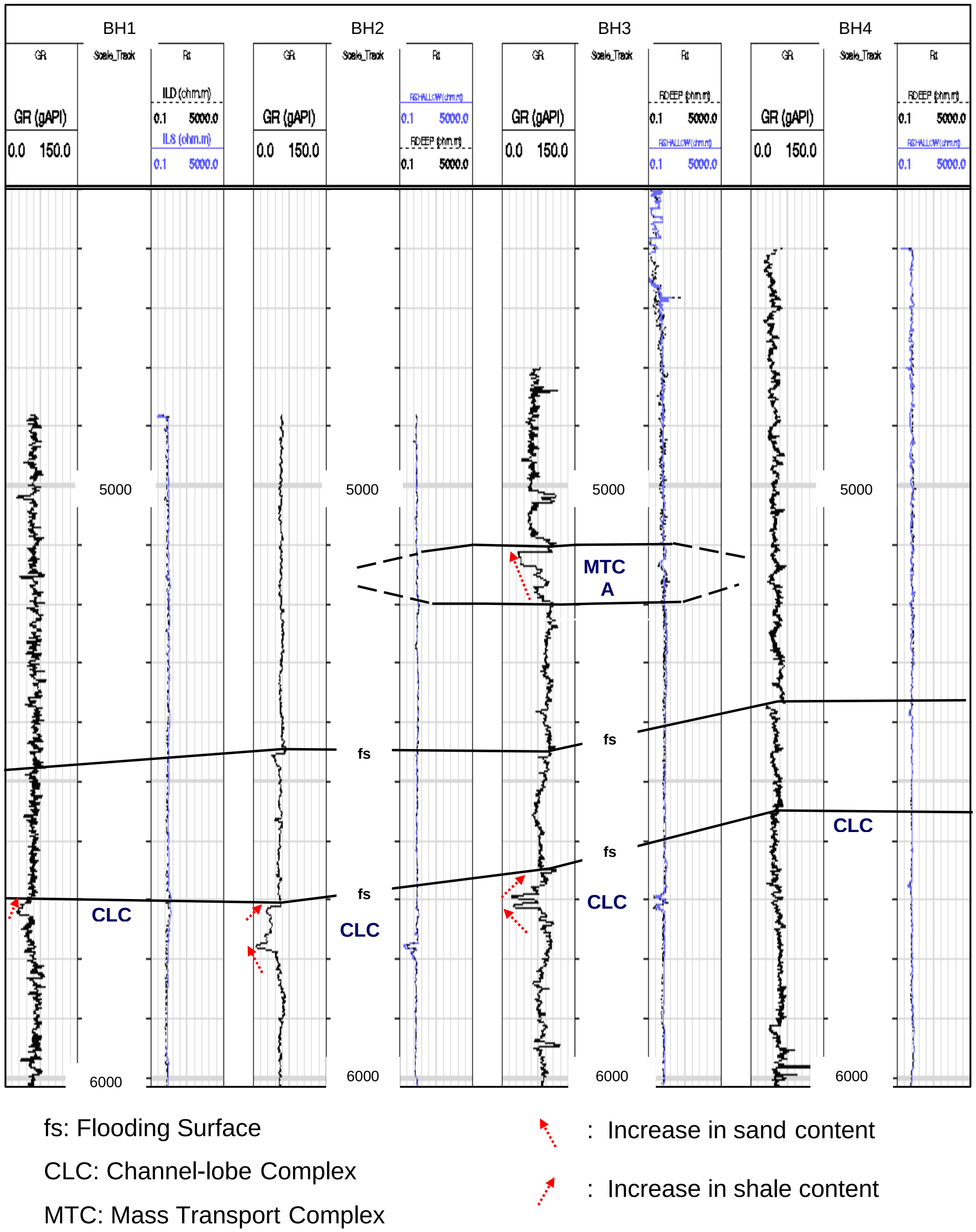

Figure 51: (a) Cross-section across well logs. The channel-lobe complex was correlated across the section; however, the localized positioning of the sand-prone unit within MTC A suggests it might be a transported block within the slump.

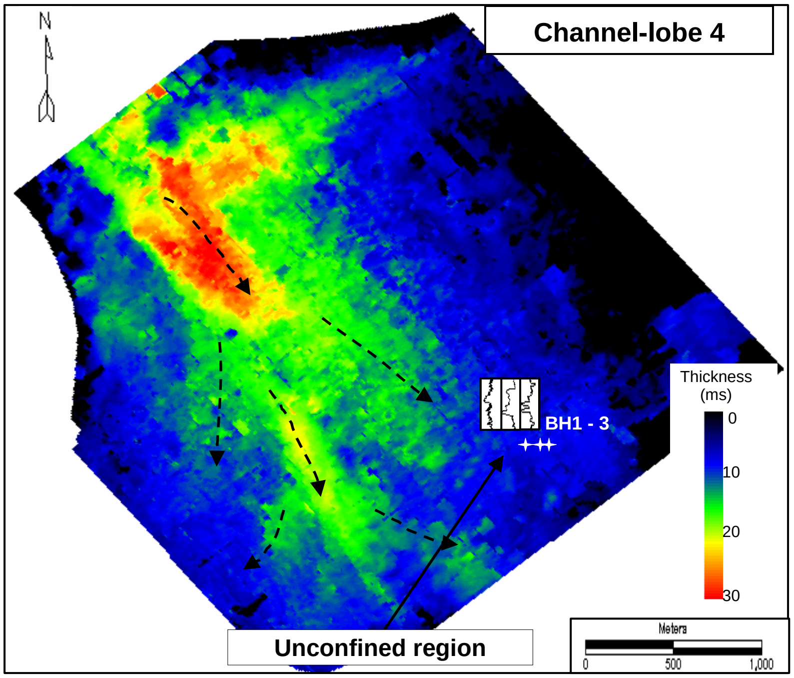

Figure 52: Isochron map of channel-lobe 4. BH1-3 interpolated on the map correlates with the unconfined region of the system which is characterized by fine-grained sediments.

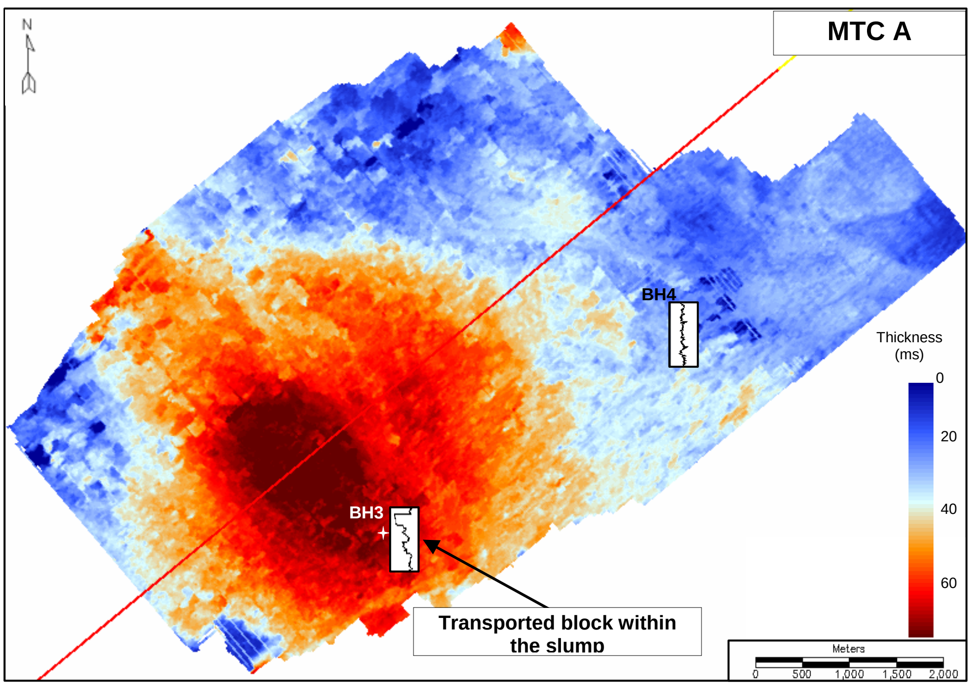

Figure 53: Isochron map of MTC A. BH3 interpolated on the map correlates with the transported block within the slump.

Chapter 5

DISCUSSION

The stratigraphic framework of my study area reveals the interplay of sediment supply and salt tectonics on depositional processes. In the previous chapter, I described how the system's facies and architecture were influenced by factors such as sediment volume, flow velocity, and slope gradient changes, which in turn determine the basin's accommodation space and sediment supply. A geologic history of the suprasalt section is presented in this chapter based on how sea level fluctuations affected sediment supply, and accommodation space within the basin. Two tools (sequence stratigraphy and chronostratigraphy) are used to achieve this objective.

5.1 SEQUENCE STRATIGRAPHY

Sequence stratigraphy describes how changes in relative sea level affect accommodation space, sediment supply, and their resultant depositional systems. Vail (1987) described how accommodation space and sediment supply could be affected by sea-level fluctuations using his "sea-slug" model (Figure 54). According to this model, a complete cycle of sea-level changes (highstand→ lowstand → highstand) is characterized by three systems tracts: lowstand, transgressive, and highstand tracts. Each system tract corresponds to a different segment of a singe sea-level cycle. The depositional elements and lithofacies associations for each segment differ based on changes in accommodation space and sediment deposition.

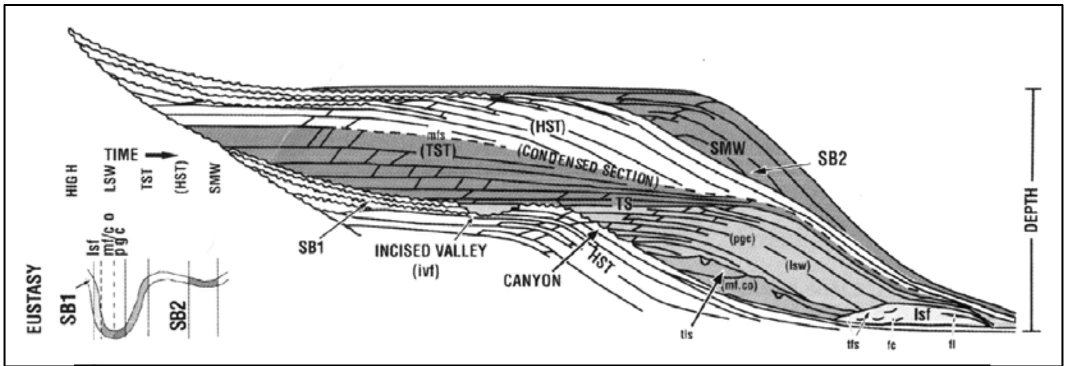

LEGEND

SURFACES

(SB) Sequence Boundaries
(SB 1) – Type 1
(SB 2) – Type 2
(DLS) Downlap Surfaces
(mfs) – maximum flooding surface
(tfs) – top fan surface
(tmf / co) – top mass flow/ channel overbank
(TS) Transgressive Surface
First floding surface above
maximum regression

SYSTEMS TRACT

HST – Highstand System Tract
TST – Transgressive System Tract
ivf – incised valley fill
LST – Lowstand System Tract
ivf – incised valley fill
lsw – lowstand wedge
pgc – prograding complex
mf/co – mass flow/channel overbank deposits
lsf – lowstand fan
fc – fan channels
fl – fan lobes
SMW – Shelf Margin Wedge System Tract

Figure 54: Sea-slug diagram illustrating the distribution of sediment and systems tracts in depth and space (modified after, Vail, 1987).

The Lowstand System Tract (LST) is initiated by a sudden drop in sea level. As a result, a reduction in accommodation space exposes the shelf thereby promoting fluvial downcutting and subsequent transport of sediments basinward. A rapid drop in relative sea level is accompanied by slumping of sediments along the continental margin and the formation of submarine canyons. The canyons subsequently connect with up-dip incised valleys, forming conduits for the basinward transport of turbidite systems and mass transport complexes. Posamentier and Allen (1999) subdivided the LST into an early and late stage (as cited on http://strata.geol.sc.edu).The Early Lowstand System Tract coincides with the initial period of falling sea level, while the Late Lowstand System Tract coincides with the slow rise in sea level following the maximum lowstand. The period at which sea level reaches its maximum is characterized by lowstand fans that are deposited at the slope/basin floor. Bouma (2001) subdivided these lowstand fan complexes into an upper fan (characterized by channel complexes), a middle fan (characterized by channel-levee systems), and a lower fan (characterized by sheet sands or depositional lobes). While, the period following the maximum lowstand when sea level rises slowly is characterized by progradational complexes or lowstand wedges that are deposited on the lower continental slope.

The Lowstand System Tract (LST) is bounded at the base by a diachronous unconformity (sequence boundary). It contains a progradational to aggradational parasequence stacking pattern, the result of the decrease in accommodation space due to increased sediment supply. In summary, the LST consists of mass transport complexes, lowstand fans, prograding complexes, and their associated depositional elements. I used the relationship between the different segments of the sea-level fall curve and their associated elements in describing the geology history of my study area.

The onset of coastal transgression is defined by the transgressive surface (TS), which defines the base of the Transgressive System Tract (TST). Increasing space caused by rising sea level promotes back stepping of the TST and the formation of retrogradational stacking patterns. During this period, sediment is trapped in the flooded incised valleys, thereby reducing the influx of clastic sediment to the marine environment.

The maximum highstand of sea level is marked by a Maximum Flooding Surface (MFS), which defines the base of the Highstand System Tract (HST). The HST is characterized by aggradational to progradational parasequence stacking pattern as a result of increase in sediment supply relative to accommodation space. During this period, clastic sedimentation is largely restricted to the shelf region; sedimentation on the basin floor is restricted to the slow deposition of hemipelagic sediments to form a condensed section. In rare occasions, basinward sedimentation does occur during the HST, either as a result of progradation of delta to the shelf edge or the presence of a conduit (submarine canyon) that allows sediment to bypass the shelf (Beard *et al*., 1982).

5.2 CHRONOSTRATIGRAPHY

This method allows for the division of strata packages into time intervals using tools such as biostratigraphy, sea-level curves, magnetostratigraphy, and isotopic indices. In most cases, accurate chronostratigraphy is best achieved by integrating all of these the different tools (Beard *et al*., 1982).

Biostratigraphy refers to the use of fossils in determining the absolute or relative ages of strata packages. The inception, extinction, and relative abundance of warm- versus cold-water fauna have been used in inferring climatic changes, including the recognition of interglacial and glacial periods and their associated stages. For instance, eight major glacio-eustatic cycles have been documented in the Pleistocene depositional record within the Gulf of Mexico province. On a more detailed level, these fossils have been correlated with sequence stratigraphic surfaces (sequence boundaries, transgressive and maximum flooding surfaces) on seismic, allowing the subdivision of the stratigraphic record into genetically related packages (Beard and Lamb, 1968; Beard, 1969; Wornardt and Vail, 1990).

Climatic changes can also been deduced from Oxygen isotope ratios in deep water foraminifera. Oxygen isotope stages characterized by more positive (heavier) oxygen isotopes correspond to periods of cold water (glacial periods). Thus oxygen isotope stages 2-4 correspond to the Wisconsinan Glacial Period and associated lowstand of sea level. Oxygen isotope stages characterized by more negative (lighter) oxygen isotopes correspond to periods of warm water (interglacial periods). Thus oxygen isotope stage 5 corresponds to the Sangamonian Interglacial Period and associated highstand of sea level (Chappell and Shackleton, 1986).

5.3 GEOLOGIC HISTORY

5.3.1 Influence of sea-level changes

I correlated five biostratigraphic-age dates obtained from BH5 with the seismic data (Figure 55b) and published oxygen isotope (and inferred sea-level) curves (Figure56). The depositional units I studied were not specifically dated. Nonetheless, the five available dates defined time intervals that, in combination with the oxygen isotope/sea-level curve, allowed me to make reasonable geologic interpretations for the units in question.

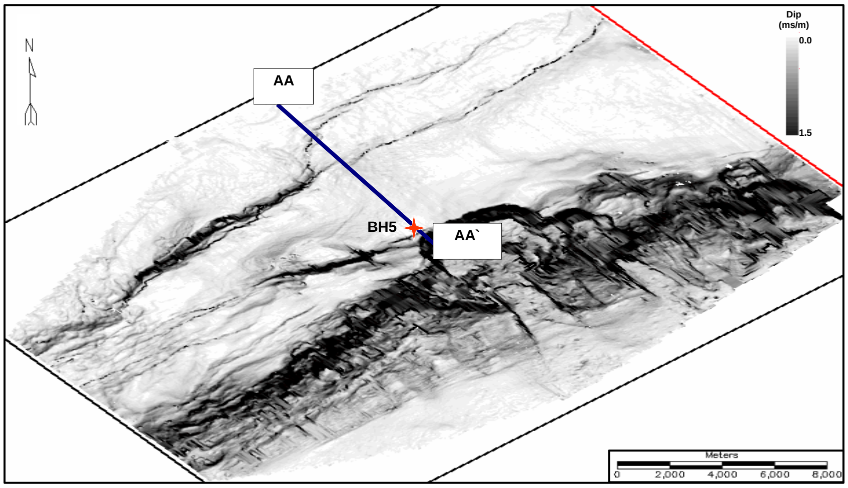

(a)

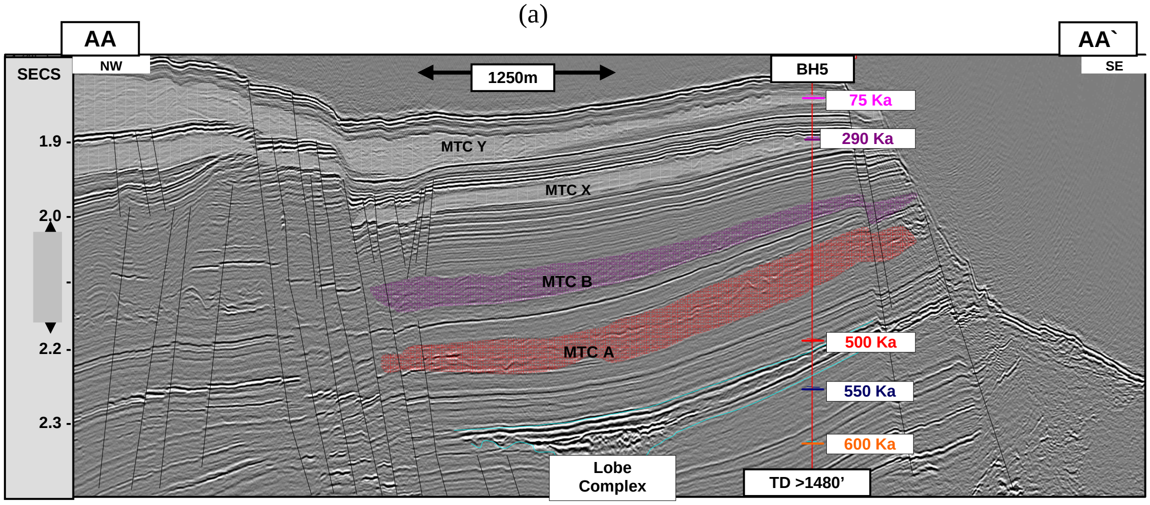

(b)

Figure 55: (a) Sea-floor dip map showing NW-SE line passing through BH5 (b) NW-SE line showing the interpolation of biostratigraphic-age dates. Dates were determined from nannofossils analysis

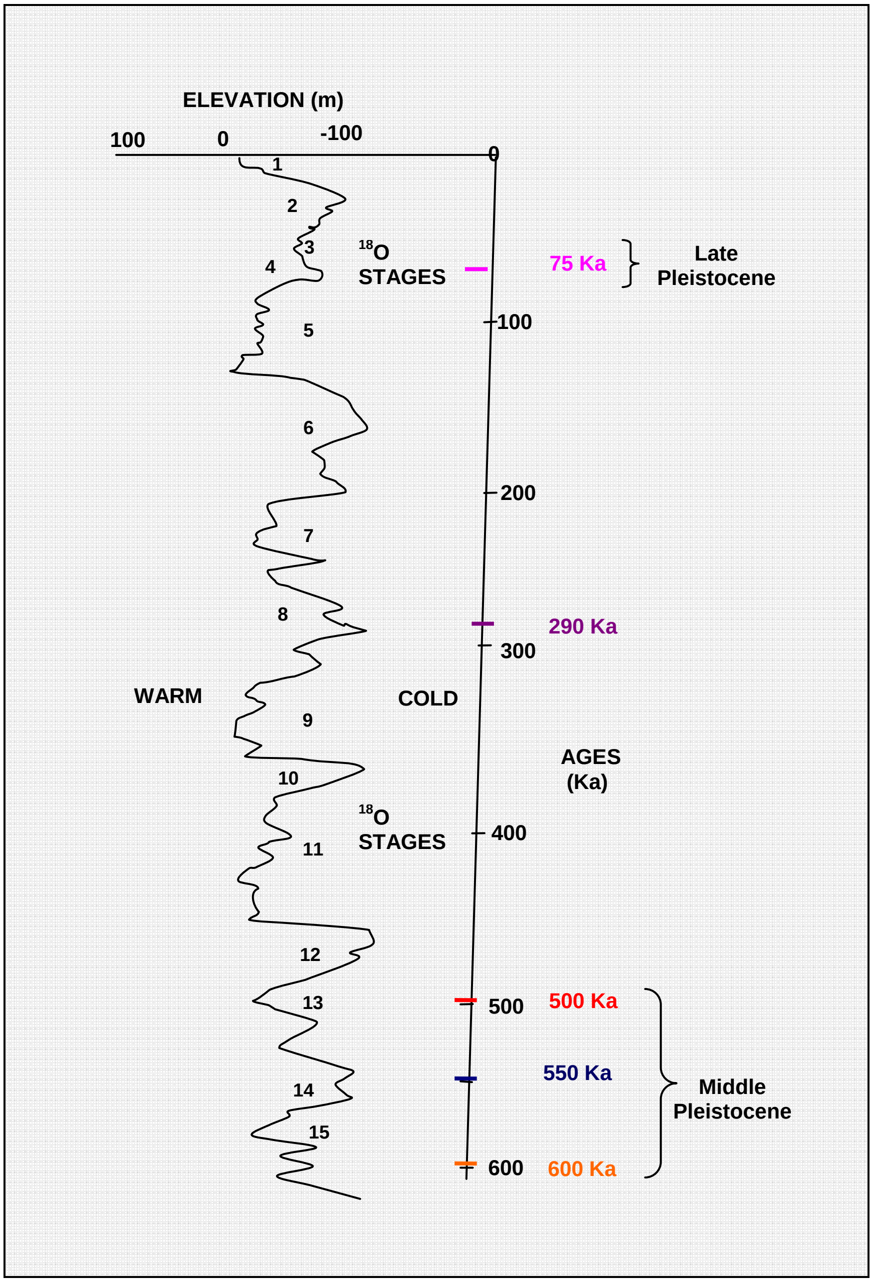

Figure 56: Diagram showing correlation between the ages and Oxygen isotope curve modified after Lamb *et al*., (1987), and Dupre' *et al*., (1991).

The oldest two dates bracket the time interval of 600 – 550 Ka. This interval coincides mainly with oxygen isotope stage 15 (a relatively warm highstand of sea level), ending with the subsequent drop in sea level associated with oxygen-isotope stage 14. On seismic data this interval corresponds to low amplitude parallel and continuous reflections characteristic of hemipelagic deposits. This correlation agrees with the sequence stratigraphy model of Vail (1987), which describes a shut down of clastic influx in the basin during highstands of sea level that results in the deposition of extensive hemipelagic sediments.

The channel-lobe complex (previously described in section 4.2.1) falls within the time interval of 550 – 500 Ka, and corresponds to oxygen-isotope stages 14 and 13. This time interval begins at a major lowstand of sea level (stage 14), and is followed by an interval of rising sea level, perhaps ending with a slight drop in sea level. I suggest that the deposition of the channel-lobe complex was initiated during the lowstand of sea level, and subsequent development of the complex continued during the early period of rising sea level. This could correspond to the Late Lowstand Systems Tract described by Posamentier and Allen (1999), during which time progradational complexes or lowstand wedges are deposited on the lower continental slope.

Alternatively, it is possible that the channel lobe complex correlates with the interval of rising sea level following oxygen-isotope stage 14. This alternative interpretation, however, contradicts traditional sequence stratigraphy models. According to Vail (1987), periods of rising sea level should be characterized by a shutdown of clastic influx into the basin and the deposition of transgressive to highstand system tracts on the shelf. This apparent contradiction could be explained by work done by Kolla *et al.*, (1993). They noted that deposition of sand-rich turbidite systems of the Mississippi fan continued into periods of sea-level rise, intervals that otherwise should be characterized by transgressive system tracts based on traditional sequence stratigraphy models (Figure 57).

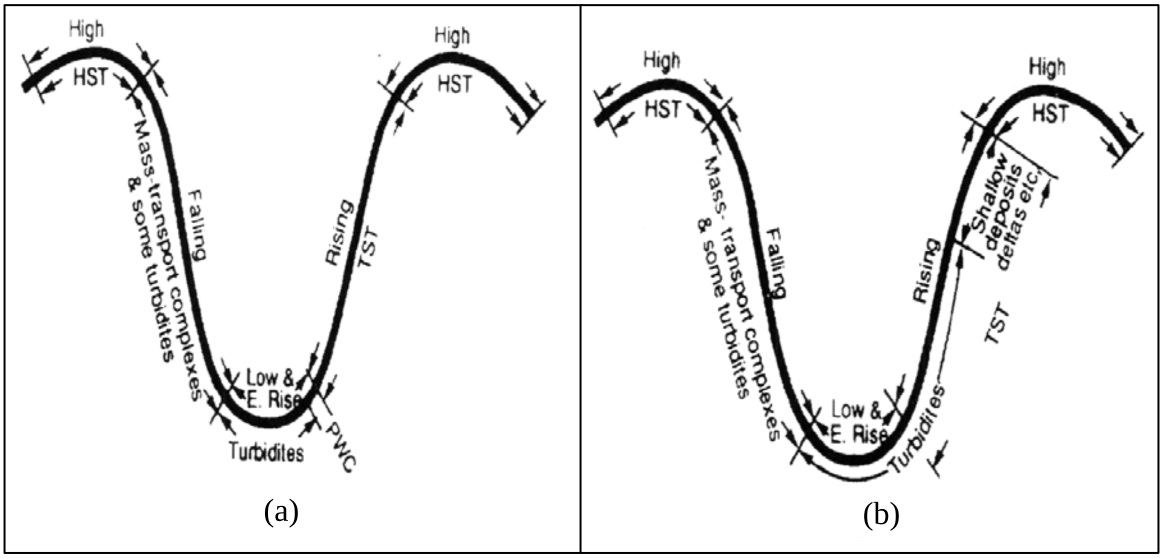

Figure 57: Depositional systems and systems tracts with respect to sea level (a) Adaptation from previous sequence stratigraphy models (b) Modified from A to show the continuation of turbidite sedimentation until a significant rise of sea level (part of TST) (Kolla *et al*., 1993).

Their association of sand-rich turbidite systems with transgressive and/or highstand systems tracts remains controversial. Nonetheless, they argued that certain factors acted to allow sediment to bypass the shelf during the rise in sea level. These factors included: (1) large sediment supply, (2) the presence of an actively connected river valley and canyon that served as a conduit, and (3) steep gradients at the head of the canyon that promoted basinward progradation of sediments. I cannot substantiate such factors in my study area; however, it is well known that the Mississippi Delta had shifted its course at least 16 different times over the past several thousand years . It is therefore possible that this could have been a time when the Mississippi Delta had prograded to the shelf edge, thereby allowing the channel-lobe complex to form during an interval of rising sea level.

The time interval between 500 and 290 Ka includes three major lowstands of sea level (oxygen-isotope stages 12, 10, and 8) and two major highstands of sea level (oxygen isotope stages 11 and 9). On the seismic record, this time interval correlates with the two large Mass Transport Complexes (MTC A and MTC B) interbedded with low-high amplitude parallel reflections. The laterally extensive, low-high amplitude parallel reflections are most likely hemipelagic deposits correlative with rising and/or highstands of sea level. It seems likely that MTC A formed during the lowstand of sea level associated with oxygen-isotope stage 12 (~470 Ka). MTC B most formed during the lowstand of sea level associated with oxygen-isotope stage 10 (~370 Ka). The BH5 well did not pass through MTC C and MTC D; however, it is likely that MTC D was deposited during a younger lowstand of sea level. This interpretation is consistent with the sequence stratigraphy model proposed by Vail (1987).

The last time interval begins at 290 Ka during a major lowstand of sea level (oxygen-isotope stage 8) and ends at 75 Ka, during the middle Wisconsinan lowstand (oxygen-isotope stage 4). This time interval on the seismic record consists of low to high amplitude parallel reflections capped by an extremely large, widespread MTC (MTC Y – not studied in this thesis). The basal 290 Ka date occurs in hemipelagic sediment immediately above another large, widespread MTC (MTC X) that almost certainly formed associated with the drop in sea level that ended in oxygen-isotope stage 8. The upper 75 Ka date occurs in hemipelagic sediment immediately above the large, widespread MTC X that almost certainly formed associated with the drop in sea level that ended in oxygen-isotope stage 4. It is interesting to note that there is no evidence in the study area of a MTC having formed during the lowstand of sea level associated with oxygen isotope stage 6. In addition, the sediments deposited during the time interval from 290-75 Ka are approximately 75m thick, whereas the sediments coincident with the time interval from 500 – 290 Ka are approximately 160m thick. These differences could be related to the volume of sediments failed and transported from the shelf to the lower continental slope during the different periods of falling sea level. A higher sediment volume was presumably transported from the shelf region onto the lower continental slope in my study area during the age range of 500 - 290 Ka in comparison to the interval of 290 - 75 Ka. In addition, differences in rates of sedimentation during these two time periods could be related to switching feeder systems, as well as the presence of up-dip intra-slope basins that could have trapped the sediments along their paths of transportation.

Chapter 6

CONCLUSION

The depositional systems mapped in my study area reflect the influence of salt tectonism and sea-level changes on the transport and deposition of sediments. The differences in their behavior and architecture show the importance of understanding the factors controlling deposition before applying a generalized depositional model for the area. My conclusions based on this study include the following:

- The sediments were deposited from the Middle Pleistocene to Late Pleistocene (mid-Wisconsinan).
- The systems deposited during the different periods of sea-level change correlates well with seismic and well log interpretation. The channel-lobe complex was interpreted to have been developed during a rise to highstand sea-level, even though such periods (rising sea level to highstand) are expected to be characterized by slow pelagic sedimentation within the basin. This might be attributed to factors (e.g. switching depocenters) that can promote clastic influx basinward during these time intervals.
- The alternating sequence of hemipelagic deposits with mass transport complexes above the channel-lobe complex correlates with intervals of rising and falling sea level. However, the absence of other turbidite systems such as channels or lobe complexes within this section (even though it experienced sea-level lowstands) could be attributed to the following factors: 1. The possibility of having switching depocenters during lowstands of sea level that would have inhibited the transport

of turbidites downslope 2. The presence of intraslope basins further updip on the slope that might also have trapped the turbidites.

- I presume that MTC A and B may have been deposited during episodic lowstands of sea level because both units are individually made up of at least 2 different flow events.
- Periods of high sediment supply probably triggered salt movement that resulted in the creation of localized accommodation for the deposition of MTC A and the channel-lobe complex. I propose that the salt movement also resulted in changes in depositional gradient that promoted the progression from confined to unconfined flow as defined by seismic attributes.
- The geometry of the channel-lobe 4 showing the bypassed and avulsed lobes suggests prolonged sedimentation as the system sought optimal pathways in an attempt to dissipate energy. The scoured nature of the inlets suggests bed-load deposition, whereas fine-grained sediments are proposed to have been deposited further downdip in the "lobe" area. This interpretation was confirmed from well logs that show intercalations of sand in shale within the same region.
- Anomalous amplitude within the basal deposits on RMS map and frequency wipe out beneath the deposits on seismic suggests the sediments are gas-charged.
- Detailed architectural and facie analysis of deposystems are enhanced with high-resolution seismic data. Results from shallow sections can therefore be used as analogues for the deeper low- resolution sections.

Chapter 7

REFERENCES

Abreu, V., Sullivan, M., Pirmez, C., and Mohrig, D., 2003, Lateral Accretion Packages (LAP): An important reservoir element in deep water sinuous channels: Marine and Petroleum Geology, v.20, p.631-648.

Al-Dossary, S., 2004, Multi-trace seismic attributes for fracture detection: Msc. Thesis (Geophysics) University of Houston, Houston, Texas.

Armentrout, J.M., Kanschat, K.A., Meisling, K.E., Tsakma, J.J., Antrim, L., and McConnell, D.R., 2000, Neogene turbidite systems of the Gulf of Guinea continental margin slope, offshore Nigeria: in A.H Bouma and C.G. Stone , eds., Fine-grained turbidite systems, American Association of Petroleum Geologists, Memoir 72/SEPM Special Publication 68, p.93 – 108.

Beard, J.H., 1969, Pleistocene paleotemperature record based on planktonic foraminifers, Gulf of Mexico: Gulf Coast Association of Geological Societies, Transactions, v.19, p.535-553.

Beard, J.H., and Lamb, J.L., 1968, The lower limit of the Pliocene and Pleistocene in the Caribbean and Gulf of Mexico: Gulf Coast Association of Geological Societies, Transactions, v.18, p.174-186.

Beard, J.H., Sangree, J.B., and Smith, L.A., 1982, Quaternary chronology, paleoclimate, depositional sequences, and eustatic cycles: American Association of Petroleum Geologists, Bulletin, v. 66, p.158-169.

Beaubouef, R.T., and Friedmann, S.J., 2000, High-resolution seismic/sequence stratigraphic framework for the evolution of Pleistocene intra slope basins, Western Gulf of Mexico: Depositional Models and reservoir analogs, *in* P., Weimer, R.M., Slatt, J.L., Coleman, N., Rosen, C.H., Nelson, A.H., Bouma, M., Styzen, and D.T., Lawrence, eds., Global deep-water reservoirs: Gulf Coast Section-SEPM Foundation 20th Annual Bob F. Perkins Research Conference, p.40-60.

Beydoun, W., Kerdraon, Y., Lefeuvre, F., Bancelin, J.P., Medina, S., and Bleines, B., 2002, Benefits of a 3DHR survey for Girassol field appraisal and development, Angola: The Leading Edge, v.21, p.1152 – 1155.

Bouma, A.H., 1997, Comparison of fine-grained, mud-rich and coarse-grained, sand-rich submarine fans for exploration development purposes: Gulf Coast Association Geological Societies, Transactions, v.47, p.59-64.

Bouma, A.H., 2000, Fine-grained, mud-rich turbidite systems: model and comparison with coarse-grained, sand-rich systems: *in* A.H Bouma and C.G. Stone, eds., Fine-grained turbidite systems, American Association of Petroleum Geologists, Memoir 72/SEPM Special Publication 68, p.9-20.

Bouma, A.H., 2001, Fine-grained submarine fans as possible recorders of long- and short-term climatic changes: *in* Fard, AM., ed., Recognition of Abrupt Climate Changes in Clastic Sedimentary Environments, Global and Planetary, v.28, p.85-91.

Bouma, A.H., Stelting, C.E., Coleman, J.M., and Kohl, B., 1987, Mississippi Fan construction and sea level fluctuation relationships (abstract): Association of Petroleum Geologists, Bulletin, v.71, p.533.

Broucke, O., Robin, C., Calassou, S., Nalpas, T., Guillocheau, F., Temple, F., and Rouby, D., 2004, The role of deformation processes on the geometry of mud-dominated turbiditic systems, Oligocene and Lower-Middle Miocene of the Lower Congo basin (West African Margin): Marine and Petroleum Geology , v.21, p.327-348.

Brown, A.R., 1996, Seismic attributes and their classification: The Leading Edge, v.15, p.1090.

Chapin, M.A., Davies, P., Gibson, J.L., and Pettingill, 1994, Reservoir architecture of turbidite sheet sandstones in laterally extensive outcrops, Ross Formation, western Ireland, *in* P.Weimer, A.H. Bouma, and B.F. Perkins, eds., Submarine Fans and Turbidite Systems: Gulf Coast Section –SEPM Foundation 15th Annual Research Conference, p.53-68.

Chappel, J., and Shackleton, N.J., 1986, Oxygen isotopes and sea level: Nature v., 324, p.137-140.

Chen, Q., AND Sidney, S., 1997, Seismic attribute technology for reservoir forecasting and monitoring: The Leading Edge, v.6, p.445-448.

Chopra, S., 2001, Integrating coherence cube imaging and seismic inversion: The Leading Edge, v.20, p.354-362.

Deptuck, M.E., Steffens, G.S., Barton, M., and Pirmez, C., 2003, Architecture and evolution of upper fan channel-belts on the Niger Delta slope and in the Arabian Sea: Marine and Petroleum Geology, v.20, p.649-676.

Droz, L., Rigaut, F., Cochonat, P., and Tofani, R., 1996, Morphology and recent evolution of the Zaire turbidite system (Gulf of Guinea): Geological Society of America, Bulletin, v.108, p.253-269.

Dupre', W.R., Morrison, R.B., Clifton, H.E., Lajoie, K.R., Ponti, D.J., Powell II, C.L., Mathieson, S.A., Sarna-Wojcicki, A.M., Leithold, E.L., Lettis, W.R., McDowell, P.F., Rockwell, T.K., Unruth, J.R., and Yeats, R.S., 1991, Quaternary geology of the Pacific Margin: *in* Morrison, R.B., ed., Quaternary Nonglacial Geology; Conterminous U.S.:Geological Society of America, The Geology of North America, v.K-2, p.141-214.

Feng, J., and Buffler, R.T., 1996, Post Mid-Cretaceous depositional history, Gulf of Mexico basin, *in* J.O., Jones and R.L., Freed, eds, Structural Framework of the Northern Gulf of Mexico: Austin, Gulf Coast Association of Geological Societies, Transactions, p.9-26.

Galloway, W.E., 1998, Siliciclastic slope and base-of-slope depositional systems: component facies, stratigraphic architecture, and classification, American Association of Petroleum Geologists, Bulletin, v.82, p.569-595.

Galloway, W.E., Garney-Curry, P.E., and Li, X., 2000, Cenozoic depositional history of the Gulf of Mexico basin: American Association of Petroleum Geologists, Bulletin, v.84, p.1743-1774.

Gersztenkorn, A., Sharp, J., and Marfurt, K., 1999, Delineation of tectonic features offshore Trinidad using 3D seismic coherence: The Leading Edge, v. 18, p.1000-1008.

Hoyal, D.C.J.D., Van Wagoner, J.C., Adair, N.L., Deffenbaugh, M., Li, T., Sun, T., Huh, C., and Giffin, D.E., 2003, Sedimentation from Jets: A depositional model for clastic deposits of all scales and environments: American Association of Petroleum Geologists, Search and Discovery Article #40082.

Humphris, C.C., 1979, Salt movement on continental slope, Northern Gulf of Mexico: American Association of Petroleum Geologists, Bulletin, v.63, p.782-798.

Jennette, D.C., Fouad, K., Wawrzyniec, T., Dunlap, D., Munoz, R., and Meneses-Rocha, J., 2003, Slope and basin-floor reservoirs from the Miocene and Pliocene of the Veracruz Basin, southeastern Mexico: Marine and Petroleum Geology, v.20, p.587-600.

Kendrick, J.W., 2000, Turbidite reservoir architecture in the Northern Gulf of Mexico deepwater: Insights from the development of Auger, Tahoe and Ram/Powell fields: Proceedings of GCSSEPM Foundation 20th Annual Research Conference Deep-water reservoirs of the world, Houston, p.450 – 468.

Kolla, V., Bourges, PH., Urruty, J.M., and Safa, P., 2001, Evolution of deep-water tertiary sinuous channels Offshore Angola (West Africa) and implications for reservoir architecture: American Association of Petroleum Geologists, Bulletin, v.85, p.1373-1405.

Kolla,V., AND Perlmutter, M.A., 1993, Timing of turbidite sedimentation on the Mississippi Fan: American Association of Petroleum Geologists, Bulletin, v.77, p.1129-1141.

Liu, J., and Watkins, J.S., 1992, Seismic facies and depositional processes on the lower continental slope, in the Mississippi Canyon Area, Gulf Of Mexico (abstract): Association of Petroleum Geologists, Bulletin, v.76, p.1462.

Martinez, J.F., Cartwright, J., and Hall, B., 2005, 3D seismic interpretation of slump complexes: examples from the continental margin of Israel: Basin Research, v.17, p.83-108.

Marton, G. and Buffler, R.T., 1993, Application of simple-shear model to the evolution of passive continental margins of the Gulf of Mexico Basin: Geology, v.21, p. 495-498.

McHargue, T.R., and Webb, J.E., 1986, Internal geometry, seismic facies, and petroleum potential of canyons and inner fan channels of the Indus submarine fan: American Association of Petroleum Geologists, Bulletin, v.70, p.161-180.

Mitchum, R.M., Sangree, J.B., Vail, P.R., and Wornar, W.W., 1991, Integrated well-log, seismic, and biostratigraphic approach to sequence stratigraphy in Late Cenozoic Expanded Sections, Gulf of Mexico (abstract): American Association of Petroleum Geologists, Bulletin, v.75, p.637.

Navarre, J., Claude, D., Liberelle, E., Safa, P., Vallon, G., and Keskes, N., 2002, Deepwater turbidite system analysis, West Africa: Sedimentary model and implications for reservoir model construction: The Leading Edge, v.21, p.1132-1139.

Nibbelink, K., 1999, Modeling deepwater reservoir analogs through analysis of recent sediments using coherence, seismic amplitude, and bathymetry data, Sigsbee Escarpment, Green Canyon, Gulf of Mexico: The Leading Edge, v.18, p.550-561.

Nibbelink, K., and Martinez, J., 1998, 3D Seismic coherence, amplitude, and bathymetry data definition of Pleistocene to recent sediments along the Sigsbee Escarpment Southeast Green Canyon, Gulf of Mexico, USA: Gulf Coast Association of Geological Societies, Transactions, v.48, p.289-299.

Niedoroda, A.W., Reed, C.W., Hatchett, L., Young, A., Lanier, D., Kasch, V., Jeanjean, P., BP America, Orange, D., and Bryant, W., 2003, Analysis of past and future debris flows and turbidity currents generated by slope failures along the Sigsbee Escarpment in the deep Gulf of Mexico: Proceedings of Offshore Technology Conference, OTC 15162, p.1-7.

Nissen, S.E., Haskell, N.L., Steiner, C.T., and Coterill, K.L., 1999, Debris flow outrunner blocks, glide tracks, and pressure ridges identified on the Nigerian continental slope using 3-D seismic coherency: The Leading Edge, v.18, p.595-599.

Orange, D.L., Angell, M.M., Brand, J.R., Thomson, J., Buddin, T., Hart, W., and Berger III, W.J., 2003, Geological and shallow salt tectonic setting of the Mad Dog and Atlantis Fields: Relationship between salt, faults and seafloor geomorphology: Proceedings of Offshore Technology Conference, OTC 15157, p.1-16.

Orange, D.L., Angell, M.M., Brand, J.R., Thomson, J., Buddin, T., Williams, M., Hart, W., and Berger III, W.J., 2004, Geologic and shallow salt tectonic setting of the Mad Dog and Atlantis fields: Relationship between salt, faults, and seafloor geomorphology: The Leading Edge, v.23, p.354-365.

Pacht, J.A., Robert, O.B., Bruce, E.B., and Bernard, L.S., 1991, Amplitude analysis within a sequence stratigraphic framework-Neogene strata of Offshore Louisiana (abstract): American Association of Petroleum Geologists, Bulletin.75, p.649-650.

Posamentier, H.W., 2003, Depositional elements associated with a basin floor channel-levee system: case study from the Gulf of Mexico: Marine and Petroleum Geology, v.20, p.677-690.

Posamentier, H.W., and Allen, G.P., 1999, Siliciclastic sequence stratigraphy: concepts and applications: Society for Sedimentary Geology (SEPM) Concepts in Sedimentology and Paleontology, No. 7, 216p.

Posamentier, H.W., and Kolla, V., 2003, Seismic geomorphology and stratigraphy of depositional deep-water deposits elements in deep-water settings: Journal of Sedimentary Research, v.73, p.367-388.

Posamentier, H.W., Meizarwin, Wisman, P.S., and Plawman, T., 2000, Deep water depositional systems - Ultra- deep Makassar Stait, Indonesia: Proceedings of GCSSEPM Foundation 20th Annual Research Conference Deep-water reservoirs of the world, Houston, p.806-816.

Prather, B., 2003, Controls on reservoir distribution, architecture and stratigraphic trapping in slope settings: Marine and Petroleum Geology, v.20, p.529-545.

Prather, B.E., Booth, J.R., Steffens, G.S., and Craig, P.A., 1998, Classification, lithologic calibration, and stratigraphic succession of seismic facies of intraslope basins, deep-water Gulf of Mexico: American Association of Petroleum Geologists, Bulletin, v. 82, p.701-728.

Rader, B., and Medvin, E., 2002, Shallow hazard detection in the near-surface, a coherence cube processing application: The Leading Edge, v.21, p.672-674.

Readings, H.G., and Richards, M., 1994, Turbidite systems in deep-water basin margins classified by grain size and feeder system: The American Association of Petroleum Geologists Bulletin, v.78, p.792-822.

Remacha, E., and Fernandez, L.P., 2003, High-resolution correlation patterns in the turbidite systems of the Hecho Group (South-Central Pyrenees, Spain): Marine and Petroleum Geology, v.20, p.711-726.

Rijks, E.J.H., and Jauffred, J.C.E.M., 1991, Attribute extraction: An important application in any detailed 3D interpretation study: The Leading Edge, v.10, p.11-19.

Saller, A.H., Noah, J.T., Ruzuar, A.P., and Schneider, R., 2004, Linked lowstand delta to basin-floor fan deposition, offshore Indonesia: an analog for deep-water reservoir systems: American Association of Petroleum Geologists, Bulletin, v. 88, p.21-46.

Salvador, A., 1987, Late Triassic –Jurassic paleogeography and origin of Gulf of Mexico basin: American Association of Petroleum Geologists, Bulletin, v.71, p.419-451.

Samuel, A., Kneller, B., Raslan, S., Sharp, A., and Parsons, C., 2003, Prolific deep-marine slope channels of the Nile Delta Egypt: American Association of Geologists, Bulletin, v. 87, p.541-560.

Sangree, J.B., Waylett, D.C., Frazier, D.E., Amery, G.B., and Fennessy, W.J., 1978, Recognition of continental-slope seismic facies, Offshore Texas-Louisiana: American Association of Petroleum Geologists, Bulletin, v.A117, p. 87- 116.

Sigismondi, M.E., and Soldo, J.C., 2003, Curvature attributes and seismic interpretation: Case studies from Argentina Basins: The Leading Edge, v.22, p.1122-1126.

Sikkema, W., and Wojcik, K.M., 2000, 3D visualization of turbidite systems, Lower Congo basin, offshore Angola: Proceedings of GCSSEPM Foundation 20th Annual Research Conference Deep-water reservoirs of the world, Houston, p.928-939.

Slatt, R.M., 2000, Why outcrop characterization of turbidite systems: *in* A.H Bouma and C.G. Stone , eds., Fine-Grained Turbidite Systems, American Association of Petroleum Geologists, Memoir 72/SEPM Special Publication 68, p.181-186.

Slatt, R.M., and Weimer, W., 1999, Turbidite systems Part 2: Subseismic-scale reservoir characteristics: The Leading Edge, v.18, p.562-567.

Slowey, N., Bryant, W.R., Bean, D.A., Young, A.G., and Gartner, S, 2003, Sedimentation in the vicinity of the Sigsbee Escarpment during the last 25,000 yrs: Proceedings of Offshore Technology Conference, Houston OTC 15159, p.1-15.

Vail, P.R., 1987, Seismic stratigraphy interpretation using sequence stratigraphy, part 1: in A.W. Bally, ed., Atlas of seismic startigraphy: American Association of Petroleum Geologists, Studies in Geology, v.1, p.1-10.

Vail, P.R., and Wornardt, W.W., 1991, Well log-seismic sequence stratigraphy analysis: An integrated approach to exploration and development (abstract): American Association of Petroleum Geologists, Bulletin, v.75, p.1423.

Van der Werff, W., and Johnson, S., 2003, High resolution stratigraphy analysis of a turbidite system, Tanqua Karoo Basin, South Africa: Marine and Petroleum Geology, v. 20, p.45-69.

Van Wagoner, J.C., Hoyal, D.C.J.D., Adair, N.L., Sun, T., Beaubouef, R.T., Deffenbaugh, M., Dunn, P.A., Huh, C., and Li, D., 2003, Energy dissipation and the fundamental shape of siliciclastic sedimentary bodies: American Association of Petroleum Geologists, Search and Discovery Article #40081.

Vitor, A., Beaubouef, R.T., and Van Wagoner, J.C., 2004, Scour Lobes: fundamental depositional elements in distributary deepwater systems (abstract): International Geological Congress, Florence, Italy.

Walper, J.L., Henk, F.H.Jr., Loudon, E.J., and Raschilla, S.N., 1979, Sedimentation on a trailing plate margin: The northern Gulf of Mexico: Gulf Coast Association of Geological Societies Transactions, v.29, p.188-201.

Weimer, P., 2000, Interpreting turbidite systems with 2D and 3D seismic data: an overview: *in* A.H Bouma and C.G. Stone, eds., Fine-Grained Turbidite Systems: American Association of Petroleum Geologists, Memoir 72/SEPM Special Publication 68, p.89-92.

Weimer, P., and Slatt, R.M., 1999, Turbidite systems, Part 1: Sequence and seismic stratigraphy: The Leading Edge, v.18, p.454-463.

Weimer, P., and Slatt, R.M., 2004, Petroleum Systems of Deepwater Settings: Society of Economic Geophysists, European Association of Geoscientists and Engineers, Distinguished Instructor Series, no. 7.

Westcott, W.A., and Broucher, P.J., 2000, Imaging submarine channels in the Western Nile Delta and interpreting their paleohydraulic characteristics from 3D seismic: The Leading Edge, v.19, p.580-591.

Wickens, H.D., and Bouma, A.H., 2000, The Tanqua fan complex, Karoo basin, South Africa-outcrop analog for fine-grained, deepwater deposits: *in* A.H Bouma and C.G. Stone, eds., Fine-Grained Turbidite Systems: American Association of Petroleum Geologists, Memoir 72/SEPM Special Publication 68, p.153-164.

Wilhelm, O., and Ewing, M., 1972, Geology and history of the Gulf of Mexico: Geological Society of America, Bulletin, v.83, p.575-600.

Winker, C.D., and Booth, J.R., 2000, Sedimentary dynamics of the salt-dominated continental slope, Gulf of Mexico: Integration of observations from the seafloor, near-surface, and deep subsurface: Proceedings of GCSSEPM Foundation 20th Annual Research Conference Deep-water reservoirs of the world, Houston, p.1059-1086.

Wood, L.J., Pecuch, D., Schulein, B., and Helton, M., 2000, Seismic attribute and sequence stratigraphic integration methods for resolving reservoir geometry in San Jorge Basin, Argentina: The Leading Edge, v.19, p.952-962.

Wornardt, W.W., and Vail, P.R., 1991, Revision of the plio-pleistocene cycles and their application to sequence startigraphy and shelf and slope sediments in the Gulf of Mexico: Gulf Coast Association of Geological Societies, Transactions, v.41, p.719-743.

Worrall, D.M., and Snelson, S., 1989, Evolution of the northern Gulf of Mexico, with emphasis on Cenozoic growth faulting and the role of salt: The Geology of North America -An overview: Geological Society of America, Bulletin, v.A, p.97 – 137.

Young, A.G., Bryant, W.R., Slowey, N.C., Band, J.R., and Gartner, S., 2003, Age dating of past slope failures of the Sigsbee Escarpment within Atlantis and Mad Dog developments: Proceedings of Offshore Technology Conference, Houston OTC 15204, p.1- 24.

Zeng, H., Backus, M.M., Barrow, K.T., and Tyler, N., 1998, Stratal Slicing, Part I: Realistic 3-d seismic model: Geophysics, v.63, p.502-513.